

# Lipid nanodispersions as drug carrier systems - a physicochemical characterization

## Dissertation

zur Erlangung des akademischen Grades  
doctor rerum naturalium (Dr. rer. nat.)

vorgelegt der

Mathematisch-Naturwissenschaftlich-Technischen Fakultät  
der Martin-Luther-Universität Halle-Wittenberg

von

Katja Jores

geboren am 10. Juni 1972 in Mainz

Gutachter:

1. Prof. Dr. rer. nat. habil. Karsten Mäder
2. Prof. Dr. rer. nat. habil. Reinhard Neubert
3. Prof. Dr. rer. nat. habil. Martin Wahl

Halle (Saale), den 8. Juni 2004

**urn:nbn:de:gbv:3-000007006**

[<http://nbn-resolving.de/urn/resolver.pl?urn=nbn%3Ade%3Agbv%3A3-000007006>]



I dedicate this thesis to all the people who have supported me.



# Table of contents

<b>1</b>	<b>Introduction.....</b>	<b>1</b>
1.1	Need of colloidal drug carriers .....	1
1.2	Overview of colloidal drug carrier systems .....	4
1.2.1	Nanosuspensions .....	4
1.2.2	Liposomes .....	5
1.2.3	Mixed micelles .....	5
1.2.4	Colloidal liquid crystalline structures .....	7
1.2.5	Microemulsions .....	8
1.2.6	Nanoemulsions.....	9
1.2.7	Nanocapsules .....	10
1.2.8	Polymer nanoparticles.....	10
1.2.9	Solid lipid nanoparticles (SLN) and nanostructured lipid carriers (NLC)...	11
1.3	Research objectives .....	13
<b>2</b>	<b>Materials.....</b>	<b>14</b>
2.1	Lipids and waxes .....	14
2.1.1	Glyceryl behenate .....	14
2.1.2	Hardfat .....	14
2.1.3	Medium chain triglycerides .....	14
2.1.4	Cera perliquida .....	15
2.2	Tensides .....	15
2.2.1	Poloxamer .....	15
2.2.2	Polysorbate.....	15
2.3	Water .....	16
2.4	Other ingredients .....	16
<b>3</b>	<b>Methods.....</b>	<b>17</b>
3.1	Preparation of lipid dispersions .....	17
3.2	Particle size determination .....	19
3.2.1	Photon correlation spectroscopy (PCS) .....	19
3.2.2	Laser diffraction (LD).....	19
3.3	Field-flow fractionation (FFF) .....	20
3.4	Nuclear magnetic resonance (NMR) spectroscopy of protons .....	20
3.5	Electron spin resonance (ESR) spectroscopy .....	20
3.5.1	In vitro determination of spin probe distribution.....	20
3.5.2	Ascorbic acid assay.....	21
3.5.3	Ex vivo measurements on human skin.....	21

3.6	Fluorescence spectroscopy.....	21
3.7	Raman spectroscopy .....	22
3.8	X-ray diffraction .....	22
3.8.1	By copper radiation .....	22
3.8.2	By synchrotron radiation.....	22
3.9	Differential scanning calorimetry (DSC).....	23
3.10	Densimetrie .....	23
3.11	Refractometry.....	24
3.12	Cryo transmission electron microscopy (Cryo-TEM) .....	24
<b>4</b>	<b>Results and discussion.....</b>	<b>25</b>
4.1	Particle size measurements by PCS and LD .....	25
4.2	Field-flow fractionation (FFF) .....	29
4.3	Nuclear magnetic resonance (NMR) spectroscopy of protons .....	32
4.4	Electron spin resonance (ESR) spectroscopy.....	37
4.4.1	In vitro determination of spin probe distribution .....	37
4.4.2	Ascorbic acid assay .....	41
4.4.3	Ex vivo measurements on human skin .....	42
4.5	Fluorescence spectroscopy.....	47
4.6	Raman spectroscopy .....	54
4.7	X-ray diffraction .....	56
4.7.1	By copper radiation .....	56
4.7.2	By means of synchrotron radiation.....	57
4.8	Differential scanning calorimetry (DSC).....	58
4.9	Densimetrie .....	60
4.10	Refractometry.....	60
4.11	Cryo transmission electron microscopy (Cryo-TEM) .....	62
<b>5</b>	<b>Summary and conclusions.....</b>	<b>66</b>
5.1	English version.....	66
5.2	German version.....	71
	<b>Bibliography.....</b>	<b>77</b>

## List of abbreviations

<sup>1</sup> H-NMR (spectroscopy)	nuclear magnetic resonance (spectroscopy) of protons
AA	ascorbic acid
CMC	critical micellar concentration
CMT	critical micellar temperature
CTFA	The Cosmetic, Toiletry and Fragrance Association, Inc.
DSC	differential scanning calorimetry
EAB	europäisches Arzneibuch (European pharmacopeia)
e.g.	exempli gratia (for example)
EPR	electron paramagnetic resonance
ESR	electron spin resonance
FFF	field-flow fractionation
GB	glyceryl behenate
GIT	gastrointestinal tract
HF	hardfat
HLB	hydrophile-lipophile balance
i.e.	id est (that means)
INCI	international cosmetic ingredients
K	Kelvin
LD	laser diffraction
MALS	multi-angle light scattering
MCT	medium chain triglycerides
MM	mixed micelle
NEmu	nanoemulsion
NMR	nuclear magnetic resonance
NLC	nanostructured lipid carriers
NR	Nile red
P3	2,2,3,5,5-pentamethyl-4-phenyl-imidazolidine-1-yloxy
PCS	photon correlation spectroscopy
PEG	polyoxyethylene glycol

PI	polydispersity index
PIDS	polarization intensity differential scattering
PMMA	poly(methyl methacrylate)
RMS	root mean square
SALATRIM	short- and long-chain acyl triglyceride molecules
SLN	solid lipid nanoparticles
TB	TEMPOL benzoate (4-hydroxy-TEMPO benzoate, 4-benzoyloxy-2,2,6,6-tetramethyl-piperidine-1-oxyl)
TEM	transmission electron microscopy
TMS	trimethylsilylpropionic acid sodium salt-2,2,3,3-D4
USP	United States pharmacopeia

# 1 Introduction

## 1.1 Need of colloidal drug carriers

High-throughput screening technologies in drug discovery present an efficient way to find new powerful substances. But in recent years it has become evident that the development of new drugs alone is not sufficient to ensure progress in drug therapy. Poor water solubility of drug molecules, insufficient bioavailability, fluctuating plasma levels or high food dependency are the main and common problems. Major efforts have been spent for the development of customized drug carriers to overcome the disappointing in vivo fates of the drug. For carriers non-toxicity (acute and chronic), sufficient drug loading capacity, possibility of drug targeting, controlled release characteristics, chemical and physical storage stability (for both drug and carrier) and feasibility of scaling up production with reasonable overall costs are requested [1-3]. Colloidal carriers have attracted the main interest because they are promising systems to fulfill the requirements mentioned above. But in the first place, nanosized carriers are treated as hopeful means to increase the solubility and therefore the bioavailability of poorly water-soluble active ingredients belonging to the classes II and IV in the biopharmaceutical classification system (BCS) [4-6].

The common characteristic of all colloidal carriers is the submicron particle size. Nanometric carriers might differ in materials, composition, drug loading and application spectrum (see chapter 1.2). Corresponding to the broad diversity of colloidal carriers, the possible administration routes vary. Dermal [7-9], peroral [10,11], parenteral [12], ocular [13] and pulmonary [14] applications are known for nanocarriers. As upper limit for intravenous administration to avoid embolism in blood vessels no particles above five micrometers and only few particles between one and five micrometers are accepted. Solid particular systems are limited to either the subcutaneous or intramuscular routes of administration, intravenous administration may result in vaso-occlusion [15].

Although biodistribution studies to organs were performed with radiolabeled carriers [16], little is known about the detailed fate of the carrier in vivo, especially concerning the uptake mechanisms, exchange processes with the physiological environment and degradation rates. Without particle modifying the phagocyte system recognizes circulating

colloidal particles in the blood as foreign material and captures them rapidly after intravenous administration [16]. While drug delivery keeps difficult to realize as long as carriers are rapidly phagocytized and drug molecules are accumulated in liver and spleen, nowadays first success was achieved for passive drug targeting to solid tumors. Tumor blood vessels present several abnormalities in comparison with normal physiological vessels. In an unspecific way, PEGylated (polyoxyethylene glycolated) particles penetrate the leaky endothelium and deliver drug inside the tumor [17-20]. These small hydrophilic carriers were found to have longer circulating half-lives in the blood than large and hydrophobic particles [21,22], due to their “water-like” aspect they are more or less invisible for the phagocytes. However, PEG-coated particles are passive systems because their modification in tissue distribution is basically a result of the difference in micro vascular permeability between healthy and altered tissue and of their long circulating properties. Active targeting has not yet been successfully established. Ideas rise up proposing new steps on the way to active targeting. E.g., polysaccharide-decoration of the surface of polymer nanoparticles should serve as anchor to cell surfaces of humans and/or bacteria and virus [23,24]. There, oligo- and polysaccharides are universally exposed and often they play a role in biologic activity which is hoped to get influenced by novel carriers.

Focusing on the biofate of lipid-containing drug carriers after peroral application, short-chain and medium-chain liquid lipids are known to be easily hydrolyzed and to be readily absorbed in the gastrointestinal tract (GIT) [25-27]. Crystalline lipids are poorly attacked by lipases and very long chains (from C<sub>18</sub> up) in solid state are poorly absorbed [28]. But not only the types of fatty acids in triglycerides, even their stereo specific distribution on triacylglyceryl structures influences the absorption fate [29]. To make use of caloric reduction to the half of conventional fats and oils, SALATRIM (short- and long-chain acyl triglyceride molecules) as fat substitute has been developed. These structured triacylglycerols are composed of at least one long-chain fatty acid (predominantly stearic) and at least one short-chain aliphatic acid (acetic, propionic, and/or butyric) [30,31].

Often penetration and uptake of entire colloidal particles in cell tissues is not probable to explain the in vivo effects of colloidal carriers [11]. More likely, due to the extremely increased surface area of nanoparticles compared to microparticles, e.g. improved drug solubility and therefore better bioavailability is given. A short calculation will demonstrate

the tremendous increase in surface area: If a substance of 1 cm<sup>3</sup> of volume is cut into small cubes of 10 μm in length, the obtained surface area will amount to 0.6 m<sup>2</sup>. Cutting the substance into cubes of only 100 nm in length, 60 m<sup>2</sup> of surface area can get in contact with the surrounding phase. Thereby, the extent of solubility of solid or liquid particles increases with their enlarging surface area (the logarithm calculated from the quotient of solubility of small and large particles correlates indirectly proportional to the particle radius [32]). Less compact particle shape may favor solubility additionally [32].

Nanosizing of a bulk material may also lead to dramatic changes of the physical properties of the substance, i.e. the depression of the melting point which results in the existence of supercooled melts [33]. In case of much decreased particle sizes the properties of the material are determined by the surface properties. Therefore colloids are not trivial systems. Furthermore, different colloidal structures might coexist.

Of course, nanometric systems have to fulfill the requests for safe drug delivery systems mentioned above. Most of all, precautions against aggregation, coalescence or Ostwald ripening [34] have to be attempted by optimized stabilization. Additionally, incorporation of sensitive drug molecules in some carrier matrices is claimed as protection against enzymatic degradation, hydrolysis or light [35-39]. That is remarkable, knowing the diffusion constant for solid materials at approximately 10<sup>-15</sup> cm<sup>2</sup>\*s<sup>-1</sup> at room temperature. According to the Einstein-Smoluchowski equation [40], within 14 h a molecule could be able to diffuse over a distance of 100 nm, what is diminished in amorphous materials to 50 s. Great attention should be paid to proposed storage stabilities of sensitive drugs in nanoparticles as far as contact to the particle surface and rapid degradation by the outer environment is rapidly possible [41]. Despite of their small size, colloidal carriers have to guarantee controlled drug release. Burst release [1,42,43] can be explained by this Einstein-Smoluchowski equation, too.

Chapter 1.2 is dedicated to several colloidal drug carriers. Entire physicochemical characterization and evaluation is not trivial because systems in the nanometric range do not offer the whole variety of investigative methods [44]. Remarkable efforts must be made to avoid artifacts due to invasive analyzing techniques [45] or only to avoid dilution which is required by many analytical methods. Special attention should be paid to other, competitive nanocompartments for the drug within a formulation [1], i.e. mixed micelles in a tenside-stabilized nanoparticle dispersion. Concerning the choice of a drug formulation,

it should be remembered that none delivery system per se meets all desired requirements for overall/general problem solution. Moreover, optimal formulations have to be chosen carefully for each drug, according to the features of the nanocarriers. The aim is to achieve desired drug release profiles in vivo by minimizing undesired side effects.

### 1.2 Overview of colloidal drug carrier systems

#### 1.2.1 Nanosuspensions

In a narrower sense, by the term “nanosuspensions” poorly water-soluble drug crystals in the nanometric range are described [46-51]. Nanosuspensions are saturated solutions. Therefore, they represent the simplest colloidal carriers with respect to composition. Their drug payload amounts to nearly 100 %. In an aqueous environment, the drug is pearl milled, precipitated or high pressure homogenized to a particle distribution mostly below one micrometer. Despite of the use of tensides, particle growth up to micrometric drug crystals may occur when the drug molecules of small particles dissolve in the outer environment and precipitate later on the surface of larger particles (Ostwald ripening). According to the Kelvin equation [52], the increased dissolution is an effect of strong particle curvature, so smaller particles are more affected than larger ones. Intravenous application of nanosuspensions stands for a risk [15].

Due to tremendous interface areas between drug and environment, solubilization velocity of the drug is increased according to the Noyes-Whitney equation [32,53]. Corresponding to the equation of Thomson-Gibbs-Freundlich, even the solubility of active substances may be increased in nanometric carriers. Attention has to be paid on drugs with small safety margins where burst release has to be avoided. But controlled release and reproducible blood levels are not easily achievable because as a release controlling barrier only the tenside layer may serve in these nanosuspensions. Suspensions of crystals in the micrometer range are already established in the market (i.e. Prednigalen<sup>TM</sup>). The only two registered nanosuspensions are Rapamune<sup>TM</sup> and Emend<sup>TM</sup> for immediate delivery.

Attention should be paid to the polymorphism of the drug, too. In contrast to the crystalline state, amorphous drug is solubilized fast. Sometimes, crystallization of the drug is retarded.

Due to the high surface-to volume ratio and due to the presence of emulsifiers supercooled melts with different physical properties are formed [54].

### 1.2.2 Liposomes

Liposomes [55-61] consist of one or more lipid bilayers of amphiphilic lipids (i.e. phospholipids, cholesterol, glycolipids). The lipophilic moiety of the bilayers is turned towards each other and creates an inner hydrophobic environment in the membrane. Lipophilic or amphiphilic drugs can be associated with the non-polar parts of lipid bilayers if they fit in size and geometry [55]. The hydrophilic molecular head groups face the outer water phase and the inner aqueous core of the vesicles. Water-soluble compounds can be included within the aqueous compartments.

Liposomes are classified as large multilamellar liposomes (MLV), large unilamellar vesicles (LUV), small unilamellar vesicles (SUV), oligolamellar large vesicles (OLV), and multivesicular vesicles (MVV), depending on their size, the number of bilayers and the existence of inner vesicles in a vesicle. The size of liposomes varies from 20 nm to few micrometers, with lipid membranes of approximately 5 nm [56].

Marketed products [62] are i.e. AmBisome<sup>TM</sup>, DaunoXome<sup>TM</sup>, and Pevaryl<sup>TM</sup>-Lipogel, indicating the parenteral and topical administration as main application routes for liposomes. Liposomes often suffer rapid degradation by the pH of the stomach, by intestinal enzymes and bile salts when they are given perorally. Further instability problems can arise during storage when the unsaturated fatty acids and the ester bindings of phospholipids are hydrolyzed and oxidized, respectively.

To overcome this last mentioned drawback, niosomes [56,63,64] were invented. Niosomes are non-ionic surfactant vesicles (NSV), resemble in their constitution to liposomes and consist of synthetic surface active molecules, i.e. alkyl polyoxyethylene ethers. Saturated hydrocarbon chains and intramolecular ether bindings increase the chemical stability of the niosomes. Whether niosomes are superior to liposomes in vivo is under investigation [63,65].

### 1.2.3 Mixed micelles

As long-chain phospholipids are known to form bilayers when dispersed in water (see chapter 1.2.2), the preferred phase of short-chain analogues is the micellar phase [66]. The

prediction of the arrangement keeps demanding, because it is related with chemical structure, temperature and water content [67,68]. In general, amphiphilic ionic, anionic or ampholytic molecules, which are able to decrease the surface tension of a solvent, arrange in micelles, as Tween<sup>TM</sup> or sodium dodecylsulfate above a certain critical concentration.

A micellar solution is a thermodynamically stable system formed spontaneously in water [69], and also in organic solvents. The latter is of less interest in pharmaceutical technology. Micelle formation can only occur above a certain solute concentration, the critical micellar concentration (CMC), and at solution temperatures above the critical micellar temperature (CMT). The small colloidal aggregates (micelles) are in rapid thermodynamic equilibrium with a measurable concentration of monomers. The size (mostly around 5 to 10 nm [70]) and shape of micelles depend ultimately on the chemical structure of the detergent. According to Small [69], spherical, rod-shaped, and discoidal micelles exist in water.

Micellar solutions exhibit solubilization phenomena. The micelle solubilizes host molecules (i.e. drugs) in any zone of the micelle volume, but the penetration into the micelle depends over all on the inner space of the micelle (as mentioned, diameter of entire micelle often below 10 nm), on the hydrophobicity of the drug and on the charge of the incorporated molecule [71,72]. The interaction between micelles and lipophilic drugs leads to the formation of mixed micelles (MM), often called swollen micelles, too. The addition of salt, alcohol etc. can vary the degree of penetration into the micelle (co-solubilization). In mixed micelles, the mobility of the micellar phase was found to be decreased due to incorporated molecules [73]. Considerably, swollen micelles are larger than the analogous “free micelles” because solubilization may result mostly from the increase in micellar size [74].

Micelles of common surfactants usually have relatively high CMC and are unstable upon strong dilution, e.g. in the blood volume. Toxic side effects of some tensides on human cells have to be considered beside bad taste of tensides in peroral liquids. Furthermore, investigations have to be focused on drug-tenside incompatibilities and on initial oversaturation [70] what would lead to later drug expulsion from the micelle. The kinetics of micelles are driven by both rapid micelle-monomer exchanges and by dissolution and new formation of micelles [75], but nevertheless the extent of water-amphiphile contact is discussed controversially [75,76]. Newer findings indicate an extensive contact between

water and methylene and methyl groups and an extreme disorder of the micelle interior. But simultaneously recent discovery excludes water penetration into the micelle although surfactants move constantly in and out of micelles [76].

Swollen micelles are fluid systems, but sufficiently stable to be used as delivery systems for stable drugs (i.e. Valium MM<sup>TM</sup>, Konakion MM<sup>TM</sup>) [77]. The hemolytic activity of bile salts is not longer present in MM, therefore they are parenterally applicable [78,79]. Latest developments for mixed micelles are presented in [80-83]. Nowadays, polymeric micelles [82,84] as pharmaceutical carriers with high solubilization capacity and rather low CMC value (to refer to arising monomer toxicity after dilution) are proposed.

### 1.2.4 Colloidal liquid crystalline structures

Liquid crystalline phases [53,70,85,86] share features from both liquids and crystalline substances. Due to their intermediate state they are named “mesophases”, too. On one hand, referring to crystals mesophases are viewed as defective crystals. Orientational order and periodicity are essential, common to all liquid crystalline states. For all liquid crystals, except cubic phases [87-89], anisometry is given. By the crystal-related phenomena they can be characterized by differential scanning calorimetry (DSC), X-ray diffraction and polarization microscopy, the latter in case of anisometry only. On the other hand, liquid crystals match partially self-organized melts in providing remarkable viscosity and diffusion characteristics.

Two liquid crystalline transitions have to be distinguished, the lyotropic and the thermotropic. Materials that form liquid crystals by addition of solvents are lyotropic liquid crystals, i.e. when in aqueous solutions the concentration of water-soluble amphiphiles is increased. The amphiphilic molecules must exhibit some chemical complexity, or otherwise the solvent will simply dissolve them [85]. Liquid crystals are typically organic molecules, ranging from small molecules, i.e. detergents, to polyelectrolytes, i.e. DNA, vegetable gums [85]. The formation of lyotropic mesophases is driven by the chemical structure of the organic molecule(s), the ratio of water to amphiphile(s), and the temperature. With decreasing concentration of water, firstly hexagonal (similar to many cylinder-like micelles) and then lamellar phases (similar to stacked bilayers, discoid) are formed. In case of very polar head groups of the molecules, together with high water binding capacities, cubic phases (“balls”) may be formed instead of hexagonal

arrangement. Drug of adequate distribution coefficient can be incorporated in between the fluid lamellar phase [53,90]. Cubosomes are submicron particles of bicontinuous cubic phases for lipophilic or amphiphilic active ingredient incorporation [91,92]. For these drugs, cubosomes have been proposed as a delivery system which may provide both a solubilization benefit (increased drug payload) and also a means for controlled or sustained release [93]. Elyzol<sup>TM</sup> as an in situ forming liquid crystalline dispersion is commercially available.

Beside the lyotropic mesophase a thermotropic transition exists. A chemically pure material does not show a clear melting point, but forms liquid crystals within a certain temperature range [85]. If the liquid crystalline state (i.e. of a drug) is maintained at lower temperatures as supercooled liquid crystals, pharmaceutical use seems to be interesting [94].

Liquid crystals as delivery systems should be able to improve the dissolution of poorly water-soluble drugs. Lyotropic liquids crystals incorporate relatively high drug amounts, but only few drugs themselves tend to build thermotropic mesophases. Disadvantageous is that the tenside concentrations are high and that colloidal dispersions of liquid crystals occur only in a thin range of parameters. Mesophases are thermodynamically stable and self-assembling, but they form reversibly the former basic micellar or molecular dispersed state by adding water.

### 1.2.5 Microemulsions

Microemulsions are optically isotropic, transparent or translucent, low-viscous, single-phasic and thermodynamically stable liquid solutions [95-98]. Critical solution is a term microemulsions are described with, reflecting their strong optical fluctuation and their solubilization capacity. As self-forming system the manufacture keeps simple. Microemulsions are bicontinuous systems that are essentially composed of water and oil, separated by surfactant and co-surfactant [34,70,95,99,100]. Microemulsions provide ultra-low interfacial tensions towards 0 mN/m despite of large oil-water interfacial areas. It is often very difficult to achieve the required interfacial area with the use of a single surfactant, hence a co-surfactant is essential.

The distinction between solubilized micellar systems (chapter 1.2.3) and microemulsions is not clear-cut since there is no well-defined transition point [101] between inverted

micelles, followed by microemulsions with comparable amounts of oil and water, and afterwards micelles if water is added continuously. Nevertheless, in this text microemulsions will be treated as bicontinuous structures only. The concept excludes aqueous surfactant solutions without added solubilizate, liquid-crystalline systems, and normal emulsions, too.

Their characterization can be done by electron microscopy and scattering methods (X-ray diffraction [102], static and dynamic light scattering) although microemulsions are unable to dilute (loss of microemulsion character in favor of micelles after dilution) and therefore size determination sometimes is difficult. Nonetheless, structures below 100 nm were often found [11,70].

Due to large interfacial areas microemulsions typically show much greater solubilizing capacities for both hydrophilic and lipophilic drugs than micellar solutions. A prominent example is Sandimmun Optoral<sup>TM</sup>/Neoral<sup>TM</sup> concentrate [11]. As reasons for better bioavailability above all the highly dispersed systems with good drug accessibility and secondary a better penetration into tissues are discussed [103].

Microemulsions are usually limited to dermal and peroral application because of their high surfactant concentration [70]. They exist in narrow regions of phase diagrams; therefore they are very restricted in tolerance to quantitative formulation changes.

### 1.2.6 Nanoemulsions

In contrast to microemulsions, emulsions are heterogeneous systems comprised of two immiscible liquids in which one liquid is dispersed as droplets in another liquid [34,104-108]. For the production [109,110] an energy input is necessary and the obtained liquid-in-liquid dispersion is thermodynamically unstable [111-115].

Oil-in water nanoemulsions present the most important parenteral drug carrier systems where lipophilic drugs are dissolved in the inner phase of the emulsion [104], i.e. Diazepam Lipuro<sup>TM</sup>, Disoprivan<sup>TM</sup>, Stesolid<sup>TM</sup> and Lipotalon<sup>TM</sup> [116,117]. Once drug-free introduced as parenteral nutrition, the ingredients of nanoemulsions are known to be physiologically well tolerable in human bodies. Degradation of the droplets containing lipophilic drug occurs very fast when administered intravenously, so retarded release is not realized [16]. After entering the blood circulation, fat emulsions would be treated as naturally-occurring fat and are therefore rapidly hydrolyzed by lipases. The phagocyte

system is only activated when certain lipids are recognized as foreign. Rapid degradation for oil droplets takes place in GIT, too, if given perorally. For topical use enhanced drug penetration is described [118].

With regard to the mobility of the oil a protection of sensitive drug molecules from hydrolysis is hindered. Moreover, sustained release and incorporation of hydrophilic components in conventional oil-in water is not realizable. Multiple emulsions (water-in oil-in water) are proposed to resolve these problems [119-121]. It has to be considered that these novel nanoemulsions again are fluid, unstable systems where the production is not easy to handle.

### 1.2.7 Nanocapsules

Oil containing nanocapsules differ from (oil-in water) nanoemulsions in providing a barrier made from polymers between the core and the surrounding environment, but as well nanoparticles with aqueous cores in an aqueous outer phase are published [122]. Suitable polymeric materials are listed in chapter 1.2.8. Often, for the preparation of nanocapsules the ways of solvent displacement [123,124] and interfacial polymerization [125] are applied.

According to the lipophilicity of the capsule content, hydrophilic and lipophilic drugs, respectively, can be dissolved [126]. Additionally, the polymeric particle surface may serve as compartment where hydrophilic drugs can be adsorbed [126]. Some encapsulated lipophilic drugs have already shown to be released in a controlled manner [127].

Encapsulation may decrease the toxicity of drugs after peroral or parenteral [2] application inasmuch as the exhibition to cells is diminished. Encapsulation saves sensitive drugs from rapid degradation. With the aim to reduce the interactions with reticuloendothelial system and to alter body distribution, the surface of nanocapsules was modified by certain materials such as surfactants (i.e. length and density of PEG chains) [128]. The complex biofate of nanocapsules is not entirely understood yet.

### 1.2.8 Polymer nanoparticles

Depending on the desired properties for polymer nanoparticles, polymers can be synthesized in a wide range of chain length, type and number. Polymers suitable for the preparation of nanoparticles include cellulose derivatives, poly(alkylcyanoacrylates),

poly(methylidene malonate), polyorthoesters, polyanhydrides and polyesters such as poly(lactid acid), poly(glycolic acid) and poly( $\epsilon$ -caprolactone) and their copolymers [2]. Obviously, toxicity of the substances, of radical starters or of solvent residues [37] has to be taken into calculation. Polymers used for parenteral delivery have to be biodegradable, they mostly belong to polyesters (i.e. polylactides) [129,130] or to the group of polyacrylates (i.e. polycyanoacrylates) [37,131]. For peroral administration, non-degradable polymers such as acrylate- and cellulose-derivatives can be used for nanoparticles designed not be absorbed [3,129]. In analogy to nanocapsules, attempts are done to modify the surface of the carriers. But again, little is known about the detailed in vivo fate of polymer nanoparticles [10,132].

For the production of polymer nanoparticles monomers can be built up to polymer particles or preformed polymers are reduced to nanoparticles. Various procedures are applied: the coacervation technique, the solvent evaporation [133] and solvent diffusion methods, the production by interfacial polymerization [37], the denaturation or desolvation of natural proteins or carbohydrates [37], and the degradation by high-shear forces (i.e. by high pressure homogenization [134] or by micro fluidization [135]). Often, particles based on polymers are reproducible to manufacture and some systems show remarkable storage stability [136]. Colloidal particles are either left as aqueous dispersion or they are converted into solid form, usually by lyophilization [129].

Nanoparticles serve as carriers for a broad variety of ingredients (i.e. conventional drugs, antigens, vaccines or enzymes). The active components may be either dissolved in the polymeric matrix or entrapped or adsorbed onto the particle surface. Depending on polymer, drug and polymer interaction and production procedure, drug release differs [137]. Polymer erosion, drug diffusion through the matrix or desorption from the surface may occur. Whereas polymeric microparticles entered the market (e.g. Enantone Depot<sup>TM</sup>), no polymeric nanocarrier is available yet.

### 1.2.9 Solid lipid nanoparticles (SLN) and nanostructured lipid carriers (NLC)

Melt-emulsified nanoparticles based on lipids (or waxes) solid at room temperature have been developed [138-142]. Advantages of these solid lipid nanoparticles (SLN) are the use of physiological well-tolerable lipids [143], the avoidance of organic solvents in some preparation processes, a wide potential application spectrum (dermal, peroral, intravenous)

and high pressure homogenization [144] as an established production method which allows large scale production. To manufacture SLN, the hot high pressure homogenization above the melting point of the lipid and subsequent recrystallization [145] is recommended (melt-emulsification), but the cold high pressure homogenization [146] (high pressure milling of lipid suspensions) for thermo labile drugs exists, too. Other production methods for SLN as the production from microemulsions [147], the precipitation [148-150] and dispersing by ultrasound [151,152] are published and differ normally in obtained particle size distribution. Noteworthy basic information concerning the structure of lipids [69,153-155] and the influence of stabilizers during production process [156-158] are provided in the literature. Additionally, for SLN improved bioavailability, protection of sensitive drug molecules from the environment (water, light) [36] and controlled release characteristics [139,141,159] have been claimed. Successful incorporation not only of lipophilic, but even of hydrophilic drug molecules has been postulated [160,161].

Common disadvantages of SLN include particle growth, particle aggregation, unpredictable gelation tendency, unexpected dynamics of polymorphic transitions, burst drug release and inherently low incorporation capacities due to the crystalline structure of the solid lipid [1,162,163]. It has been proposed that this last mentioned drawback can be overcome by oil loaded solid lipid nanoparticles (also described as nanostructured lipid carriers or NLC) [164,165]. Liquid lipids solubilize drugs to a much higher extent than solid lipids. In a preferred scenario, the liquid lipids form droplets within the solid lipid particles matrix. According to this model, the NLC nanoparticles would provide a high incorporation capacity (due to the liquid lipid) and control of drug release (due to the encapsulating solid lipid). It has been postulated that medium chain triglyceride (MCT) molecules can replace glyceryl behenate (GB) molecules in the crystal lattice in a random distribution up to a MCT load of 16 % (weight % of total lipid) [164,166]. Even higher oil loads up to 38 % have been described to be incorporated as MCT clusters inside the solid matrix. Thereby, the solid particles are described to be spherical [7,165,167,168] what should offer a maximal volume for oil and drug incorporation.

Despite of reinforced investigation efforts, until today neither SLN nor NLC are clinically used.

### 1.3 Research objectives

On the one hand, for SLN nearly 100 % incorporation rate, controlled release and protection from the outer environment were claimed. On the other hand, laws of nature i.e. restricted incorporation capacities for host molecules in crystalline matrices and very short diffusion times for drugs in colloidal carriers, lead to call the SLN testimonies into question.

To clarify the contradictions, the topic of the present thesis is the physicochemical characterization of lipid nanodispersions. The work is focused especially on SLN and NLC, but corresponding lipid systems as nanoemulsion or microemulsion have to be always under investigation, too, as far as comparisons of novel carriers to already established systems are important for final judgments.

By a physicochemical characterization detailed knowledge will be gained concerning the

- Drug localization in SLN
- Drug and oil localization in NLC
- Particle shape of SLN and NLC
- Accessibility of surrounding aqueous phase to the incorporated (model) drug, closely related to drug stability in the nanometric carriers
- Behavior of lipid nanodispersions on human skin (*ex vivo*).

The appropriate characterization of SLN and NLC is highly challenging due to their small particle sizes. Any particle separation from the aqueous environment or only dissolution with water could easily lead to misleading results due to particle aggregation and changed samples if stabilizers are removed from the particle surface. Therefore, non-invasive investigation techniques without the need of dilution have been applied whenever possible. Nuclear magnetic resonance ( $^1\text{H-NMR}$ ) and electron spin resonance spectroscopy (ESR), fluorescence spectroscopy, X-ray diffraction, measurements of refractive index and density, Raman spectroscopy were used beside invasive methods (transmission electron microscopy (TEM), field-flow fractionation (FFF), photon correlation spectroscopy (PCS) and laser diffraction (LD)). Moreover, the broad variety of techniques should help to minimize artifacts linked to many techniques. Combining the results gained by different methods, the data provide a more complete understanding of lipid nanodispersions.

## 2 Materials

### 2.1 Lipids and waxes

#### 2.1.1 Glyceryl behenate

Compritol 888 ATO (INCI: tribehenin, USP: glyceryl behenate, GB) is a mixture of approximately 15 % mono-, 50 % di- and 35 % triglycerides of behenic acid (C<sub>22</sub>) while other fatty acids than behenic acid account for less than 20 %. The melting point lies between 69 and 74 °C. It was a gift of Gattefossé (D-Weil am Rhein) where it is offered as product with lubricant and binding properties in tablets and capsules.

According to the lipid classification of Small [69], all mono-, di- and triglycerides belong to the group of polar lipids. Both di- and triglycerides are regarded to class I which stands for insoluble non-swelling amphiphiles. These non-swelling amphiphiles in water form a stable monolayer at the water-air interface as well as monoglycerides in water do. But monoglycerides additionally tend to form liquid crystals in water, they are grouped in class II (insoluble swelling amphiphiles). Monoglycerides provide already stabilizing capacities for water-insoluble components.

#### 2.1.2 Hardfat

Witepsol W25, donated by Condea (D-Witten), is a hardfat mixture (65-80 % tri-, 10-35 % di- and 1-5 % monoglycerides, fatty acid chain lengths 12-18, hydroxyl value between 20 and 30; HF) with a melting interval from 33.5 to 35.5 °C.

#### 2.1.3 Medium chain triglycerides

Miglyol 812 (DAC: oleum neutrale; CTFA: caprylic/capric triglyceride (caprylic acid: C<sub>8</sub>, capric acid: C<sub>10</sub>), medium chain triglycerides; MCT) is an at room temperature liquid lipid (oil) of low viscosity. Usually, fatty acid composition in MCT is dominated by C<sub>8</sub> fatty acids (50 to 65 %), followed by C<sub>10</sub> (30 to 45 %), C<sub>12</sub> (max. 5 %) and C<sub>6</sub> (max. 3 %) [169]. The oil is known to be faster biodegradable than lipids with longer fatty acid chains. Due to missing toxicity on skin and mucous membrane MCT found use as in dermal product

where it enhances permeation and spreading, as lubricant and drug solvent in peroral products, as solution enhancer in parenteral formulations [169]. MCT was purchased at Caelo (D-Hilden).

### 2.1.4 Cera perliquida

Cera perliquida is used for the preparation of the microemulsion (used as reference in chapter 4.4.3). It is a thin liquid wax consisting of iso-octyllaureate and iso-octylmyristate and was obtained from Pharma GmbH (D-Pößneck) by the name Onicetan 148<sup>TM</sup>. Cera perliquida shows good tolerance on skin [169].

## 2.2 Tensides

### 2.2.1 Poloxamer

Lutrol F 68 (poloxamer 188; a water-soluble non-ionic polyoxyethylene-polyoxypropylene polymer) was donated by BASF (D-Ludwigshafen). Its value in the HLB system (hydrophile-lipophile balance) amounts to 29. The stabilizer and solution enhancer does not cause toxic reactions after parenteral, dermal or peroral administration [169]. Moreover, the transition time of gut is not influenced in GIT of rats [169]. Tenside micelles are not likely to occur in the concentration range of poloxamer used in this study. Poloxamer 188 arranges only at higher concentrations and temperatures in form of micellar structures [68,170].

### 2.2.2 Polysorbate

Tween<sup>TM</sup> 80V Pharma is the trade name of polysorbate 80 (polyoxyethylene sorbitan fatty acid ester) and was a gift from Uniqema (B-Everberg). Its HLB value is 15. It was used for the microemulsion which was applied on human skin, where polysorbate does not provoke irritations [169].

### 2.3 Water

By means of double reverse osmosis (Milli-Q plus, Millipore, USA-Billerica) water corresponding to the monograph for highly purified water (EAB 4) was obtained. Immediately before the preparation of lipid dispersions the water was micro-organism-reduced by boiling for one minute.

### 2.4 Other ingredients

For  $^1\text{H-NMR}$  deuterized water, chloroform-D1 and Uvasol<sup>TM</sup> (tetramethylsilane) were obtained from Merck (D-Darmstadt). Trimethylsilylpropionic acid sodium salt-2,2,3,3-D4 (TMS) from Deutero (D-Kastellaun) with its sharp signal at 0 ppm served as a NMR reference.

For ESR lipophilic spin probes were used as model drugs: TEMPOL-benzoate (4-hydroxy-TEMPO-benzoate, 4-benzoyloxy-2,2,6,6-tetramethyl-piperidine-1-oxyl, TB; melting point: 99–101 °C, partition coefficient for octanol/water  $\gg 100$  [171]) was obtained from Aldrich Chemicals (USA-Milwaukee) and 2,2,3,5,5-pentamethyl-4-phenyl-imidazolidine-1-yloxy (P3; melting point: 45-46 °C) from Magnettech (D-Berlin). They are both crystalline paramagnetic nitroxyl radicals of strong red-orange color. Ascorbic acid (AA) reduces the ESR-active probes to ESR-silent hydroxylamines. AA sodium salt for the reduction assay was ordered from Fluka (D-Steinheim).

For spectrofluorometric studies Nile red (Nile blue A oxazone; 9-diethylamino-5H-benzo[ $\alpha$ ]phenoxazine-5-one; NR) was obtained from Sigma (USA-St. Louis). The intensively pink-colored dye exhibits a sharp melting point at 192/193 °C. The partition coefficients of NR in several organic solvents (e.g. chloroform, xylene) relative to water were found to be approximately 200 at 4 °C.

For the preparation of the microemulsion propylenglycol (1,2-propylenglycol) and dodecyl alcohol (n-dodecenal, lauryl alcohol) were needed. Both were provided by Merck (D-Darmstadt).

Human skin was obtained from the abdomen of a female person (32 years old) during a plastic surgery. Immediately after the fat layer was cut and the skin was cryo-conserved and stored at  $-22$  °C.

## 3 Methods

### 3.1 Preparation of lipid dispersions

Table 1 gives an overview of the prepared samples.

Usually, the total lipid concentration in our dispersions amounts to 10 % (w/w). For TEM measurements, the total lipid concentration was reduced to 1.5 %. To prepare solid lipid nanoparticles GB was melted in a water bath at 85 °C and HF at 65 °C, respectively. In general, it is recommended to destroy any crystal center of the bulk material by a long heating phase clearly over the melting point with the aim to avoid the lipid memory effect and to make new crystallization possible [172]. In the case of NLC, different fractions of the GB were replaced by MCT (2 %, 4 %, 10 %, 15 %, 20 %, 25 %, 30 %, 40 %, 50 % and 75 % (w/w) MCT, referred to the total lipid phase). For ESR measurements, in the hot lipid 1 mmol TB, referred to TB end concentration in the sample (corresponding 0.276 % (w/w<sub>lipids</sub>)), or 5 mmol P3, respectively (corresponding 1.167 % (w/w<sub>lipids</sub>)), were dissolved and for fluorescence spectroscopy 8.75 µg NR per 35 g sample (corresponding 0.00025 % (w/w<sub>lipids</sub>)).

The hot lipid phase was given to an aqueous solution of 2.5 % poloxamer 188 (0.5 % for TEM samples) of the same temperature and a dispersion was formed using a rotor-stator mixer (ultra turrax, IKA, D-Staufen) for 30 s at 8,000 rpm. The premix was passed three times through a Lab 40 high pressure homogenizer (APV Gaulin, D-Lübeck) [173] at 85 °C (65 °C for HF-sample) and 500 bar. The hot dispersions were filled in silanized glass vials and cooled to room temperature by placing them in a water bath at 22 °C.

The nanoemulsions (NEmu-0.2%, NEmu-0.4%, NEmu-1%, NEmu-2.5%, NEmu-5%, NEmu-7.5%, NEmu-10%) were prepared in exactly the same manner with MCT instead of GB as the lipid phase. Mixed dispersions (MIX) were prepared by mixing of separately prepared solid (SLN) and liquid (NEmu-10%) lipid nanodispersions. Through simple dispersion by means of an ultra turrax at 8,000 rpm for 30 s microparticles (Micro-GB and Micro-MCT) are obtained, according to the procedure for the above mentioned premix. If necessary, recrystallized melts made from MCT and GB bulk mixtures were prepared by simple heating up to 85 °C in a water bath under shaking, followed by a cooling step in water of 22 °C.

Table 1: Sample composition.

Sample	% lipid* (w/w)	% GB** (w/w)	% MCT (w/w)	% poloxamer* (w/w)	Production Procedure
SLN	10	10	0	2.5	Homogenization of hot dispersions composed of single lipid or mixture of lipids and aqueous poloxamer solution
NLC-0.2	10	9.8	0.2	2.5	
NLC-0.4	10	9.6	0.4	2.5	
NLC-1.0	10	9	1	2.5	
NLC-1.5	10	8.5	1.5	2.5	
NLC-2.0	10	8	2	2.5	
NLC-2.5	10	7.5	2.5	2.5	
NLC-3.0	10	7	3	2.5	
NLC-4.0	10	6	4	2.5	
NLC-5.0	10	5	5	2.5	
NLC-7.5	10	2.5	7.5	2.5	
NEmu-0.2%	0.2	0	0.2	2.5	
NEmu-0.4%	0.4	0	0.4	2.5	
NEmu-1%	1	0	1	2.5	
NEmu-2.5%	2.5	0	2.5	2.5	
NEmu-5%	5	0	5	2.5	
NEmu-7.5%	7.5	0	7.5	2.5	
NEmu-10%	10	0	10	2.5	
Mix-0.2	10	9.8	0.2	2.5	Separate preparation of SLN and MCT-nanoemulsion (NEmu-10%); followed by mixing of both dispersions in desired ratio
Mix-0.4	10	9.6	0.4	2.5	
Mix-1.0	10	9	1	2.5	
Mix-1.5	10	8.5	1.5	2.5	
Mix-2.0	10	8	2	2.5	
Mix-2.5	10	7.5	2.5	2.5	
Mix-3.0	10	7	3	2.5	
Mix-4.0	10	6	4	2.5	
Mix-5.0	10	5	5	2.5	
Mix-7.5	10	7.5	2.5	2.5	
Micro-GB	10	10	0	2.5	Preparation by ultra turrax
Micro-MCT	10	0	10	2.5	
Bulk mixture	100	98	2	0	Melting and recrystallizing of lipid bulk ware melt

\* for TEM measuring 1.5 % lipid and 0.5 % poloxamer

\*\* in case of HF-SLN use of hardfat instead of GB

The microemulsion was prepared by adding two components. Component I of the microemulsion consists of 34.5 % polysorbate 80, 44.8 % propylenglycol, 10.35 %

dodecanol and 10.35 % cera perliquida. Dissolution is given by lukewarm conditions. To component I (70 % (w/w)) component II (30 % (w/w)), water) was added under soft shaking.

All samples were stored at 22 °C, protected from light. The measurements described below were performed one day after sample preparation and within one month in case of TEM studies.

## **3.2 Particle size determination**

### **3.2.1 Photon correlation spectroscopy (PCS)**

As an estimate for the size of the lipid particles the intensity weighted mean diameter (often called effective diameter or z-average diameter) and the polydispersity index were determined by photon correlation spectroscopy (PCS; Zetasizer 4, Malvern Instruments, UK-Malvern; He-Ne-laser of 633 nm) at 25 °C under an angle of 90°. All samples were diluted with demineralized particle-free water to an adequate scattering intensity prior to the measurement.

Each dimensional information gained by PCS is expressed as median plus/minus range of three experiments, each performed in triplicate.

### **3.2.2 Laser diffraction (LD)**

Beside PCS, the dispersions were investigated by laser diffraction (LD; Coulter LS 230, USA-Miami; He-Ne-laser of 633 nm) after dilution with particle-free water. By its additional polarization intensity differential scattering (PIDS) technology this instrument is capable to measure particles down to 40 nm. For the calculation of PIDS data and for the evaluation with the Mie theory refraction has to be estimated for the particles. 1.456 as real and 0.01 as imaginary refractive index were assumed for the particles. The average particle size is expressed as the median volume diameter (50 % of the particle volume are below this value). LD 99 % values indicate the percentage of particle volume below a certain size.

Each dimensional information gained by LD is expressed as median plus/minus range of

three experiments, each performed in triplicate.

### **3.3 Field-flow fractionation (FFF)**

Symmetric FFF was performed in a FFF PMMA channel of 30 cm length and 350  $\mu\text{m}$  height, constructed with an trapezoidal spacer of maximal width of 25 mm at the inlet (Eclipse F, Wyatt Technology Europe, D-Woldert), lined with a membrane made from regenerated cellulose (cut off 10,000) at the bottom side. 20  $\mu\text{l}$  of water-diluted sample (1:100) were injected. Elution medium was particle-free water. The channel flow amounted to 1 ml/min. The cross flow was set to 3 ml/min and was stopped after 26 min.

The MALS detector (DAWN EOS, Wyatt Technology, USA-St. Barbara) was coupled online with the FFF channel and eluting fractions were analyzed according to the average mass weighted radius (RMS radius). The MALS detector is equipped with a He-Ne-laser of 690 nm and the scattered light is recorded with detector elements in eighteen different angles. The result is given in mean RMS radii. Errors are taken from ASTRA analysis report (Version 4.9.07).

### **3.4 Nuclear magnetic resonance (NMR) spectroscopy of protons**

$^1\text{H}$ -NMR spectra were recorded by an Avance DPX 400 spectrometer (Bruker, D-Rheinstätten), operating at 400 MHz and 20 °C. An aliquot of each aqueous nanodispersion was filled in a NMR-tube. Accurately weighted quantities of deuterized water (for all aqueous samples) or chloroform- $\text{D}_1$  (for measurement of MCT/GB bulk ware) were added for field lock and TMS was added as reference for 0 ppm.

### **3.5 Electron spin resonance (ESR) spectroscopy**

#### **3.5.1 In vitro determination of spin probe distribution**

An ESR (synonymously EPR, electron paramagnetic resonance) equipment of 1.5 GHz (L-band) from Magnettech (D-Berlin) was used. The measurements were done at room temperature. The following typical parameters were used: modulation frequency, 100 kHz; microwave power, 50 mW; modulation amplitude, 0.01 mT; time constant, 0.06 s; scan

time, 1 min; scan range, 10 mT. Localization of spin probe in different nanocompartments was determined on probe containing samples. Further information on distribution of TB in the samples were obtained by adding spin probe to probe-free dispersions and following ESR measurements.

Simulation of the ESR spectra was performed by means of the PEST-software from NIH, USA.

#### 3.5.2 Ascorbic acid assay

The used equipment and measurement conditions were the same as declared in chapter 3.5.1. The reduction kinetics of the spin probe in the samples were gained by time depending ESR measurements after mixing (1:1 (V/V)) with 1.6 mmolar aqueous solution of sodium ascorbate.

#### 3.5.3 Ex vivo measurements on human skin

Again, the equipment mentioned in chapter 3.5.1 was used. The measurements were done at room temperature. The following typical parameters were used: modulation frequency, 100 kHz; microwave power, 50 mW; modulation amplitude, 0.1 mT; time constant, 0.06 s; scan time, 3 min; scan range, 8 mT. In contrast to viable epidermis, enzymatic activity and enzymatic metabolism of cryo-conserved skin are decreased, but no differences in penetration and permeability are expected for cryo-conserved skin [174]. Three weeks after surgery experiments on the skin were carried out. Circular pieces of 2 cm in diameter were stamped out; rests of disinfectants (due to surgery) were dabbed away by water soaked wads of cotton wool and stuck on a glass plate by instant adhesive to avoid artificial wrinkles due to drying of the skin during the experiment. 10  $\mu$ l of formulation were applied on 1 cm<sup>2</sup> human skin and immediately the measurements were started non-invasively. During the experiments storage took place at 32 °C over a saturated solution of sodium chloride (corresponding approximately 40-44 % relative humidity of air).

### 3.6 Fluorescence spectroscopy

Emission fluorescence spectra were determined with a Perkin Elmer luminescence spectrometer LS 50 equipped with a 50 Hz xenon flash lamp and a concave grating

monochromator. Perkin Elmer names wavelength accuracy for  $\pm 1$  nm. The spectra were recorded at room temperature with both slit widths set at 4 nm. The excitation wavelength was fixed at 546 nm and the emission spectra were recorded from 550 to 700 nm with a scanning speed of 100 nm/min. Simulation of the fluorescence spectra was performed by means of the Origin software from OriginLab Corporation, USA.

### 3.7 Raman spectroscopy

Raman scattering at an angle of  $180^\circ$  relative to the incident beam was recorded by an Fourier transform Raman spectrometer RFS 100/S (Bruker, D-Karlsruhe). The excitation source was a diode-pumped Nd:YAG laser with an operating wavelength of 1064 nm. Spectra were acquired with 200 scans and a laser power of 350 mW at sample location. The interferograms were treated with the Black-Harris four term function and Fourier transformed to give spectra with a resolution of  $4\text{ cm}^{-1}$ .

The samples were placed in glass tubes (diameter 5 mm) and non-invasively analyzed at room temperature. Spectra processing was carried out using the Bruker OPUS software. Raman intensities were determined as integrated band intensities.

### 3.8 X-ray diffraction

#### 3.8.1 By copper radiation

Wide angle X-ray scattering (WAXS;  $2\theta = 4 - 40^\circ$ ) was done by a Philips X-ray generator PW 1830 (Philips, NL-Amelo), equipped with a copper anode (40 kV, 25 mA, wavelength 0.154178 nm) and a mobile counting tube (Goniometer PW 1820). Steps of 20 s per  $0.04^\circ$  were chosen, so the measurement time amounts to approximately four hours. Against loss of water, liquid samples were held in the carrier by a Mylar film. Its own narrow diffraction signal could be eliminated mathematically by subtraction of a blank.

#### 3.8.2 By synchrotron radiation

Hard X-rays with wavelengths in the range from 0.01 nm to 0.1 nm are available from synchrotron sources. They have penetration depths in matter in the order of several

centimeters as compared with those of conventional X-rays which are in the order of 10 to 100  $\mu\text{m}$ . Synchrotron radiation also has a very small angular divergence which is necessary to obtain well resolved diffraction diagrams of crystalline materials with lattice constants as studied in this investigation. The high penetration depth allows obtaining diffraction patterns of crystalline materials in an aqueous environment and even in a glass container. This makes this radiation an excellent tool for the investigation of materials as studied in this work.

We used the beam line BW5 at the storage ring DORIS in HASYLAB (Hamburger Synchrotron Laboratorium) at DESY (Deutsches Elektronen Synchrotron) in Hamburg. The diffractometer at this beam line is equipped with a two-dimensional, position sensitive detector (area detector) as described by Weislak et al. [175]. The detector is about 1 m behind the sample. The sample was exposed to the radiation in a conventionally used glass vial, at room temperature. As the used wavelength was about ten times smaller than the wavelength of a copper X-ray tube, the corresponding diffraction angles are in the order of  $< \sim 5^\circ$  so that the detector, in this distance, catches the complete diffraction diagram.

The synchrotron data obtained from the channel numbers of the detector had to be calibrated to the value of scattering vector. The value of scattering vector is the main parameter which characterizes the position of a diffraction peak. Furthermore, for the correct evaluation of reflection positions the non-linear background had to be subtracted. By use of the software PeakFit calculations were done.

#### **3.9 Differential scanning calorimetry (DSC)**

Differential scanning calorimetry (DSC) was performed by a Mettler DSC 821 (Mettler Toledo, D-Gießen). In 40  $\mu\text{l}$  aluminum pans accurately weighted dispersions (around 15 mg) were filled. Then, the pans were hermetically closed. DSC scans were recorded at a heating and cooling rate of 5 K/min, in comparison with an empty pan. It was made use of nitrogen as flush gas (80 ml/min). Melting points correspond to the maxima of the DSC curves.

#### **3.10 Densimetric**

Density was analyzed by an Anton Paar DMA 5000 (AU-Graz), an instrument based on the detection of density dependent shifts in the resonance frequency of a flexural resonator

filled with the undiluted sample liquid. Each formulation was measured three times at 25 °C. Each densimetric data point is expressed as median plus/minus range of three experiments.

#### **3.11 Refractometry**

Refractive indices were determined with a refractometer of Zeiss (D-Oberkochen). As light source an electric light bulb served. Other wavelengths except the wavelength of sodium vapor lamp (589 nm) are filtered. Measurements were done at 20 °C with the original undiluted nanodispersions and each data point was performed five times. The data are expressed as median plus/minus range of the five experiments

#### **3.12 Cryo transmission electron microscopy (Cryo-TEM)**

A drop of dispersion prepared for TEM measurements was placed on a bare copper grid and plunge frozen in liquid ethane at approximately 100 K. The sample was transferred into a cryoelectron microscope (CEM902a, Zeiss, D-Oberkochen, Philips CM120, NL-Eindhoven) operated at 80 kV respectively 120 kV. Samples were viewed under low-dose conditions at a constant temperature around 77-100 K. Images were acquired by a Dage SIT low intensity TV camera system and processed by a Kontron IBAS image processing system in the case of the Zeiss CEM902A and a Tietz Fastscan CCD camera system for the Philips CM120.

## 4 Results and discussion

### 4.1 Particle size measurements by PCS and LD

Particle size was determined by photon correlation spectroscopy (PCS), a dynamic particle size measurement technique [176,177]. Smaller isometric particles in a liquid diffuse faster than bigger ones, causing faster fluctuations in the intensity of scattered light, which is recorded in the experiment. PCS measures the diffusion coefficients of particles, and under the assumption of spherical particle shape autocorrelation analysis yields a mean particle diameter. Sedimentation of particles sets the upper size limit because for particles large enough to sedimentate (e.g. often microparticles), sedimentation is superimposed on diffusion. Weak intensities of scattered light and the required ability of fast data processing determine the lower size limit. Anisometric particles have smaller diffusion coefficients in comparison to spherical particles of the same volume and therefore their hydrodynamic diameter determined by PCS is larger. Information concerning the size homogeneity of the particles within the sample is provided by PCS in term of polydispersity index (PI).

As a further technique to obtain information on the particle size laser diffraction (LD) was employed. Diffraction patterns of particles are recorded. According to the Mie theory, the particle radius is calculated from the diffraction angle, the optical properties of the particle and the suspension medium. Larger particles scatter light at smaller angles. Mie theory provides a complete solution of the scattering problem for spherical particles. For non-spherical particles the theory yields the equivalent sphere diameter. LD was mainly used in this study to prove the absence of microparticles what can not clearly be evaluated by PCS.

The particle sizes obtained by static (LD, PIDS included) and dynamic light scattering (PCS) methods are in the same range but the LD median diameters are always smaller than the diameters obtained by PCS (table 2). Usually, differences in the results of two methods are not unexpected when they rely on different measurement principles. In this context, the differences can be elucidated. Particle sizes obtained by LD are always a bit smaller than those of PCS (and FFF), because the latter determine the hydrodynamic radii which are larger than the real radii of the spheres. Furthermore, intensity-weighted particle distribution (PCS) result always in larger particle sizes than volume-weighted distributions (LD) because larger particles provoke higher intensities in the particle analysis and no strong linearity is given

#### 4 Results and discussion

Table 2: Dependence of particle size on the oil load of the dispersions, determined by LD and PCS, expressed as median  $x$  ( $x_{\min}$ ;  $x_{\max}$ ).

<b>Sample</b>	<b>LD: 50 % (V) of all particles smaller than [nm]</b>	<b>LD: 99 % (V) of all particles smaller than [nm]</b>	<b>PCS: Average par- ticle size [nm]</b>	<b>PCS: Polydispersity index (PI) [ ]</b>
SLN	163 (140;216)	614 (591;711)	250 (215;287)	0.334 (0.290;0.381)
NLC-0.2	181 (133;209)	618 (509;652)	274 (206;301)	0.332 (0.252;0.370)
NLC-0.4	162 (114;185)	575 (528;607)	271 (218;305)	0.292 (0.243;0.331)
NLC-1.0	173 (148;205)	572 (532;634)	276 (241;338)	0.209 (0.180;0.225)
NLC-1.5	155 (112;202)	519 (493;576)	260 (249;325)	0.177 (0.153;0.226)
NLC-2.0	142 (121;149)	538 (482;568)	266 (238;310)	0.165 (0.149;0.181)
NLC-2.5	139 (102;173)	568 (480;550)	262 (238;311)	0.162 (0.126;0.191)
NLC-3.0	125 (114;170)	586 (447;518)	242 (241;295)	0.159 (0.104;0.181)
NLC-4.0	166 (133;190)	550 (489;575)	216 (210;281)	0.155 (0.107;0.181)
NLC-5.0	168 (145;200)	544 (515;562)	217 (212;244)	0.171 (0.128;0.189)
NLC-7.5	175 (120;214)	585 (558;610)	211 (200;276)	0.184 (0.130;0.192)
NEmu-10%	139 (128;144)	571 (508;593)	178 (170;185)	0.143 (0.120;0.150)
Mix-0.2	193 (127;227)	598 (509;659)	277 (224;281)	0.362 (0.313;0.379)
Mix-0.4	176 (137;215)	595 (511;647)	266 (222;270)	0.334 (0.307;0.370)
Mix-1.0	165 (125;192)	600 (552;672)	269 (218;272)	0.350 (0.299;0.390)
Mix-1.5	184 (133;228)	604 (587;624)	246 (220;268)	0.337 (0.318;0.354)
Mix-2.0	162 (144;187)	596 (560;607)	235 (216;288)	0.331 (0.322;0.345)
Mix-2.5	154 (128;188)	554 (536;649)	225 (207;262)	0.307 (0.257;0.331)
Mix-3.0	154 (132;192)	558 (542;574)	222 (210;247)	0.275 (0.265;0.292)
Mix-4.0	159 (135;202)	579 (550;601)	235 (199;269)	0.318 (0.258;0.325)
Mix-5.0	153 (105;187)	578 (514;640)	208 (185;219)	0.224 (0.200;0.236)
Mix-7.5	149 (106;180)	566 (518;579)	199 (172;211)	0.209 (0.193;0.228)
Micro-GB	15,830	43,310	2,404*	1.000*
Micro-MCT	19,320	32,390	8,177*	0.634*
Wi-SLN**	112	375	181	0.165

\* PCS is not a suitable method for particles in the micrometer range.

\*\* The data of a nanoemulsion are captured (measurements done at room temperature).

between intensity and particle size.

As all measurements are done at room temperature, colloidal dispersions made from HF are not crystallized at room temperature (no melting event in DSC recordable) and represent supercooled melts, therefore the particle sizes of an emulsion are captured.

Owing to increased homogenization efficiency, however, the samples used for TEM in this study showed PCS and LD particle sizes in general 50 to 60 nm below the sizes of conventionally high concentrated SLN and NLC, maintaining the same PI values.

The presence of considerable amounts of micrometer particles can be excluded for all samples under investigation from the LD results (apart from the microparticles, of course). LD indicated that more than 99 % (V) of the particles were smaller than 620 nm in all cases.

Comparing the SLN, NLC and NEmu formulations there is no clear correlation between LD particle size and oil load. And again, in PCS, only a trend towards smaller particle size with increasing oil content of the dispersions seems to be given, but has to be carefully discussed against the background of wide data ranges and high PIs. The PCS method is not sensitive enough to characterize clearly differences in these demanding, similarly composed samples. But the differences found by PCS between SLN and NEmu-10% are reliable. They are correlated to differences in particle shape – if a comparable particle volume for both can be assumed.

As the viscosity of MCT and melted GB at temperatures above 70 °C is similar [178], differences in homogenization efficiency as a result of different viscosities can be excluded as a cause for different size phenomena. Directly after hot high pressure homogenization all lipids should form droplets of similar size. The subsequent crystallization should, however, influence the shape of the nanoparticles.

Anisometric particles have smaller diffusion coefficients than spherical particles of the same volume [179-181] and - since slower Brownian motion is correlated to apparently larger sphere sizes - their hydrodynamic diameter is larger. Assuming similar particle volumes after homogenization, the faster diffusion (and thus apparently smaller size) of NEmu-10% droplets compared to SLN indicates an anisometric shape of SLN. By inversion of an argument, the larger sizes of SLN should reflect their anisometric shape.

Only if oil loading amounts to 40 % (NLC-4.0) the particle size approaches the size of the nanoemulsion. The particle character seems to turn more and more towards the spherical shape of the oil droplets (see results of TEM measurements in chapter 4.11).

The reflection of differences in particle shape in PCS results has already been reported previously for triglyceride nanoparticles in the solid and liquid state, respectively [181-183]. For GB nanoparticles, a direct comparison of the PCS particle size in the solid and liquid state was not possible since, in contrast to triglyceride nanoparticles, they cannot be maintained in the liquid state at temperatures much below their melting point.

The droplets of the nanoemulsion have a much smaller polydispersity index (as a characteristic parameter for the width of the particle size distribution) than all of the GB-containing dispersions. For anisometric particles - but presumably comparable in volume - a more non-monodisperse autocorrelation has to underlie for the measured data. The PI describes the deviation of the measured autocorrelation function from that of a dispersion of monodisperse spheres with the same diameter. Summarizing, the width of the particle size distribution as reflected by the PI is strongly driven by the anisometry of particles. Comparatively high PI values of SLN and NLC could support the idea of non-spherical platelets, if presupposing that mainly the viscosity of lipids during emulsification drives the particle sizes of the final formulations.

For the dispersions from the MIX series (made from physical mixtures of NEmu-10% and SLN) there is a trend towards decreasing particle size and increasing homogeneity with increasing oil load in all particle size measurement results. The mixing ratio determines size and PI data. The higher the amount of NEmu-10% the more the particles resemble pure NEmu-10% in all PCS and LD 50 % data while LD 99 % as indicator for maximal size always shows the presence of SLN despite of high NEmu-10% admixture.

Comparing the MIX series with NLC different PI data are determined whereas differences in particle sizes are small. Despite the same sample composition more homogeneous particle distributions (smaller PI values) are characteristic for NLC, especially in case of high MCT loading. This result indicates that co-processed MCT and GB form the mixed NLC particles after lipid crystallization whereas in MIX samples they remain as separate MCT and GB particles, respectively, after mixing.

Real or potential influences on the particle sizing results should be considered. LD data are valuable, but uncertainty remains on the optical properties of the particles needed for PIDS measurements; these particle parameters are not easy to obtain. No influence should be present in the investigated samples due to surfactant micelles which “disturb” as competitive nanocompartments because poloxamer 188 is known to arrange in micellar structures only at

higher concentrations and temperatures [68,170]. But the high dilution of the samples in water required for both LD and PCS measurements may result in surfactant diffusion from the particle surface. A lack of stabilizing surfactant may cause the particles to aggregate. Particle sizes and polydispersity index should thus not be taken as absolute.

Attempts to characterize dispersions of solid lipid nanoparticles without any dilution by a HPPS-ET (High performance particle sizer, Malvern Instruments, UK-Malvern) yielded interesting additional data. While the results for latex particles differed only by 30 nm when measured with/without dilution, e.g. for SLN 198 nm in diluted samples (1:100, with water) and 735 nm in undiluted samples were found. Dilution did also affect the measured particle size of the nanoemulsion, but to a smaller extent (undiluted: 267 nm; diluted: 156 nm). The PCS method bases on particle diffusion. If free diffusion is hindered due to high concentration of the dispersions, a shorter diffusion length will result. As a result, the PCS algorithm translates this into a higher particle size. The restriction is larger for anisometric particles. One hundred-fold dilution leads to a low particle concentration in which particles are able to diffuse independently. Moreover, our findings support the superposed SLN arrangements which are already described in the literature [184].

Particle sizes remained unchanged over a period of at least four weeks. During long-term storage for more than one month sometimes unpredictable gelation occurred in solid lipid containing samples. Gels are more structured than liquids. Again, SLN are able to organize themselves in superstructures.

### **4.2 Field-flow fractionation (FFF)**

Field-flow fractionation (FFF) separates particles due to their Stokes radius [185,186]. The Stokes radius drives their diffusion coefficient (in analogy to PCS). In the FFF-technique particles are placed in a parabolic flow profile such that smaller particles are transported faster and eluted earlier. This is achieved by applying a force field perpendicular to the transport direction [187]. Injecting particles of equal volume and different shape, the isometric particles will be eluted earlier than the asymmetric particles.

Looking more into detail, FFF forces all particles to suffer the same cross flow and to move in direction to the accumulation wall with the same velocity. According to the individual diffusion behavior of a particle, it will be relocalized and after various equilibria (between cross flow and diffusion forces) eluted from the channel. This retention time is indirectly

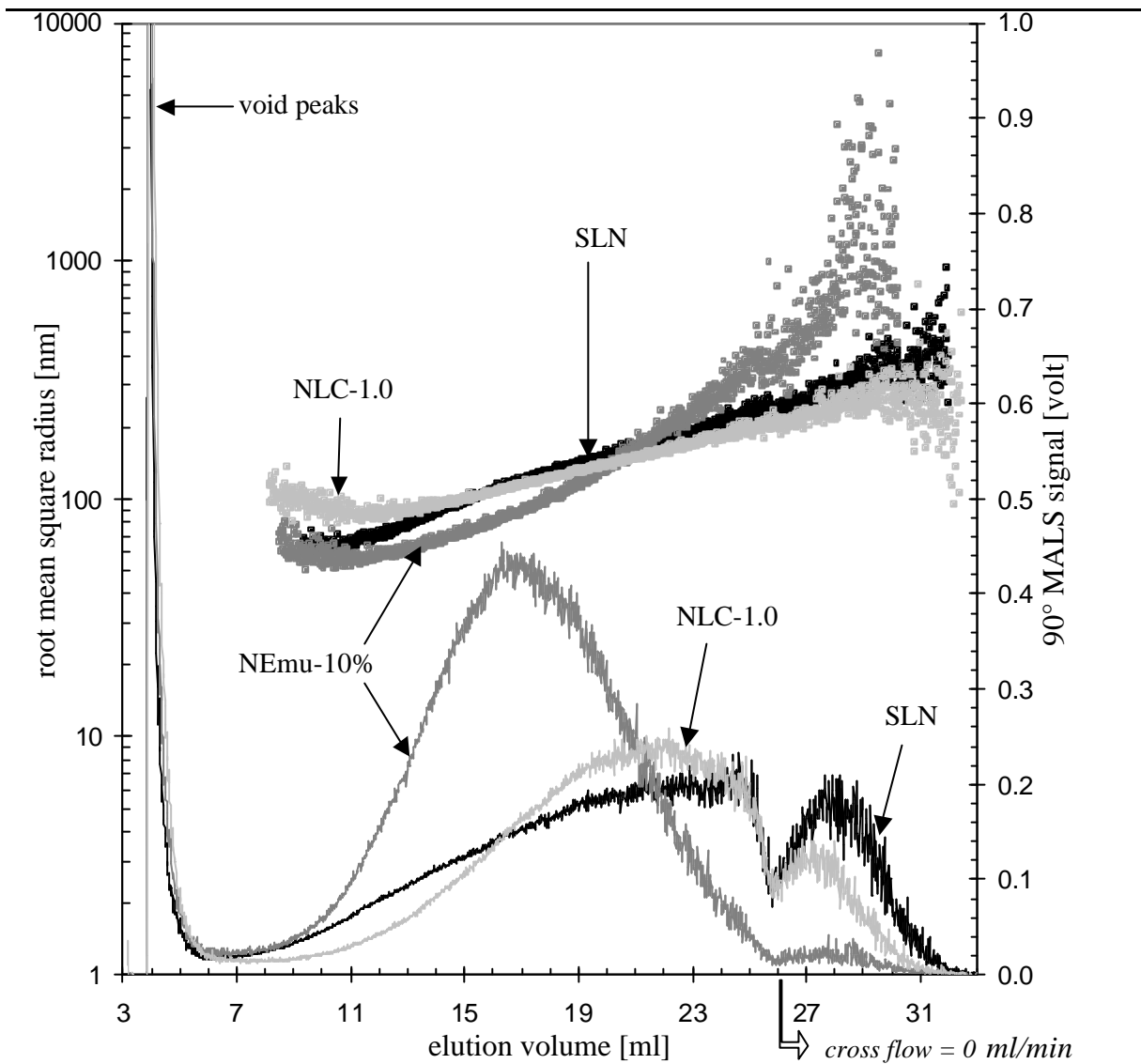
proportional to the diffusion coefficient.

All eluted fractions were continuously analyzed by multi-angle light scattering (MALS) where a photometer records the scattering signals of the particles and where the result is given in average size-weighted radius (RMS (root mean square) radius) [180]. MALS allows to measure particle radii from 10 nm up to approximately one micrometer. MALS works parameter-free, i.e. knowledge of particle shape or refraction index is not needed.

Figure 1 provides information about the laser light intensity arising from the samples SLN, NLC-1.0 and NEmu-10% after elution from the FFF channel. Sample NEmu-10% is eluted earlier and the RMS radius is smaller compared to the other two samples at the same retention time below 19 ml. This is an indication of smaller particles (as seen by PCS, e.g.) and different shape. For spheres the RMS radius is expected to be smaller compared to an anisotropic shaped particle of the same volume. Because of their compact shape the droplets of NEmu-10% are less retarded than the particles of the solid dispersions.

When the cross flow was stopped after 26 min solid particles are still localized in the channel and start to move out whereas the elution of the droplets is nearly completed at this time. The SLN and NLC are anisometric with higher hydrodynamic radius. Until this time, due to the cross flow especially platelets with lower diffusion coefficients were held more effectively in the channel than the nanodroplets. The equilibrium between diffusion and retardation is shifted in favor of retardation. The MCT load on NLC-1.0 seems to lead to slightly less irregular particles compared to SLN but NLC-samples with oil loads different from NLC-1.0 should be investigated by FFF before this fact can be stated clearly.

The particle size data plotted in the upper part of figure 1 and evaluated in the table below are in good correlation to the values found by PCS for NLC and SLN (table 2). The measuring principle of both FFF and PCS bases on particle diffusion. The high MALS value for NEmu-10%, especially detectable in the second part of the run, is remarkable. Even few particles in the upper nanometer range or even in the micrometer range increase the LS diameter drastically. This phenomenon is probably an artifact due to coalescence of MCT droplets. Coalescence may occur due to focusing of the sample at the channel inlet and due to particle-particle interactions on the membrane, respectively. Washing off the poloxamer molecules from the particle surface by the elution medium may facilitate droplet growth. SLN and NLC suffer the same conditions, but they are solid and maintain their particulate character.



Formulation	Z-average radius [nm] (elution by FFF and subsequent LS measurements of elutes gained in between 8th and 26th minute)	Z-average radius [nm] (elution by FFF and subsequent LS measurements of elutes gained in between 8th and 32nd minute)
SLN	185 +/- 4	300 +/- 9
NLC-1.0	160 +/- 3	198 +/- 5
NEmu-10%	273 +/- 9	723 +/- 18

Fig. 1: Elution behavior of lipid nanodispersions in cross flow FFF, subsequently detected by MALS (top curves: RMS radii; bottom curves: intensities of scattered light). Table at the bottom: z-average particle sizes of the nanodispersions obtained from the upper graphic.

In FFF analysis, the width of the particle size distribution is reflected in milliliters of elution volume in which particles can be detected. The results confirm the increased polydispersity observed by PCS for SLN and NLC-1.0 (table 2). Of course, retardation favors peak broadening additionally, but particle size distribution should be mirrored well by the elution volume.

### 4.3 Nuclear magnetic resonance (NMR) spectroscopy of protons

$^1\text{H}$ -NMR spectra of the colloidal GB nanosuspension (formulation SLN) and the nanoemulsion made from MCT (formulation NEmu-10%) are shown in figure 2. In the SLN sample only poloxamer derived, but no GB related signals are observed. This finding indicates that the nanoparticles have crystallized. The presence of supercooled melts, which have been observed by NMR for other “SLN”-samples [163,182] and which may exist even twenty and more Kelvin below the melting temperature of the lipid bulk phase [188] can therefore be excluded.

In order to facilitate the assignment of the peaks to the ingredients in the complex colloidal mixtures, NMR spectra of aqueous poloxamer solution, of poloxamer-free homogenized MCT-water mixtures and of GB-water mixtures were recorded (figure 3). Despite the absence of poloxamer, both lipid dispersions showed a remarkable short term stability (LD 99 % < 3 microns after 1 day), which permitted the NMR measurements. The absence of  $-\text{CH}_2-$  and  $-\text{CH}_3$  NMR signals in GB-water mixture was expected, because solid ingredients are not detected under the experimental conditions due to very short relaxation times. The ppm-values of the MCT methyl and methylene protons ( $-\text{CH}_3$ : 0.9 and  $-\text{CH}_2-$ : 1.3) are typical for alkyl chains of triglycerides. Protons located near or at the glycerol part of the lipid have higher ppm values. The ppm values for methyl and methylene groups of poloxamer can easily be distinguished from MCT signals, because they are shifted to higher values ( $-\text{CH}_3$ : 1.2 and  $-\text{CH}_2-$ : 3.7) due to the presence of oxygen in the polymer backbone. The assignment of the NMR signals of MCT and poloxamer are in agreement with the literature (e.g. NMR databases and [189]).

The samples NEmu-0.2, NEmu-0.4 and NEmu-1.0 are pure nanoemulsions with very low oil load (0.2, 0.4 and 1 % (w/w) MCT and 2.5 % poloxamer). NMR spectra were recorded without any sensitivity problem, which demonstrates that even such little oil amounts are

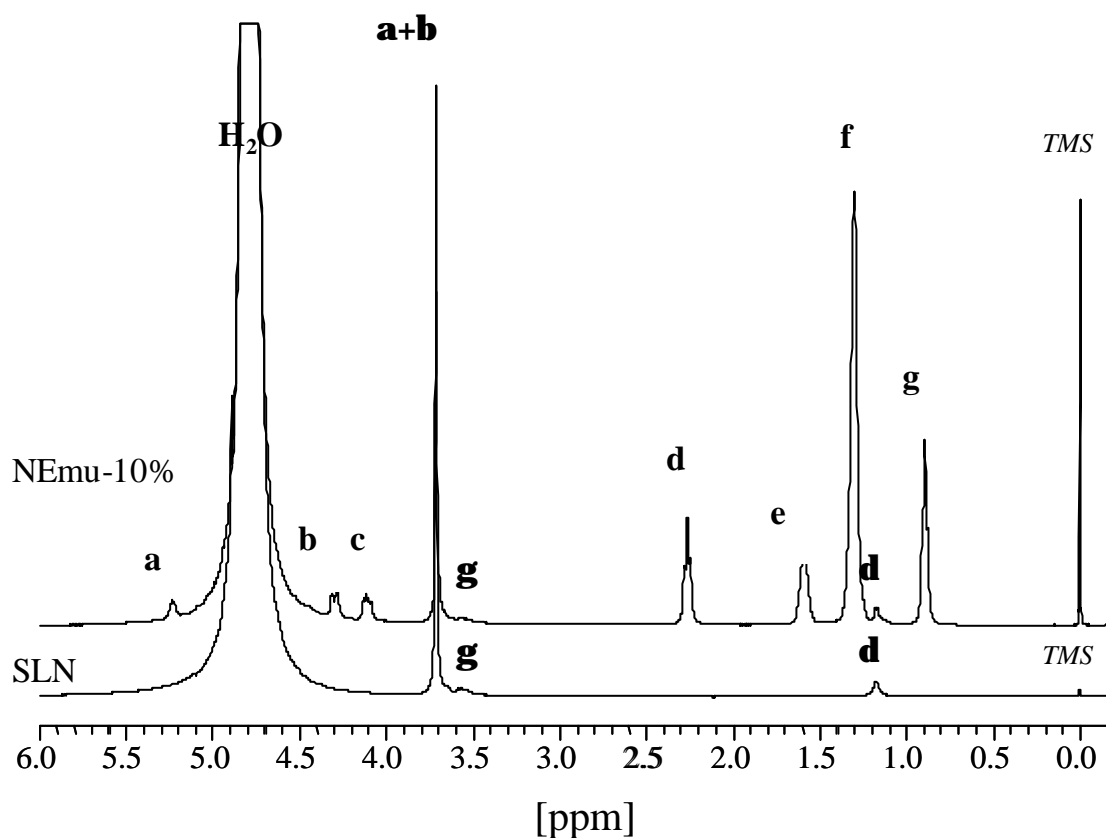
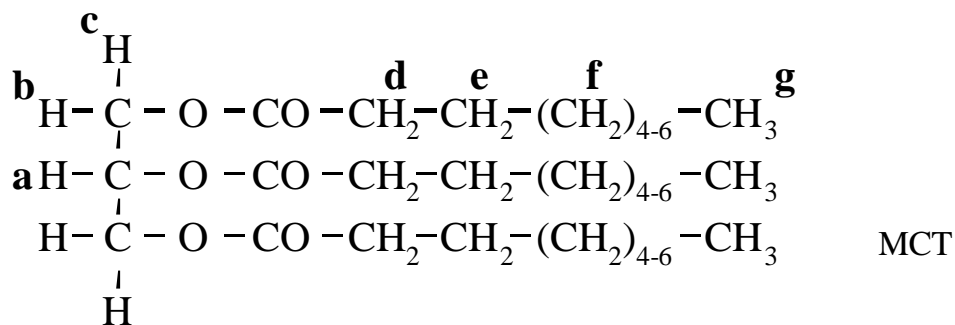
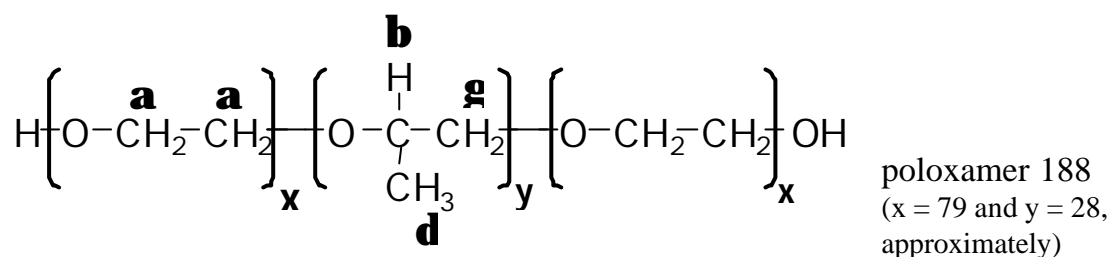


Fig. 2: <sup>1</sup>H-NMR spectra of the SLN formulation made from GB (below) and of the MCT nanoemulsion (above). All signals are signed corresponding to the positions of the protons in the chemical formula above.

detectable by means of NMR (spectra not shown). It was surprisingly found that the line widths of the MCT methylene protons in nanoemulsions are slightly smaller than those of MCT bulk, because broader lines due to restricted mobility of MCT molecules on the nanodroplet interface and line broadening caused by phase boundaries could be expected. Different viscosities could be one possible explanation. MCT formulated as nanodroplets experiences lower viscosity of the surrounding outer phase (viscosity of water: 1 mPa\*s) whereas MCT bulk is more viscous (30 mPa\*s). Moreover, for methylene protons of the bulk a very slightly more asymmetric signal was detected. Traces of water in the bulk could structure the oil and broaden the signal due to superposition of different species. Additionally, phase boundaries with different magnetic susceptibilities might increase the NMR line width due to the introduction of local non-homogeneities of the magnetic field.

The NMR spectra of NLC and MIX samples are quite different, although the chemical composition is the same and the sizes of the colloidal particles are comparable (figure 4). The MCT alkyl signals in NLC samples have much lower signal amplitudes due to broader lines, especially at lower oil loads. In contrast, alkyl signals of the MIX samples are comparable to pure nanoemulsions and the line width is equal for all MCT loads. The reason for increasing line widths and decreasing maximum amplitudes in the NLC samples is due to strong interaction of the oil molecules with solid GB what leads to an increased immobilization of the MCT molecules. Their relaxation is faster than that of unbound oil in the mixtures [190,191]. Furthermore, the increase in line widths was more pronounced for the methyl end group of the lipid chain. The oil should be adhered on the solid lipid surface mainly by molecular affinities between lipophilic groups.

Previously described chemical shifts [166] of the fatty acids in GB-MCT systems can not be confirmed. The chemical environment of the oil molecules does not differ in particles with either high or low oil load. In this way, it can not be assumed that for low oil supplementation the oil molecules are surrounded by a matrix of solid GB, just as little higher oil loads form clusters inside the particle. Most probable is the localization of the oil at the particle surface between solid glyceride and tenside layer [192,193]. The extent of immobilization of the alkyl signals can be quantified by means of the widths at half height of the signal amplitude (table 3).

Attempts to quantify the immobilization of the MCT protons by adding the signal amplitude of the internal standard trimethylsilylpropionic acid sodium salt-D4 (TMS, signal at 0 ppm)

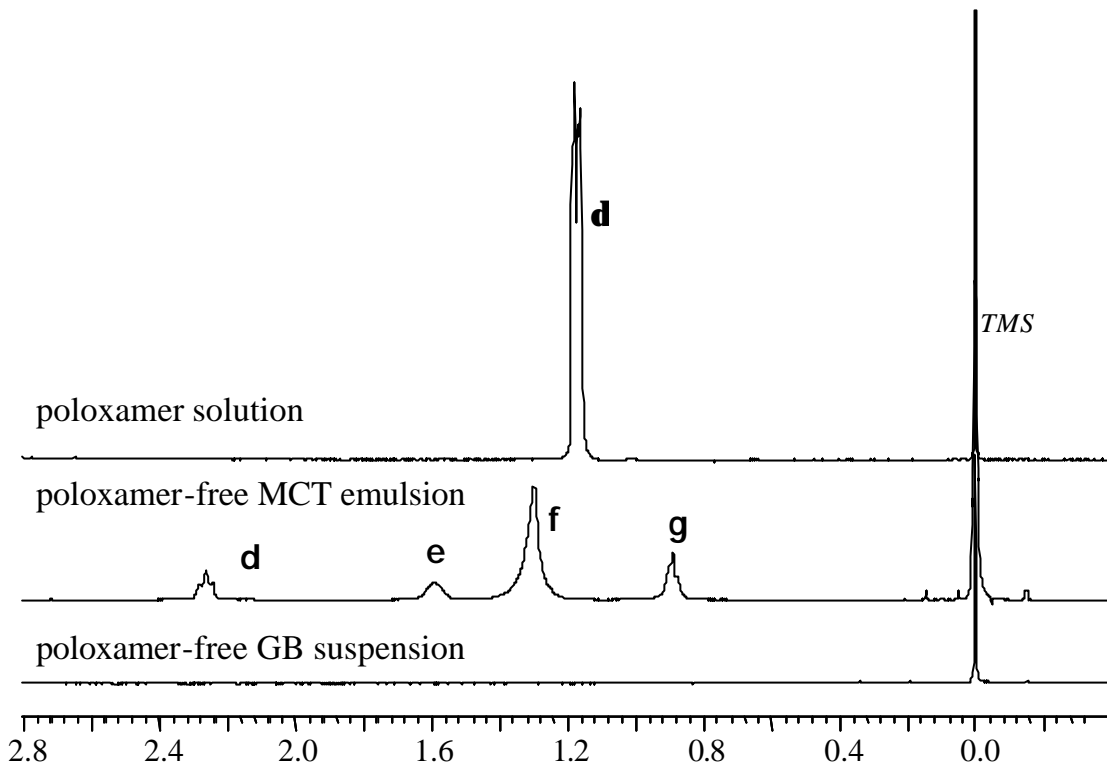


Fig. 3: <sup>1</sup>H-NMR spectra of a non-stabilized GB dispersion, of a non-stabilized MCT emulsion and of an aqueous poloxamer solution (from the bottom to the top).

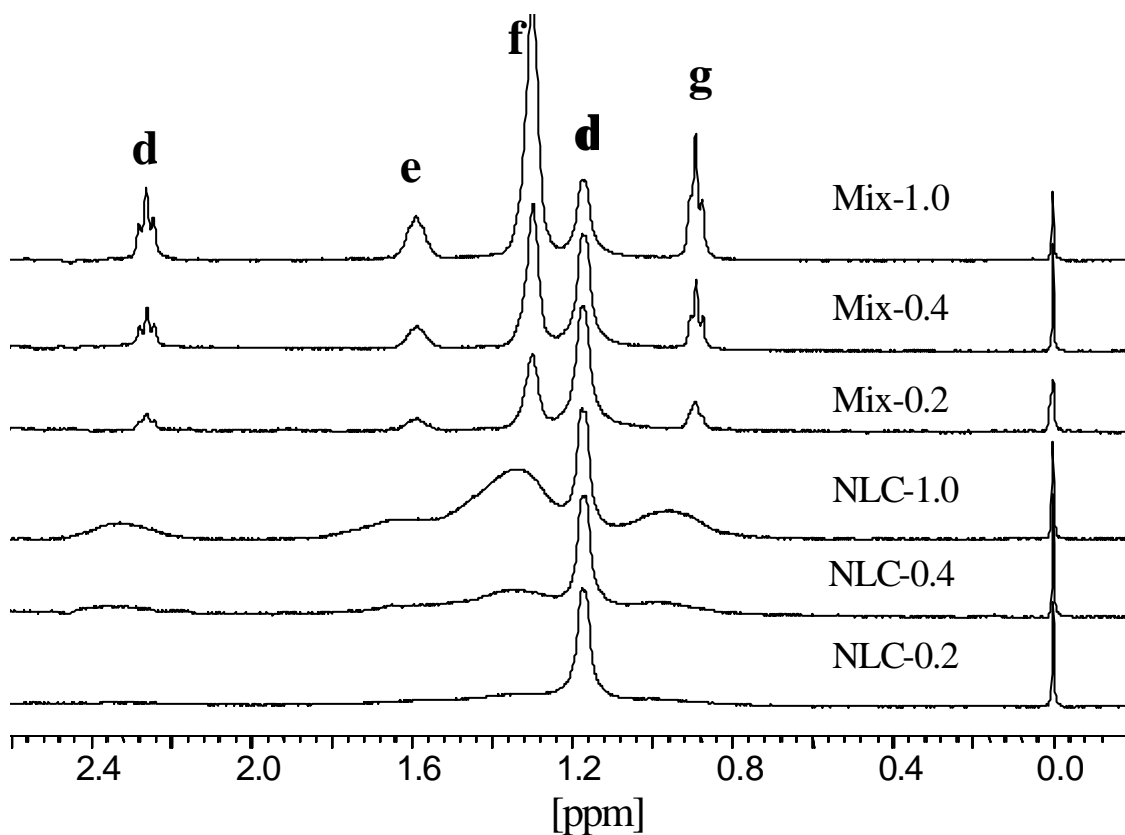


Fig. 4: <sup>1</sup>H-NMR spectra of hybrid lipid nanoparticles (formulations NLC-0.2, NLC-0.4, NLC-1.0), and mixtures from GB-SLN and MCT nanoemulsions (Mix-0.2, Mix-0.4, Mix-1.0) (from the bottom to the top).

Table 3: Increased widths at half height of  $^1\text{H}$ -NMR signals as a feature of immobilized chemical groups.

Formulation	NMR-line width at half amplitude [Hz]		
	LIPID-Protons		POLOX-AMER
	“f”-signal 1.3 ppm	“g”-signal 0.9 ppm	“d”-signal 1.15 ppm
SLN	-	-	3.9
NLC-0.2	approx. 96	approx. 21	3.9
NLC-0.4	96.0	20.2	3.8
NLC-1.0	89.6	18.6	3.6
NEmu-10%	15.2	3.5	3.5
NEmu-0.2%	13.2	1.1	2.9
NEmu-0.4%	13.2	1.1	2.9
NEmu-1.0%	13.2	1.1	3.0
Mix-0.2	14.8	2.8	4.0
Mix-0.4	13.6	1.2	3.7
Mix-1.0	14.0	1.5	3.7
GB-dispersion without poloxamer	-	-	-
MCT-dispersion without poloxamer	13.2	1.4	-
MCT bulk (oil)	20.8	3.4	-
aqueous solution of poloxamer	-	-	2.9
recrystallized melt of GB containing 2 % oil (bulk-mixture)	signals unseparated: 296		-

failed due to the line broadening of TMS in solid lipid containing samples. This line broadening is caused by adsorption and magnetization transfer processes similar to processes described by Mayer [194]. The line broadening was considerable less pronounced in samples containing no solid lipid material. We attribute the higher increase in line width due to an increased surface area (platelet structure) and the higher rigidity of the interface.

The NMR line widths of the MCT protons in the MIX samples are in the range of the nanoemulsion. The NMR spectra of the mixed samples represent – in contrast to NLC – a

superposition of the NMR spectra of SLN and NEmu. The small line widths of the MCT protons indicate no interaction of the liquid oil with the solid lipid. It can be concluded that steric stabilization stabilizes the particles very efficiently.

The recrystallized melt of GB bulk containing 2 % MCT is of great interest. A strong immobilization of MCT is given due to the rigid solid lipid matrix. In comparison even to the 2 % oil loaded SLN, the bulk system led to broadened unseparated alkyl signals.

Concerning the tenside, slightly lower values for the widths at half height were obtained through increasing MCT load on the SLN. The reason can be found in different particle shapes: Higher oil content leads to more spherical particles and therefore less surfactant molecules are needed to stabilize the decreased surface area. During crystallization of the melt-emulsified glycerides poloxamer is able to stabilize the new areas efficiently enough to prevent particle agglomeration. In pure emulsions of absolutely low oil amounts the mobility of poloxamer is equal to an aqueous poloxamer solution. Furthermore, higher lipid content requires more tenside molecules which causes a higher level of immobilized molecules. In mixtures, the influence of the SLN on the widths at half height is predominant because of SLN's higher quantitative mixing ratios. Last of all, poloxamer seems to immobilize partly the alkyl groups of oil droplets what is shown in the comparison of a unstabilized nanoemulsion with its stabilized counterpart.

Briefly, the NMR results show an immobilization of the oil in the NLC formulations. The immobilization in MCT-GB particles (formulations NLC-0.2, NLC-0.4, NLC-1.0) is not at all comparable to high immobilization extent of the recrystallized melt of GB bulk containing 2 % oil. This is a strong indication that MCT molecules are not well fixed in the solid matrix of the particles. But clear statements if the liquid lipid molecules stay in the inner part of the solid matrix or stick on its outer surface finally will not can be done by NMR. For further information ESR studies were carried out.

### **4.4 Electron spin resonance (ESR) spectroscopy**

#### **4.4.1 In vitro determination of spin probe distribution**

In the ESR spectra only paramagnetic (e.g. TB) but not diamagnetic substances as the used lipid or tenside provoke signals [195]. TB (4-Hydroxy-2,2,6,6-tetramethylpiperidin-1-oxyl;

figure 5) belongs to the group of stable nitroxyl radicals. It is an at room temperature solid crystalline red substance of high lipophilicity (distribution coefficient n-octanol/water approximately 300).

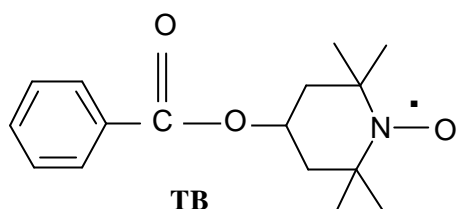


Fig. 5: Chemical structure of TEMPOL benzoate.

ESR permits the measurement of the molecular mobility (spectral shape) and the polarity of the molecular environment of the probe TB (hyperfine splitting constant  $a_N$ ). The ESR spectra indicate that TB experiences different environments in nanoemulsions, SLN- and NLC-dispersions (figure 6).

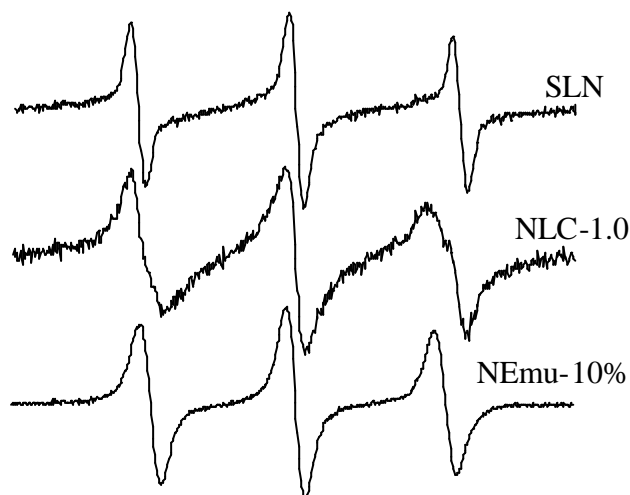


Fig. 6: GHz ESR spectra of TB in NEmu-10%, in NLC-1.0 and in SLN (from the bottom to the top).

Spectral simulation (figure 7) permits a quantitative characterization (figure 8) of the ESR spectra. The spectrum of the nanoemulsion can be simulated with a single species of high mobility in a lipophilic environment. This result agrees well with the expectation. Due to the high lipophilicity, the nitroxide almost completely dissolves in the oil. The ESR spectra of the SLN can be simulated by three different species. Species I ( $a_N$  between 1.51 mT and 1.58 mT is molecular solubilized in a lipophilic environment and has considerable mobility despite the use of a solid lipid. It can be attributed to TB molecules molecular dissolved in the lipid alkyl chains. Species II has a very small line width and a large hyperfine splitting of 1.72 mT. It has exactly the same spectral pattern as TB solubilized in water or in

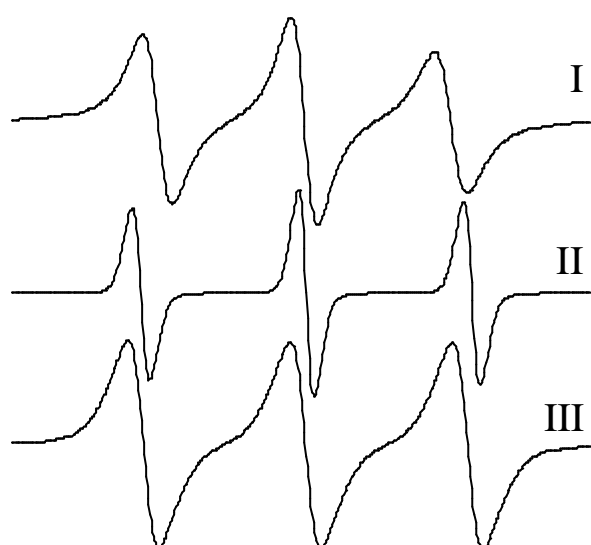


Fig. 7: Simulated compartments for TB in NLC-1.0 (lipophilic (I), very hydrophilic (II), moderate hydrophilic (III)).

2.5 % aqueous poloxamer solutions. Therefore, species II can be attributed to TB molecules which are molecular solubilized in the aqueous phase. A competitive nanocompartment for TB in form of tenside micelles can be excluded because poloxamer 188 is known to arrange in micellar structures only at higher concentrations and temperatures [68,170].

A further species (III) has large line widths indicative of spin exchange processes due to a high local concentration. The hyperfine splitting constant (ranges from 1.65 mT to 1.68 mT) indicates a polar

environment. Species III represents TB molecules which are localized in a high local concentration on the surface of the SLN particles. It can be concluded that crystallization of the molten lipid nanodroplets (obtained after high pressure homogenization) leads to an expulsion of the majority of TB molecules (about 70 %) onto the particle surface and into the aqueous phase. The ESR spectra of the TB-loaded NLC represent also the three different species. Increasing oil loads lead to decreasing concentrations of species II (TB in the outer aqueous phase). However, increased concentrations of lipid-solubilized TB are only observed at 10% oil load of the lipid phase (NLC-1.0). At lower oil loads (NLC-0.2 and NLC-0.4), TB is preferentially localized in high local concentrations at the particle surface in a more polar environment (species II).

Changes in the ESR patterns during storage could not be observed, neither for samples stored at room temperature nor for them at 8 °C. Following these ESR results annealing might not play an important role for GB because of its high melting point and its high solidification degree in nanodispersions.

Additional experiments were performed where TB was added to the TB-free lipid nanodispersions after the homogenization and tempering steps. The majority of the TB remained as non-dissolved crystals and diffusion of TB through the water phase is the

velocity determining factor in this experiment. But after seven days some TB molecules were dissolved and distributed in the sample. The recorded ESR spectra were comparable to the regular produced samples at this time point. This indicates that TB can access all compartments if it is added after the production of the nanodispersion.

A non-invasive determination technique for model drug localization offers superior information as long as separation of colloidal particles and following quantitative analysis of the drug often is a challenge [37,44]. For the investigated lipid dispersions common separation techniques let to disappointing results. (Ultra-) centrifugation did not show sharp separation because lipid platelets and aqueous environment do not provide distinct difference in densities. The use of Centrisart<sup>TM</sup> tubes did not allow drug-only composed particles or even large unbound molecules as poloxamer or drug to cross the inner filter and favors aggregation due to concentration effects at the filter membrane. In case of GB particles there was no possibility to redisperse agglomerates to solitaire particles. Incomplete drug capture, drug inclusion in the lipid agglomerates or uncontrolled drug release due to carrier changing are thinkable. Dialysis was found to be time consuming and requires particle dilution with unknown consequences for the carrier fate.

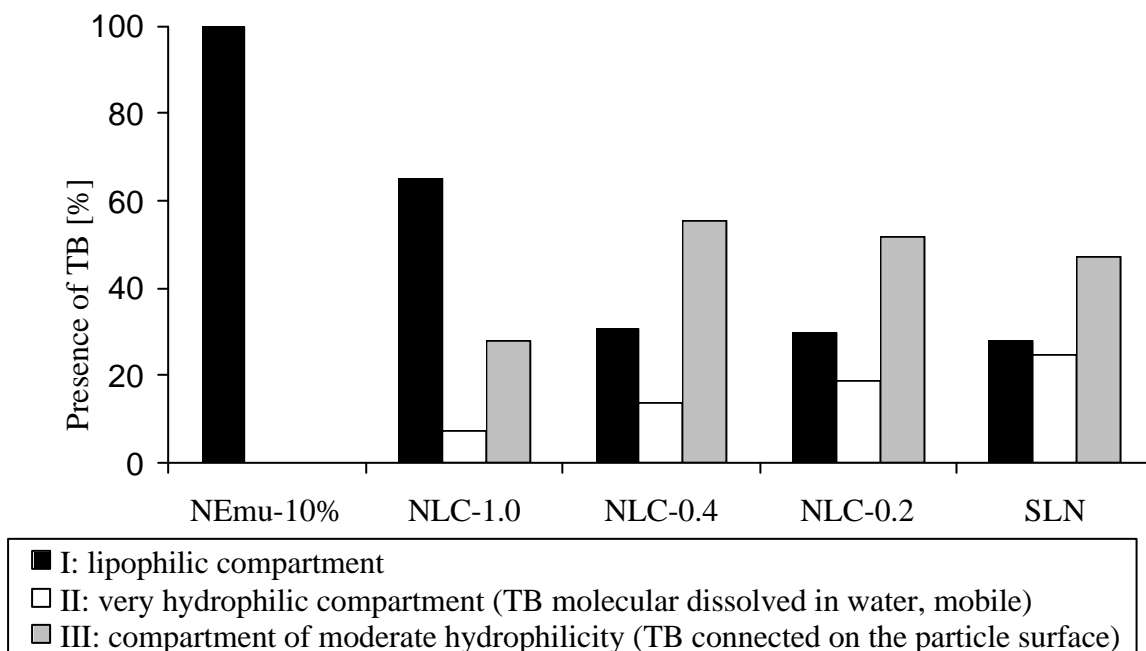


Fig. 8. Localization of TB in lipid nanodispersions – results of simulation of the ESR spectra by means of NIH-pest software.

## 4.4.2 Ascorbic acid assay

The hydrophilic ascorbic acid reduces accessible TB to an ESR-silent hydroxylamine. The ascorbic acid assay with aqueous ascorbic acid solution demonstrates that the examined SLN are not able to protect the lipophilic TB molecule from aqueous reduction medium as it would be expected if liquid lipid domains are surrounded by a solid lipid matrix (figure 9). The best protection for the probe is given in a nanoemulsion which generally is not known as an most favorable system of prolonged release. The fastest reduction was observed for SLN, which

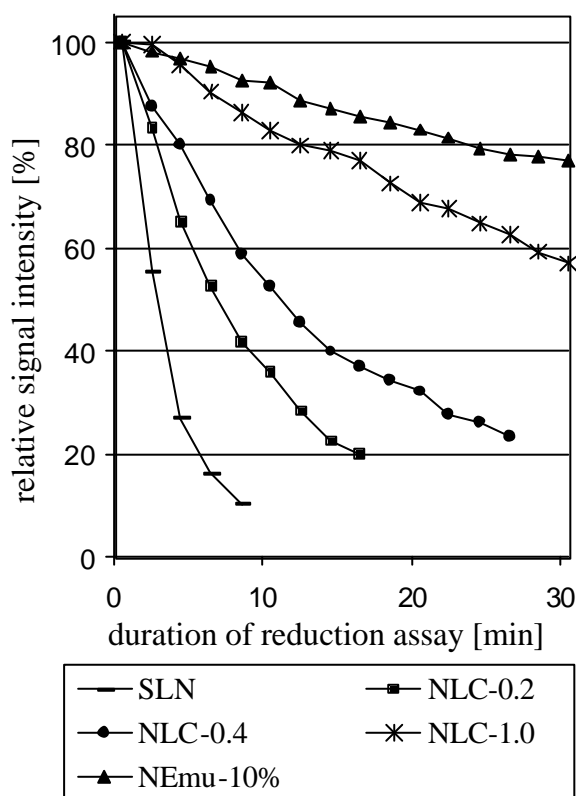


Fig. 9: Decrease of ESR signal intensity (time against changes in the signal area) of different nanocarrier systems during the ascorbic acid reduction assay.

TB species localized in a polar environment (species II and III) decrease faster than the signal intensity of species I (non-polar lipid compartment). Interesting conclusions concerning the distribution processes of TB between the polar and the non-polar microenvironment can be drawn. In a first scenario, no changes would be seen if distribution happens very fast (e.g.

agrees with the results of the spectral simulation, where the highest amount of TB was attributed to nitroxide molecules localized in polar environments. Generally, diffusion of TB inside the particle is rapidly possible due to the very short diffusion length and due to the considerable mobility the TB molecules inside the lipid. Reaching the surface, TB becomes access to the reducing AA (see figure 9: the remaining TB concentration in SLN after only 8.5 minutes is very low). Therefore, the packaging lattice of the small GB platelets must be very loose and incompact, and, above all, diffusion over nanometric distances is always very fast (see chapter 1.1).

Changes of the spectral shape were observed during the reduction experiments. The signal intensities of the

within milliseconds). If the distribution of TB between the different compartments would occur very slowly (e.g. hours), a rapid decrease of the hydrophilic species would be seen and the lipophilic species would remain and dominate the ESR spectrum (scenario two). Our findings correspond to an intermediate scenario where we can clearly detect changes in the spectral shape, but we do not see a dominating signal of the lipophilic species. So the distribution process of TB between the polar and the non-polar microenvironment must be comparable to the reduction kinetics of the hydrophilic species and therefore in the order of seconds to minutes.

It is noteworthy, that classical release experiments can not be performed on SLN and NLC due to their colloidal size. Determination of release kinetics for emulsions can be done either by Franz flow-through diffusion cells (initially developed for skin permeation studies) or by diluting the formulation in the medium of conventional tablet dissolution testers and later separation of the particles from the medium. Loss of water, choice of membranes/cell layers/media, dilution and separation processes often do not lead to meaningful and comparable data [196] or can even cause artifacts [1,196]. So long as these problems exist, ESR spectroscopy at least provides interesting information concerning the accessibility to the drug molecules contained in colloidal carriers, even in a non-invasive way.

### 4.4.3 Ex vivo measurements on human skin

Beside peroral and parenteral application routes for SLN often a dermal administration is proposed. For effective topical treatment of skin diseases and transdermal drug therapy, it is imperative that the topically applied drug enters the epidermis or the dermis of the skin or the peripheral blood, respectively. Skin penetration and permeation of the drug after topical administration depend on the physicochemical properties of the drug molecule and on the function of the skin as a transport barrier (stratum corneum, above all) and can be influenced by the applied formulation. Formulations with supersaturated drug concentrations, with penetration enhancers or with moisturizer favor the diffusion of lipophilic drugs into deeper skin layers. In addition, the bioavailability of an active substance may be influenced by first pass metabolism.

Up to now, the dermal application of SLN was investigated by skin-destructive methods or by in vitro models [38,197,198]. Penetration of active substances into the skin can only be determined by the tape stripping method or by skin slicing in e.g. steps of 100 nm. Occlusion

tests work on pure in vitro models without use of skin when the loss of water from a beaker glass covered with filter containing samples is determined. Dissolution tests are performed membrane-free as diffusion into an appropriate acceptor medium [199] or by Franz cell experiments. The latter can be conducted by a filter membrane, by viable skin or by reconstructed epidermis onto which the test formulation is given. Released drug concentrations are analyzed in the elution media floating at the bottom side of the barrier. Often problems arise from poor drug diffusion into the acceptor medium or bad reproducibility of the results. Special equipments are on the market for skin characterization (e.g. viscoelasticity by cutometer, humidity by corneometer), but each determine one certain parameter only.

ESR spectroscopy should allow following the fate of lipid systems on ex vivo skin in a non-invasive way, by a more simultaneous view on drug distribution, sample changes or possibly pH changes. The method could be applied on in vivo test conditions easily.

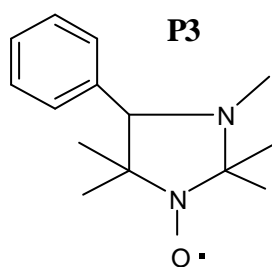


Fig. 10: Chemical structure of P3.

Before starting the skin experiments the ESR spectrum of P3 (figure 10) loaded SLN sample was recorded (figure 11). P3 was used instead of TB because less reduction to ESR silent hydroxylamines is expected. The spectrum indicates a low incorporation rate of P3 in the solid lipid and the localization of the probe in a rather polar environment. These conclusions are drawn from considerations as described in chapter 4.4.1. In good agreement to the results gained on the lipophilic spin probe TB, the results are not unexpected.

After application of the SLN on human skin, water starts to evaporate. Spectral changes are observed (figure 11, above). The immobilization of P3 increases what is indicated by a decrease in signal intensity (figure 11, on the right, above). Furthermore, P3 distributes to a more lipophilic environment, seen by smaller coupling constants and broader lines. Lipids of the skin create this lipophilic environment. That is proven by SLN applied on a glass surface (figure 12), no lipophilic compartment is available and immobilization increases drastically. Spin-spin exchanges occur due to high local concentrations on the glass panel and the spectra demonstrate a superposition of aggregated P3. For SLN on human skin no further changes are detected after 90 minutes due to a nearly completed water loss from the SLN formulation.

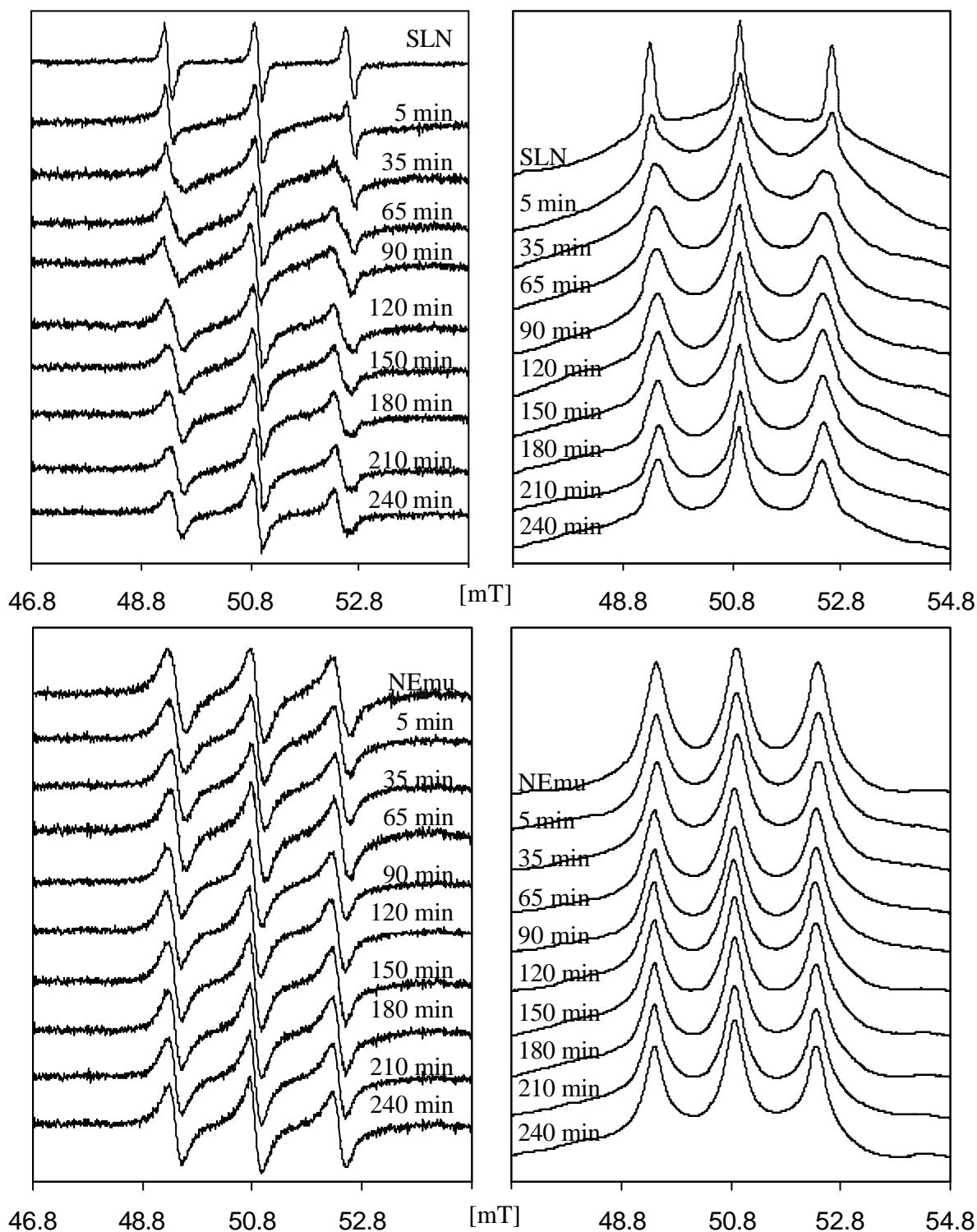


Fig. 11: In-vitro ESR spectra (on the left) and their integrations (on the right) of P3-loaded SLN (on the top) and of NEmu-10% (at the bottom), gained on human skin.

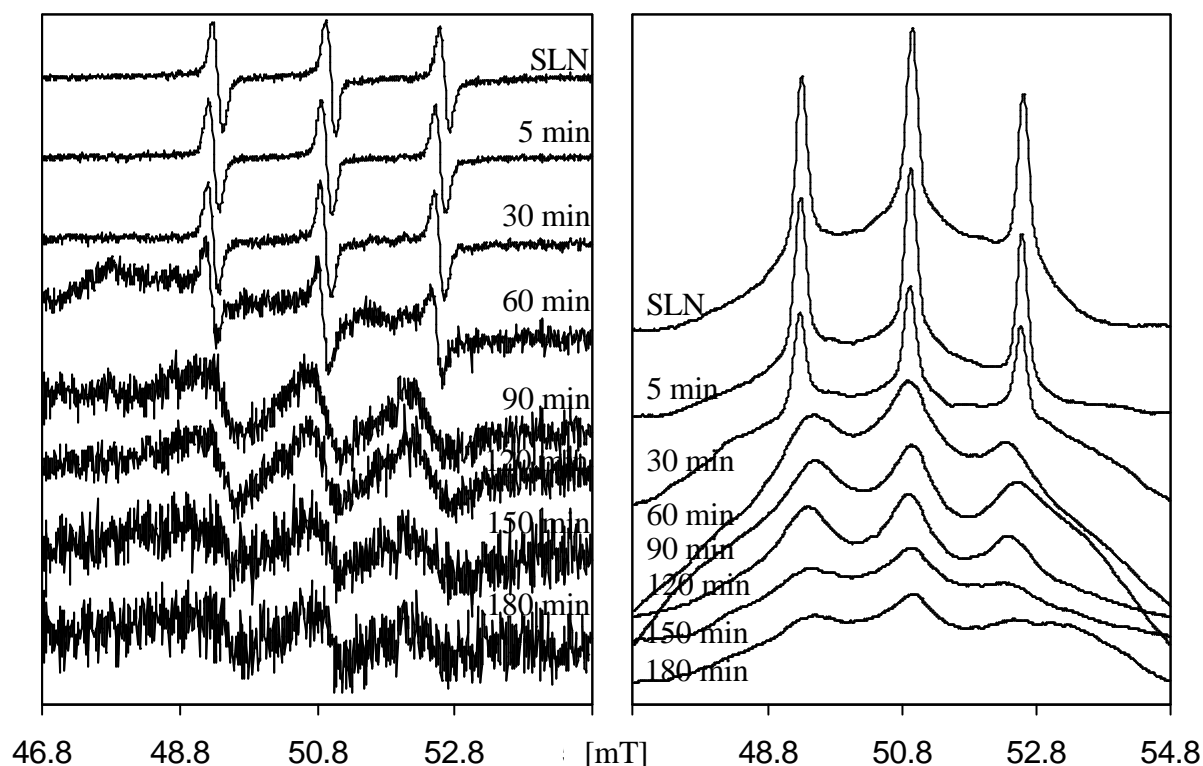


Fig. 12: ESR spectra (on the left) and their integrations (on the right) of P3-loaded SLN, applied on a glass surface.

Comparing to the nanoemulsion NEmu-10% (figure 11, below) the mobility of P3 is maintained in spite of water evaporation (constant signal intensity). The hydrophobic spin probe is still localized in oil (smaller coupling constant and broader lines) where it is not affected from changes in the outer phase, i.e. evaporation.

SLN and NEmu-10% are compared to a conventional microemulsion described in chapter 3.1. Microemulsions are systems known for good dermal penetration because their high tenside content interacts with cell barriers; supersaturated microemulsions work even more [200,201]. Reliable simulations of P3 localization in different compartments of the three formulations are not possible since loss of water in SLN leads to probe aggregation. But comparing the aspects of other spectra, the investigated microemulsion showed the same results as the nanoemulsion, due to a high liquid lipid content where P3 is preferentially localized.

Important information is obtained from the experiments where the sample has been removed from the skin surface after 1 h by dabbing with cotton wool. For all samples SLN, NEmu-

10% and microemulsion the signal intensity decreases, but a medium amount of model drug is already distributed to deeper skin areas of higher lipophilicity (figure 13). Again, simulations are not possible, the low spin probe concentrations left after dabbing can not be calculated with acceptable error range. But the total integrated areas after dabbing could be compared by subtraction (data not shown). The interesting result was that SLN are not superior in penetrating deeper skin layers compared to the formulations NEmu-10% and microemulsion.

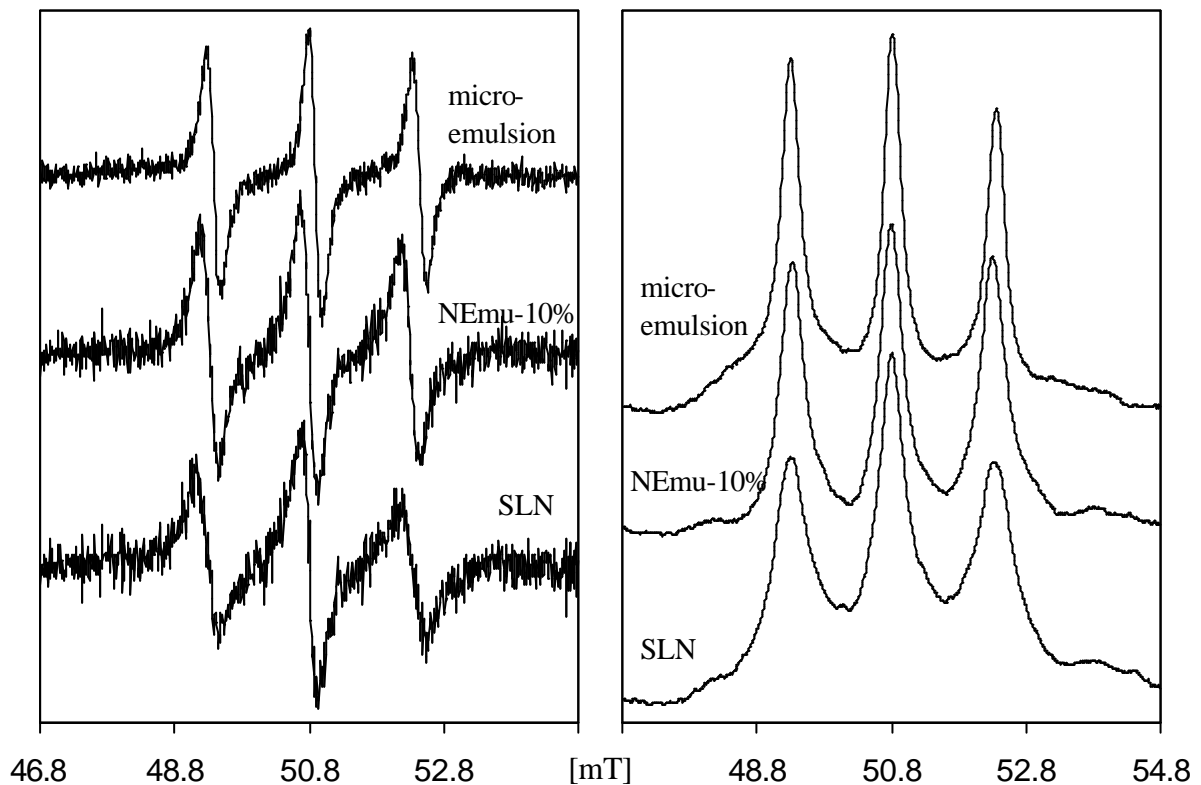


Fig. 13: ESR spectra gained on human skin (on the left) and their integrations (on the right) after incubation (1 h) and subsequent removing of P3-loaded samples (from the bottom to the top: SLN, NEmu-10% and microemulsion).

To find an explanation for these data one should remark that even from microemulsion and NEmu-10% not all P3 molecules are released and delivered to the skin because P3 remains in an oily film which is easily removed from the skin surface. When starting the SLN experiments, P3 is localized on the surface of SLN, in accordance to the former conducted simulations in chapter 4.4.1. From there, high thermodynamic activity leads to distribute the

hydrophobic probe to skin compartments of better solubility. But thereby, the finely and highly distributed model on the large surface area of the solid lipid platelets does not correspond to an increase in drug release (as expected). Solid lipid film building on the skin after water evaporation hinders drug transport.

Summarizing, the “net P3 amount” contained in human skin after incubation (1 h) and after removing of excessive formulation from the skin surface show that SLN do not release a higher amount of the model drug than already established nanoemulsion or microemulsion systems. The human stratum corneum could not be entered significantly by SLN.

#### 4.5 Fluorescence spectroscopy

Similar to in vitro ESR analysis, fluorescence spectroscopy offers a non-invasive determination possibility for the distribution of a model drug [37].

The lipophilic benzophenoxazone dye NR (figure 14) is known to show strong fluorescence in a wide range of organic solvents. Its partition coefficient is noted at 196 for chloroform/water (4 °C) and less than 1 µg NR is soluble in 1 mL of water [202]. However, fluorescence is totally quenched in aqueous medium. NR dispersed into a poloxamer solution loses its fluorescence and becomes a clear colorless solution. Distribution experiments

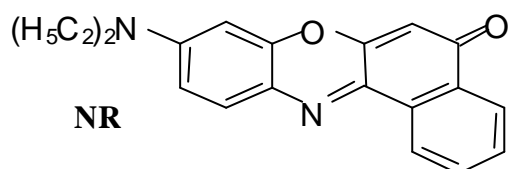


Fig. 14: Chemical structure of Nile red.

where NR was added to NR-free lipid nanodispersions failed because of the irreversible quenching phenomenon before reaching the lipid matrix. Therefore, the disappearance of the fluorescence can not – in contrast to the claims made by Olbrich et al. [203] – be discussed as an absence of the Nile red in the water phase.

The emission spectra of many fluorescent substances are dependent on the physicochemical properties of the solvents. NR shows solvatochromism [204], its absorption band varies in spectral position, shape and intensity with the nature of the solvent. As a rule, in solvatochromism the spectrum preserves its essential form, merely shifting to longer or shorter wavelengths if the quantitative relation in a solvent mixture is changed [205]. Alterations in the spectral curves can not only be found in organic solvents of different dielectric constants and refractive indices, but also in various structured colloid lipid preparations like liposomes and microemulsions [202].

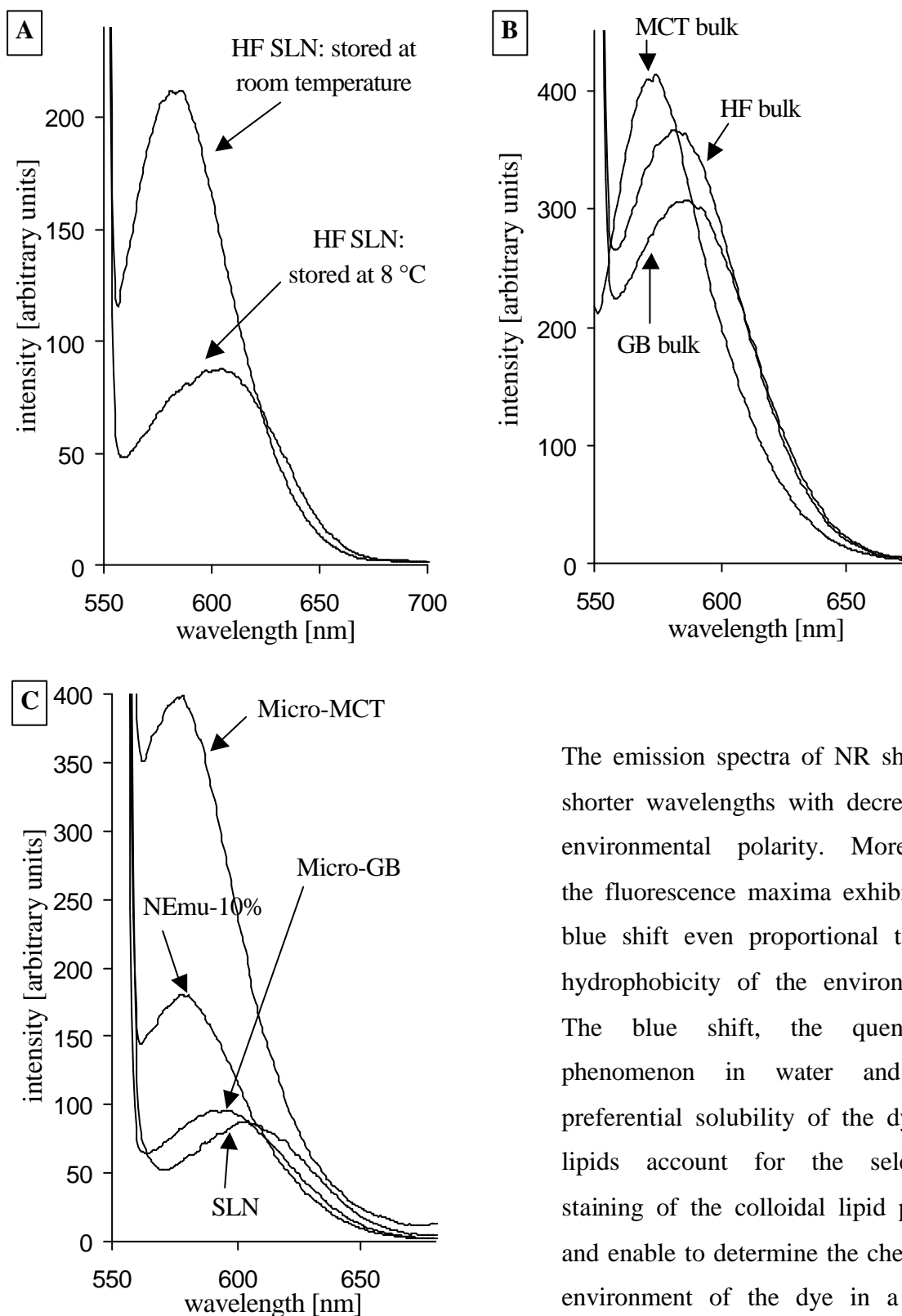


Fig. 15: Fluorescence spectra of NR (A) in HF SLN stored at different temperatures, (B) in HF bulk ware, and (C) in aqueous dispersions containing particles of different sizes.

The emission spectra of NR shift to shorter wavelengths with decreasing environmental polarity. Moreover, the fluorescence maxima exhibit the blue shift even proportional to the hydrophobicity of the environment. The blue shift, the quenching phenomenon in water and the preferential solubility of the dye in lipids account for the selective staining of the colloidal lipid phase and enable to determine the chemical environment of the dye in a non-invasive way.

Confirming this notion, NR-doped SLN made from HF were

investigated. Due to the low melting point of HF and due to the colloidal size of the carrier [33,206] at room temperature HF-SLN possess a liquid lipid matrix [207] what causes the lack of signals by X-ray and differential scanning calorimetry measurements (data not shown). Temperatures well below room temperature (8 °C) are required to solidify the lipid matrix within hours to days. The emission maximum moves to a longer wavelength (figure 15 (A)), indicating a more hydrophilic environment for NR. Furthermore, a reduction of the fluorescence intensity is observed, which indicates that more NR molecules interact with water and lose their fluorescent properties. Both from the shift of the fluorescence spectra and the loss of fluorescence intensity it is to conclude that the solidification of the lipid matrix leads to the expulsion of NR from the lipid matrix to the surface of a crystalline particle.

For a better understanding, the fluorescence properties of NR in bulk were examined (figure 15 (B)). The triglyceride MCT creates a more hydrophobic environment than the partial glycerides contained in HF and GB, above all (see lipid composition described in chapter 2.1). Intensities decrease in solid lipids, the higher melting GB bulk pronounces even less solubility for NR than the crystal lattice of HF.

The influence of the particle size on the fluorescence properties was investigated by comparing lipid nanoparticles (GB-SLN) with lipid microparticles (Micro-GB). Micro-GB accommodates slightly higher numbers of NR molecules in a more hydrophobic compartment than the nanoparticles can do (figure 15 (C)). Both, the Micro-GB and the SLN provide a crystalline matrix with low incorporation capacity and therefore the model drug is exposed to water. This finding is consistent with the fact that GB-SLN crystallize as very thin platelets with a thickness of very few lipid layers: In this thesis on hand, for the first time GB containing nanoparticles are reported to be platelets instead of spheres. It will be later demonstrated by TEM images (chapter 4.11), e.g. In contrast, the environment for the dye in both kinds of MCT particles is less changed. Micro-MCT protects more NR molecules against quenching than NEmu-10% with considerable larger size dependent surface area.

The emission spectra of the nanoparticle formulations with varying oil loads are shown in figure 16 (upper graphic). Even small changes in the MCT:GB ratio lead to remarkable different spectra in the fluorimeter. The intensive signal at 546 nm arises from the reflection of the entering excitation light on the particle surfaces. To get exact figures from the shifted peaks fits are drawn to describe the experimental spectra as good as possible. On closer inspection two simulated curves will be necessary to describe the data exactly in case of

samples NLC. The simulation by one (SLN) and two (samples NLC and NEmu-10%) curves, respectively indicates nanocompartments of different polarity (see figure 16 (graphics below)).

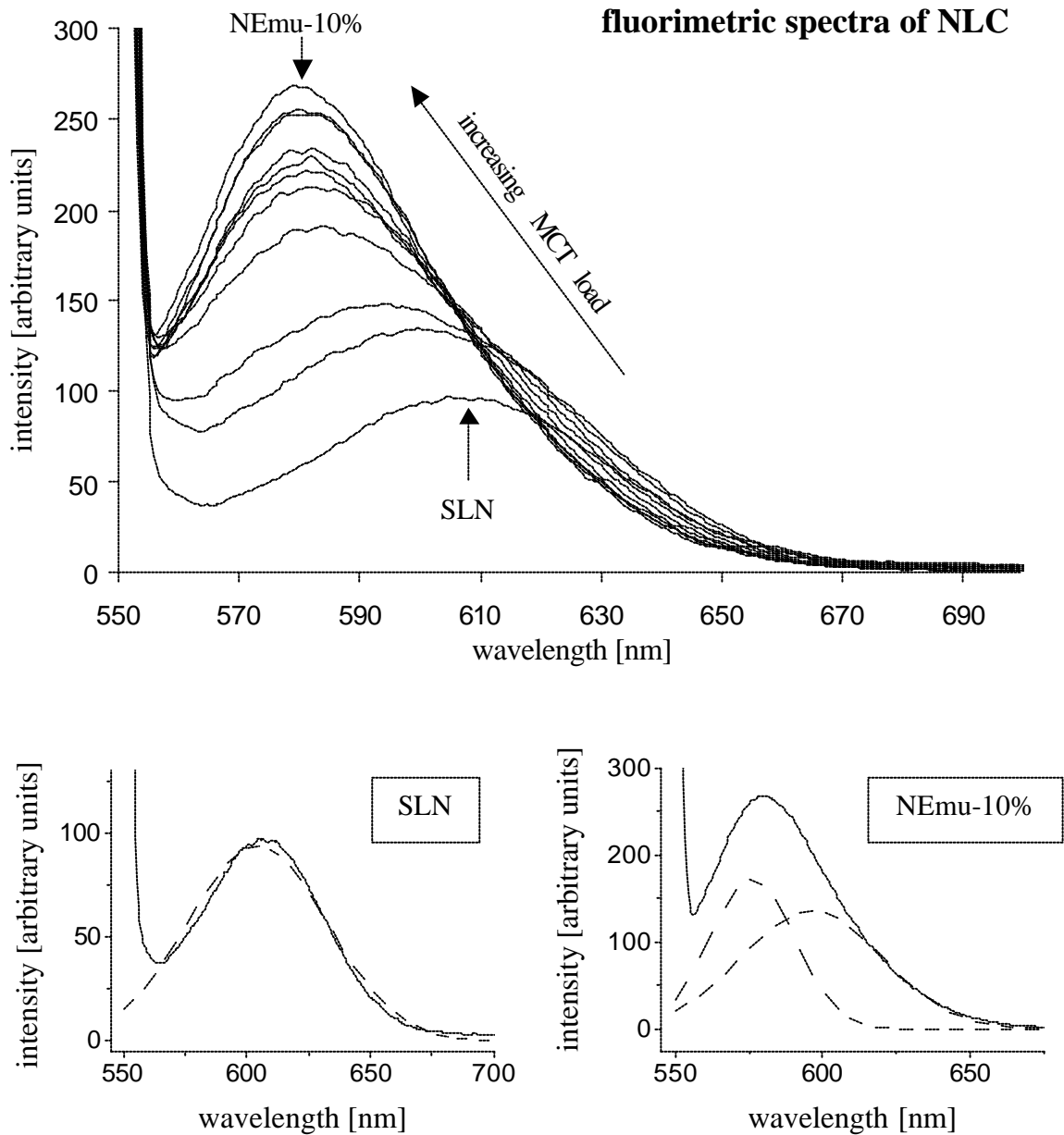


Fig.16: Fluorimetric spectra of formulations SLN, NLCs, NEmu-10% (above) and simulated fits (dashed lines) of the shifted signals of SLN and of NEmu-10% (on the bottom).

The following conclusions can be drawn by closer look on the peak fits:

- The fluorescence spectra of pure SLN can be simulated with one fitting curve with a wavelength maximum in a range of 604 nm, which indicates an remarkable polarity (for comparison: NR in acetone yields an emission maximum at 608 nm [202]). NR should be localized on the particle surface of SLN!
- Oil load creates always an additional second (apolar) compartment at approximately 578 nm for the fluorescent marker (for comparison: NR in chloroform yields an emission maximum at 595 nm and in xylene at 565 nm [202]). NR is either localized on the solid particle surface or accommodated in an oily compartment. The expressive polar compartment known from SLN disappears suddenly if oil load amounts to more than 20 %. 20 % oil load and more correspond to an oil concentration enough to host preferentially nearly all marker molecules of the sample. But even in NEmu-10% a small compartment with medium polarity (at 585 nm) remains where always some NR is localized on the droplet surface whereas the majority of NR is dissolved in the droplets (578 nm).
- It can be proven that protecting incorporation characteristics in the solid matrix are failed. The dye is exposed to an aqueous environment where approximately 2/3 of the marker are quenched (see loss in intensity in figure 16 at SLN in contrast to NEmu-10%, quantified in figure 17). Best protection from the outer environment is given in the nanoemulsion.
- The same quantification of peak areas was performed for MIX samples (figure 17). Again, increasing MCT content in the MIX samples increases quenching protection. Above all, regarding samples with low oil content, peak areas were diminished up to 20 %, i.e. up to 20 % less protected NR in MIXes were found in comparison with NLC. Decreased NR protection in MIXes confirm the short diffusion pathways and rapid distribution of NR into oily compartments of NLC. In MIXes diffusion possibility from GB to MCT is failed (due to the presence of the aqueous diffusion barrier between liquid and solid particles and due to quenching effects in water).

It is very important to mention the relation between fluorescence properties and concentration of NR. In figure 18 both the emission maxima and the fluorescence intensities vary with the concentration of NR employed. A general rule is that a linear response will be obtained until the concentration of the fluorescent substance is sufficiently large so as to absorb significant

amounts of the exciting light [208]. Non-linear response would provoke artifacts because peak shifting and quenching phenomena could not be correlated accurately to changed sample composition. The employed concentration of  $0.25 \mu\text{g NR per 1 g}$  formulation combines linearity with sufficient fluorescence intensity.

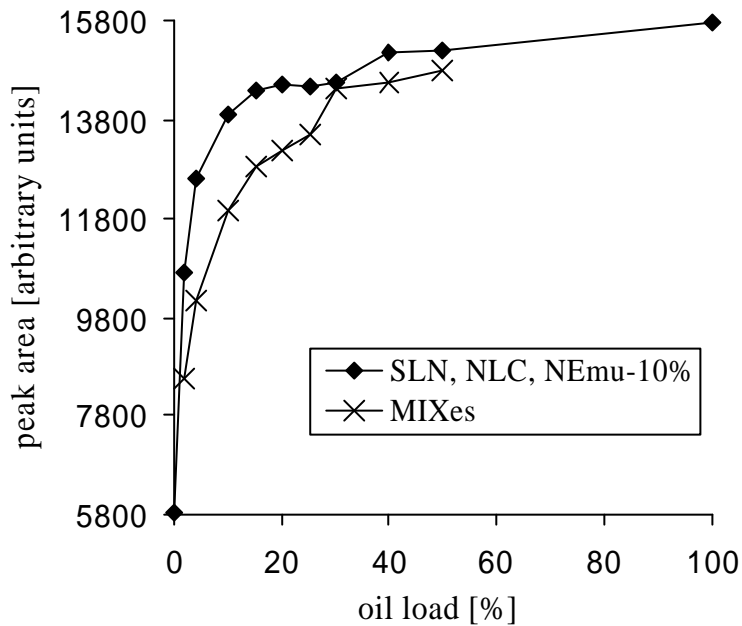


Fig. 17: Dependency of the peak area on the oil content of the samples.

Summarizing, spectrofluorometric studies show a poor incorporation capacity of the marker NR in SLN and NLC. Even the bulk ware of solid lipids can not accommodate reasonable amounts of the dye. Concerning incorporation capacity and protection from the outer water phase SLN and NLC are surpassed by a common nanoemulsion. It should be clearly pointed out that the concentration of NR was  $0.25 \mu\text{g/g}$  formulation, so the nanoparticles are only negligibly loaded.

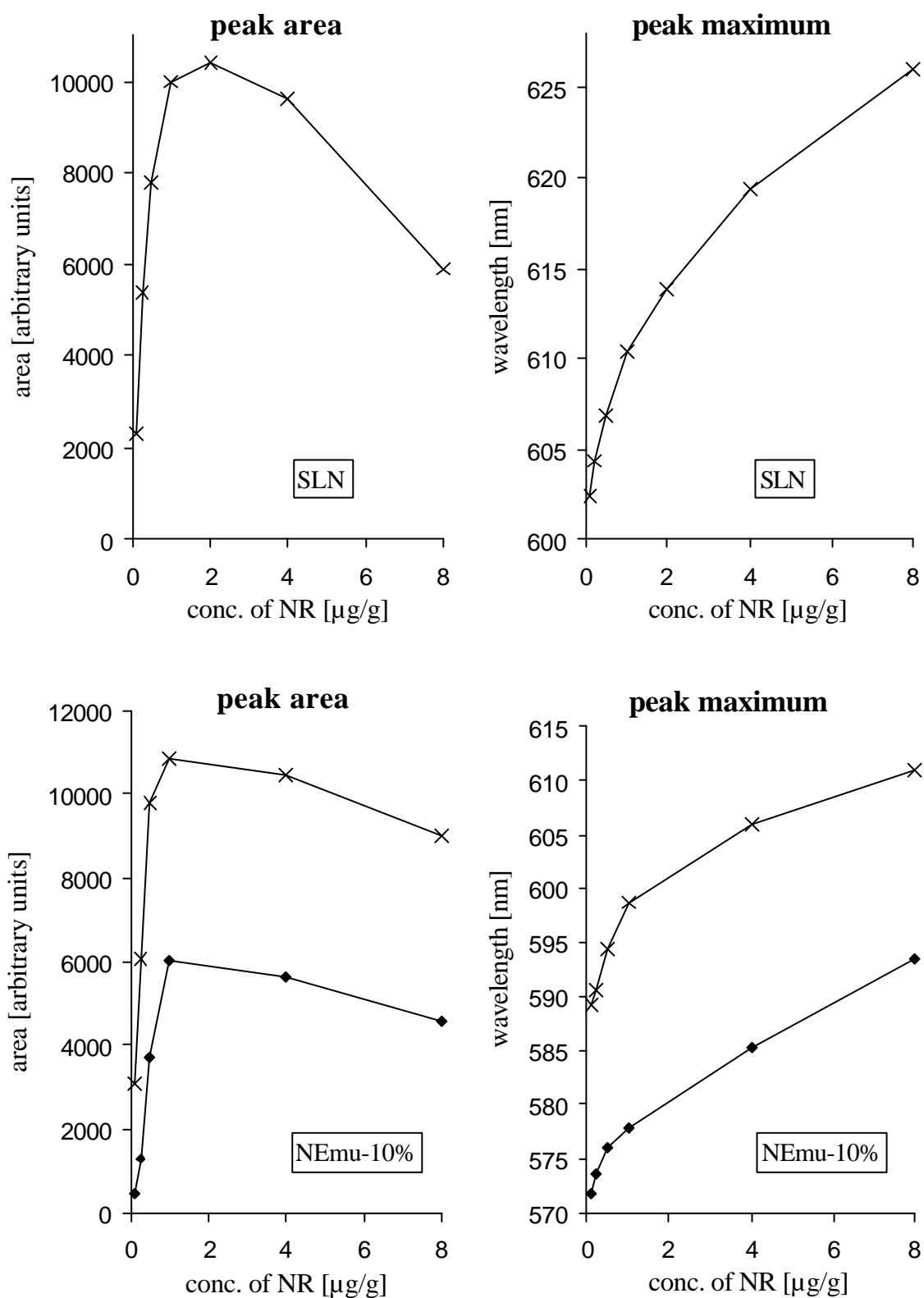


Fig. 18: Dependency of peak area and of peak maxima on the Nile red concentration in GB-SLN (upper graphics) and in MCT nanoemulsion (after fitting; lower graphics).

#### 4.6 Raman spectroscopy

In analogy to the infrared absorption spectroscopy (IR spectroscopy), the Raman spectroscopy detects vibrations of molecules after excitation by an intensive laser beam [209-212]. Characteristic Raman bands were obtained from apolar functional groups (e.g. C-C bindings) which are inaccessible for IR measuring. Instead of providing a dipole (indispensable for IR spectroscopy), molecular groups have to show polarizability of electrons as the key factor for Raman spectroscopy. Both techniques, the IR and the Raman spectroscopy give often complementary information.

In a non-invasive way, the sample is exposed to the laser beam. Approximately less than 1 % of the exciting light quanta donate a certain part of their energy to the sample molecules to activate molecular vibrations. The scattered light is recorded and the donated energy is

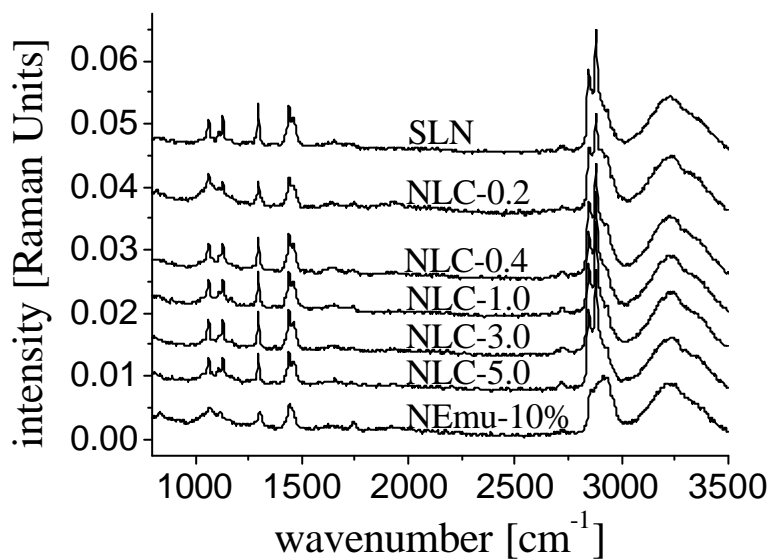


Fig. 19: Raman spectra of different lipid nanodispersions.

expressed in form of smaller wave numbers. In a Raman spectrum the differences in wave numbers are correlated to specific molecular vibrations. The position and widths of the bands are sensitive to the conformation of the molecule. Figure 19 represents the Raman spectra of SLN, NLC-0.2, NLC-0.4, NLC-1.0, NLC-3.0, NLC-5.0 and NEmu-10%. SLN show a similar pattern as the formulation NLC, but NEmu-10% is found to differ. In table 4 the bands are assigned to different molecular vibrations. Water and poloxamer solution, respectively cause only broad peaks at  $3,500\text{ cm}^{-1}$  (data not shown) and they are well separated from the interesting lipid signals. Regarding the aspect of oil incorporation in the crystal lattice, bands indicating the order of lipid chains are of high interest. The symmetric stretching of the methylene groups

(at  $2,842\text{ cm}^{-1}$ ) is an indicator for the degree of chain order and occurs in SLN and in all formulations NLC. In contrast NEmu-10%: For the liquid lipid the signal at  $2,842\text{ cm}^{-1}$  is completely missed and less pronounced concerning the factor splitting group. Moreover the band at  $2,852\text{ cm}^{-1}$  occurs which indicates failing order. Oil loading did not lead to changed lipid chain arrangement and oil incorporation could not be confirmed by these data.

Table 4: Observed Raman bands and assignments to molecular vibrations.

Band position [ $\text{cm}^{-1}$ ]	Assignment	“Diagnostic value”
between 800 to 900	$\text{CH}_3$ rocking	Sharp band indicates 3 consecutive trans
1060	C-C asymmetric stretching	Sharp band indicates 3 consecutive trans
1130	C-C symmetric stretching	Sharp band indicates 3 consecutive trans
1295	$\text{CH}_2$ twisting	
1420/1440/1465	$\text{CH}_2$ scissoring	Indicator of packing behavior
2842/2852	$\text{CH}_2$ symmetric stretching	Low band position and high intensity indicate trans
2880	$\text{CH}_2$ antisymmetric stretching	Sharp band indicates 3 consecutive trans

No significant differences have been found between the experimental spectra of NLC-0.2 and the superposition of the corresponding NEmu-10% and SLN spectra. NLC-0.2 reacts in Raman spectroscopy as it would be composed of a nanoemulsion and of a nanosuspension, without interaction of both lipids.

Despite of DSC, NMR, ESR and X-ray measurements which did not show remarkable changes in the solid lipid dispersions, Raman spectroscopy seems to indicate further lipid ordering during storage (figure 20). The signal at  $1,420\text{ cm}^{-1}$  becomes more pronounced, i.e. the packaging density is changed. Often the more pronounced signals are accompanied by gelation of the samples. At the investigated sample on hand (NLC-1.0), gelation has already begun after 49 days, seen by slightly increased viscosity. While storage over nearly five months took place, NLC-1.0 solidified totally.

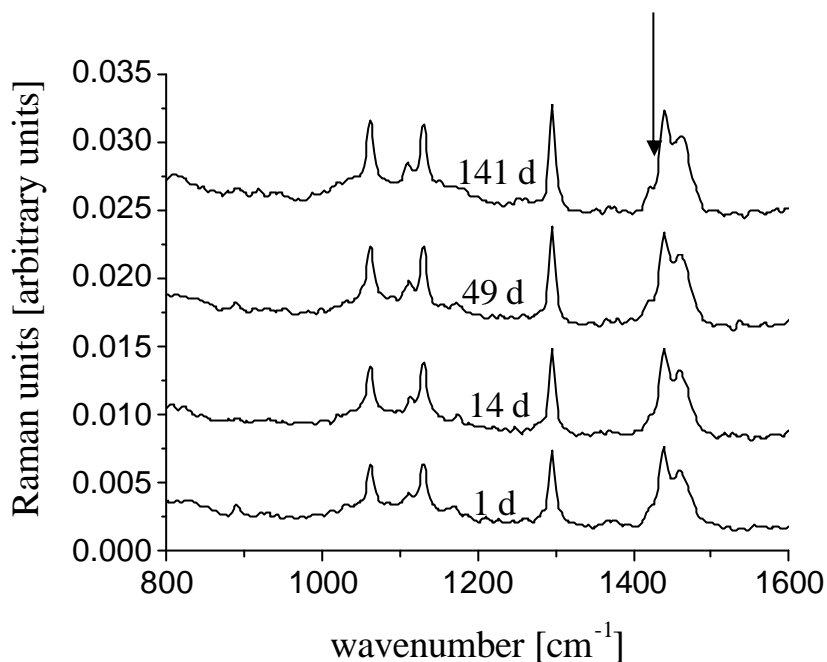


Fig. 20: Raman spectra of the formulation NLC-1.0 during storage process. After 49 d, the sample has already started to build a gel, and after 141 d, it was solid.

## 4.7 X-ray diffraction

### 4.7.1 By copper radiation

Triglycerides occur in three main modifications  $\alpha$ ,  $\beta'$  and  $\beta$  which differ in the arrangement of the fatty acids. The arrangement of fatty acid chains can be determined by X-ray measurements. X-ray diffraction patterns [213] of the investigated samples result in constant reflexes with their maxima at the angles  $2\theta$  21.2 and 23.3 (figure 21). This corresponds to short spacings of the chains at 0.42 and 0.38 nm what is attributed to the  $\beta'$ -modification of the solid lipid [69,214]. The presence of diglycerides is known to favor the  $\beta'$ -modification of the lipid [215,216]. MCT did not lead to changed patterns, so the lipid crystal structure in X-ray measurements do not seem to be disturbed by the oil adding. Even after six months of storage the X-ray patterns remain unchanged.

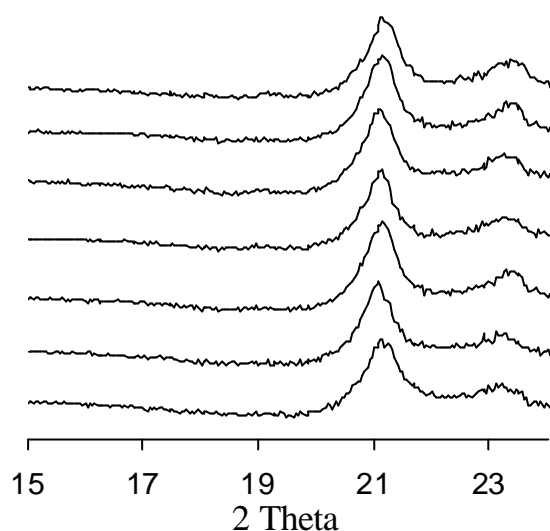


Fig. 21: X-ray (copper anode) diffraction patterns of formulations SLN, NLC-0.2, NLC-0.4, NLC-1.0, Mix-0.2, Mix-0.4 and Mix-1.0 oil load (from the bottom to the top). Formulation NEmu-10% does not provoke reflexes.

For the sake of completeness it should be mentioned that attempts failed to modify the  $\beta'$ -modification in favor of the  $\alpha$ -modification. The  $\alpha$ -modification has a comparatively higher incorporation capacity for host molecules due to more irregular lipid structure, but is less thermodynamically stable. Therefore, attempts have been made to stabilize the alpha-modification by additives. Cocoa butter containing GB nanoparticles remained in  $\beta'$ -modification (ad-mixture of 3 or 4 % cocoa butter to food lipids is a common mean to stabilize the lower

melting  $\alpha$ -modification in chocolate [217] or after producing with the  $\alpha$ -tending substance polyglycerol-polyricinoleate [120]. Rapid crystallization forced at 5 °C resulted in  $\beta'$ -modification. By shock cooling in liquid nitrogen the GB-SLN directly after melt-emulsification transformed into a gel. Moreover, it is doubtful if, firstly, the concept of  $\alpha$ -lipids realizes a remarkable increase in drug or oil incorporation. Still, the lipid is an structured crystal what usually hinders an uptake of foreign molecules. Secondly, the  $\alpha$ -modification is thermodynamically unstable and tends to build the more stable  $\beta$ -modifications. It will be difficult to guarantee  $\alpha$ -modification over long-term storage. Also, the possible advantage of the higher incorporation rate is probably paid of by the enhanced diffusion coefficients [162].

#### 4.7.2 By means of synchrotron radiation

During conventional X-ray analysis the samples are faced to high energetic radiation over long exposure times of approximately four hours. It is thinkable that lipid modifications are changed due to calorific input. Synchrotron measurements are fast-recording X-ray diffraction measurements. They should elucidate this possibility of modification change.

Synchrotron radiation is a very intensive beam of high parallelism in spreading direction of

the rays. In contrast to the measurements performed with copper radiation, synchrotron measurements were performed within seconds.

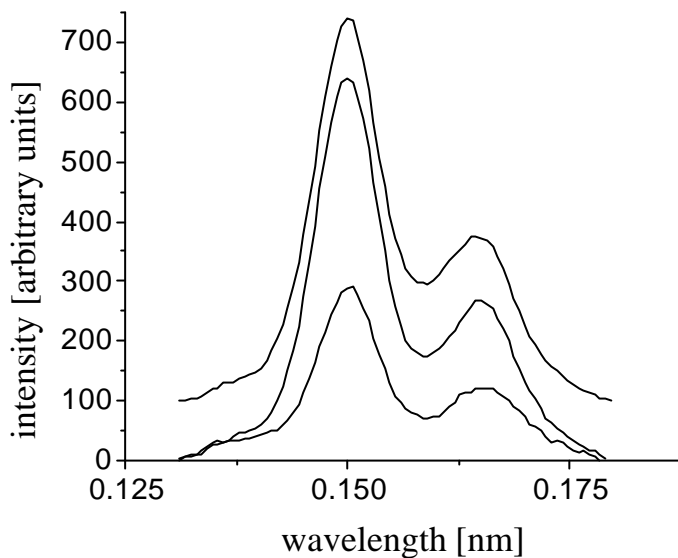


Fig. 22: Synchrotron diffraction patterns after background subtraction of formulations NLC-5.0, NLC-0.4 and SLN (from the bottom to the top; SLN curve shifted by +100 units on the y-axis). Formulation NEmu-10% did not provoke reflexes.

all, with the accuracy smaller than 1 % all synchrotron reflections are unchanged for synchrotron samples among themselves (SLN, NLC-0.4 and NLC-5.0). Once again, oil load did not lead to changed crystal lattices what must be assumed as prerequisite for oil incorporation. The short spacings of the lipid chains were found at 0.42 nm and 0.39 nm, again indicating the  $\beta'$ -modification. [218-220].

#### 4.8 Differential scanning calorimetry (DSC)

Liquids as water, supercooled glyceride fractions and MCT can not be registered using the described temperatures and analyzing conditions. As melting events of GB were detected (figure 23), supercooled GB particles can be excluded (in agreement with the NMR results presented in this thesis) [206]. Measurements one day and four weeks after production led to the same melting pattern.

While the later from a nanoemulsion and from SLN mixed formulations did not differ in their melting behavior compared to formulation SLN, the MCT loaded samples did. Firstly, a

Synchrotron results are presented in figure 22. As the used wavelength is about ten times smaller than the wavelength of the copper X-ray tube (approximately 0.15 nm), the corresponding diffraction angles are ten times smaller and lie below 0.5 nm. The diffraction patterns of the samples SLN, NLC-0.4 and NLC-5.0 resemble the patterns previously gained by copper X-ray measurements. Therefore, the former conducted X-ray experiments are reliable. Above

depression of the GB melting point can be mentioned which keeps nearly linear even with oil loads up to 75 % (figure 24). Secondly, the difference between the onset point and the peak maxima increased with higher oil load, a signal for more irregular arrangement of molecules

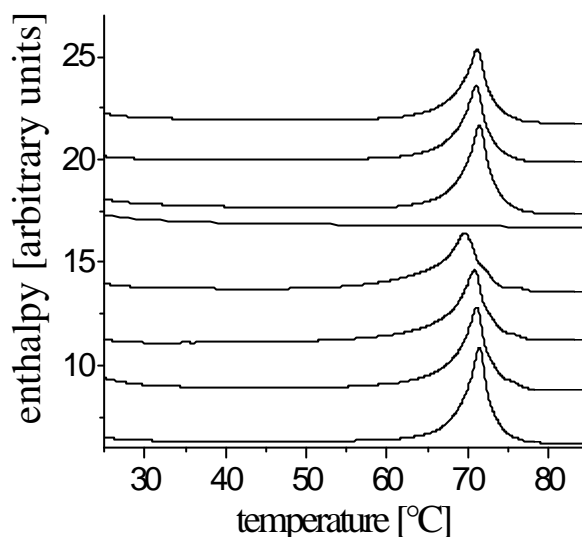


Fig. 23: DSC heating curves (5 K/min) of formulations SLN, NLC-0.2, NLC-0.4, NLC-1.0, NEmu-10%, Mix-0.2, Mix-0.4 and Mix-1.0 (from the bottom to the top).

(values range from 2.6 K at formulation SLN to 3.9 K at formulation NLC-1.0). These two phenomena show an interaction of oily molecules with the crystalline matrix, but an incorporation can not be claimed necessarily. A depression of the melting point in these fine GB platelets can be provoked even through oil spots or layers on their surface. Just particle shape, colloidal character and particle environment have a big impact on the melting point [33] as particle size distribution [221,222], too.

It was claimed that MCT localization inside GB particles could be characterized by freezing out the dispersion downwards to temperatures of approximately minus 60 °C [223]. Interrelated MCT molecules should result in an endothermic crystallization event whereas statistically over the whole GB matrix distributed oil molecules should not be able to form MCT crystals with specific crystallization energy due to the hindering GB barrier. This method was found to be unsuitable for the given measuring problem. Freezing let to crystallize the outer water phase of the dispersion first and unpredictably other components were precipitated in this step. DSC results should be always discussed carefully because the method is invasive and the recorded measuring signals may come from a sample possibly changed by the temperature regimen.

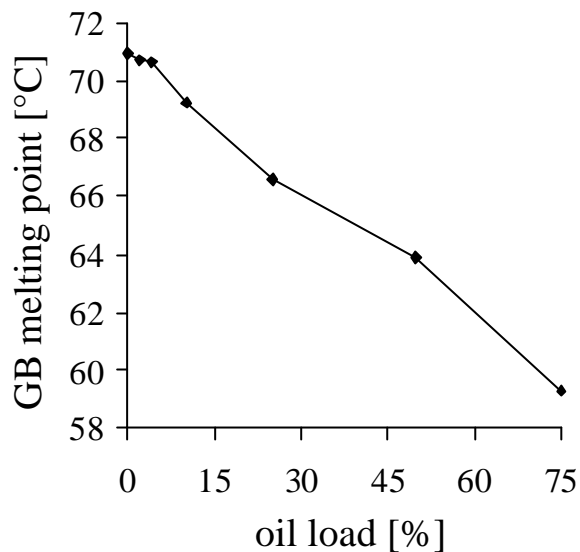


Fig. 24: Decrease in GB melting point with increasing MCT load of NLC (experiments done with oil loads from 0 to 75 %).

#### 4.9 Densimetric

Density is known to vary with the different modifications of a lipid. From earlier examinations [224] we know that oil load does not change the modification of GB.

Increasing MCT content lowered in strong linearity the density of the samples (figure 25). Due to the linearity it can be assumed that the packing density of the GB lattices is not disturbed or changed. MCT molecules are not incorporated in between the chains of the solid matrix. Moreover, because of the similarity to the densities gained with MIXes separated nanocompartments consisting of MCT or of GB make more sense. A disturbed packing density was claimed in [223] due to wrong interpretations of imprecise measurements.

#### 4.10 Refractometry

Further results on the interaction of the oil with the solid lipid matrix were obtained by refractometry (figure 26). Increasing MCT loads lower the refractive indices linearly correlated. For both samples NLC and MIX separated nanocompartments (MCT and GB) can be observed. Particles in the given nanometric range interact less pronounced but clearly detectable with light of 589 nm. Advantageous is the bright color of the thin lipid particles for the detection of light refraction.

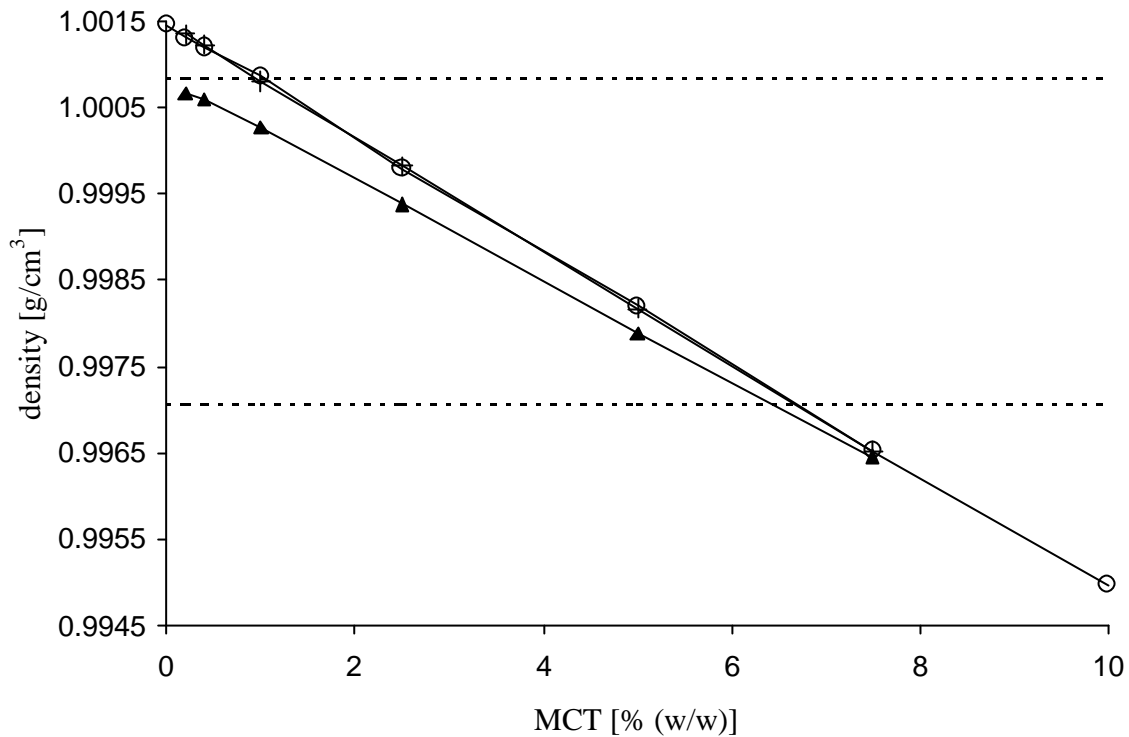


Fig. 25: Dependence of the density on the oil content at 25 °C (legend: circle for formulations of different oil loads (SLN, NLCs and NEmu-10%); cross for MIXES; triangle for samples NEmu; upper dashed line for a lipid-free poloxamer solution; lower dashed line for water). The density for MCT bulk was determined at 0.941569 g/cm<sup>3</sup>. Statistical ranges of each measuring point are too small to be drawn in the figure.

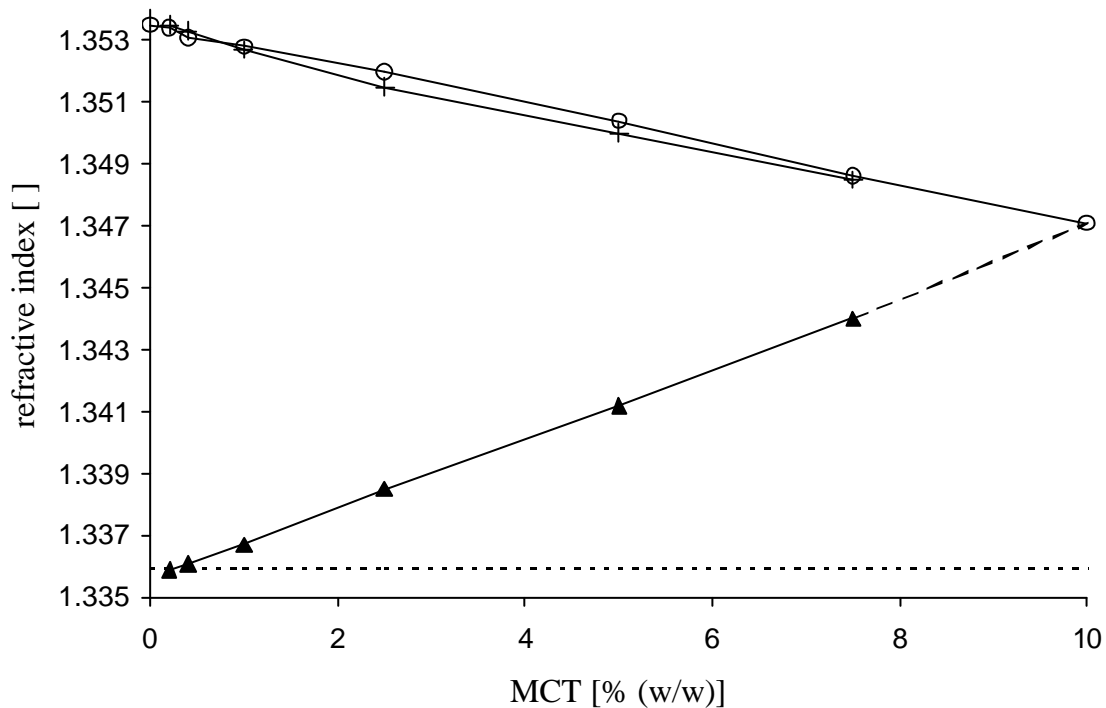


Fig. 26: Dependence of the refractive index on the oil content at 20 °C (legend: circle for formulations of different oil loads (SLN, NLCs and NEmu-10%); cross for MIXES; triangle for samples NEmu; horizontal dashed line for a lipid-free poloxamer solution). The maximal range for a median amounts to  $\pm 0.0003$  what makes possible differences between the two upper curves negligible, but what is too small to be drawn in the graphic.

To proceed on the rough assumption based on the claims in the literature that incorporated oil molecules are covered by the solid lipid matrix and that oil (and sensitive drug molecules inside the oily domains of NLC) are protected from rays of light, oil should not contribute to the refractive index. But the opposite was found, MCT contributes to the refractive index. Hence, light-sensitive drug molecules are not protected by NLC.

Failing light protection can be stated clearly. Nevertheless, by refractometry the model of expelled MCT from the solid core can not be confirmed for certain because little is known on light-particle interaction. Artifacts could be possible since a high penetration depth of light may capture incorporated oil in the solid core itself.

### **4.11 Cryo transmission electron microscopy (Cryo-TEM)**

The ultra structure of single lipid particles is revealed in the electron microscopic studies (figure 27).

The micrograph of NEmu-10% shows only circular dark structures which are attributed to spherical nanodroplets (figure 27, image A). The SLN dispersion has a completely different electron microscopic appearance (image B): weak circular and ellipsoidal structures represent thin platelets in top view. If the particles are viewed edge-on, they appear as dark rods or “needles” since, in this position, the increased thickness of the structures leads to a darker appearance. The rod- or needle-like particles in the electron micrographs were typically of a thickness of about 10 nm and below. It should be noted, however, that very large and thus potentially thicker particles may not be detected in this position since their dimensions may exceed the thickness of the sample film. Generally, cryoelectron micrographs tend to be strongly biased towards small particles as a result of the preparation technique. After applying the liquid sample to the microscopic grid excess liquid is removed with a piece of filter paper until only an extremely thin sample film remains in the holes of the grid, particularly in their center. Structures larger than the thickness of this film are either removed or relocated to thicker film areas (which are usually too sensitive towards the electron beam to be reliably investigated) during this process. Anisometric particles - such as platelets - may align in such a way that their largest dimension is stretched out in the plane of the film. As a result, a direct comparison of particle sizes observed in cryo TEM with the results of particle sizing techniques such as PCS or LD should not be performed for the dispersions under investigation.

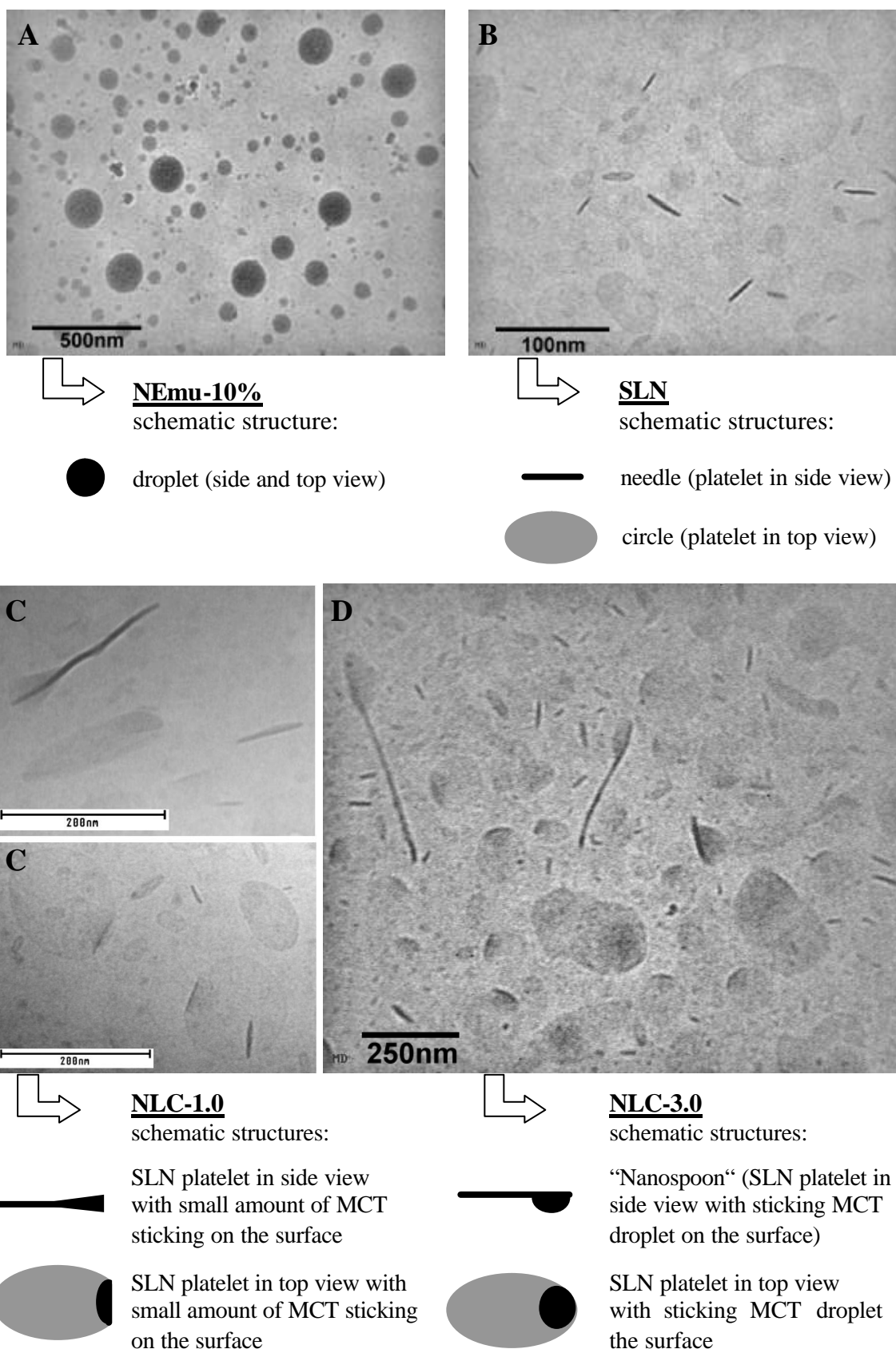


Fig. 27: Cryo-TEM images of lipid nanodispersions and proposed interpretation of the structures observed.

NLC-particles with an oil-load of 10, 30 and 50 % of the lipid phase were also under investigation. Examples of the results are shown in images C and D. From these micrographs, which show quite heterogeneous structures, it has to be concluded that GB-nanoparticles loaded with MCT represent “hybrid” structures between NEmu and SLN. As in the SLN dispersion (image B), “needles” and circular structures characteristic of crystalline, platelet-shaped particles can be detected. But compared to SLN, these structures are of modified appearance, e.g., with darker spots on the circular structures, or “caps” on the needles projected in side view. These spots and caps can be attributed to the presence of liquid oil on the surface of the crystalline GB particles. In some cases, the darker, crystalline lipid in side-view seems to be slightly bent around the oil fraction or even folded up. Already at a low oil load of only 10 % (image C) there are indications for the presence of two-phase particles. At an increased MCT load of 30 % (image D) among others a characteristic “nanospoon” structure can be observed where the liquid oil is localized as distinctive droplet with lower contrast on the solid lipid platelet projected in side view. In top view, the MCT spots appear darker than the platelet itself since their presence increases the thickness of the structure. Even though some particles seem to contain liquid oil on both platelet surfaces the localization on one side of the particle only seems to be energetically favorable compared to an even distribution over the whole particle surface as was previously also been observed for triglyceride nanoparticles loaded with the supercooled liquid drug ubidecarenone [192].

The question if the low MCT load of 10 % leads to asymmetric and non-spherical GB circles in top view and if the liquid MCT enables the platelet to fold up will require further investigations on these novel structures. The most important result of the electron microscopic investigations seems to be the oil separation as own nanocompartment within the nanoparticles. Moreover, the TEM analysis clearly reveals the anisometric shape of the particles with a high amount of solid lipid with particle sizes being in the range of that indicated by the light scattering techniques (table 2).

In contrast to some literature reports, where SLN are often assumed to be spherical [7,165,167,168] GB nanoparticles without oil load are imaged as thin platelets with circular to irregular contours (figure 27, image B). Particles with thicknesses as low as about 10 nm and below were observed in the GB dispersion. This corresponds to one or two molecular layers assuming a short spacing of 6.16 nm as reported for the  $\beta'$ -modification of GB [162]. Platelet-like particles consisting of a few molecular layers only have already been observed in

dispersions of saturated monoacid triglycerides in the  $\beta$ -modification [221,225]. Our present results lead to the conclusion that they can also form in dispersions of a complex glyceride mixture with comparatively low triglyceride content.

## 5 Summary and conclusions

### 5.1 English version

The aim of the present study was a physicochemical characterization of lipid nanodispersions, especially focused on colloidal solid lipid particles. The experiments should lead to a better understanding of structure and behavior of these very complex drug carrier systems.

SLN and nanoemulsions are easily to produce at small and large scale. All prepared samples are very well short-time stable over at least one month with respect to particle size, DSC, X-ray, NMR and ESR characteristics. Especially for GB particles strong ageing effects could not be observed in the studies, too, only by Raman spectroscopy slight changes in the spectra are detected during storage. But sometimes unpredictable gelation of SLN occurred during long-term storing what – in contrast - was never seen for nanoemulsions.

The NMR results show an immobilization of the oil in the NLC formulations. The immobilization in MCT GB particles is not at all comparable to high immobilization extent of the recrystallized melt of GB bulk containing 2 % oil. This is a strong indication that MCT molecules are not well fixed in the solid matrix of the particles. But clear statements if the liquid lipid molecules stay in the inner part of the solid matrix or stick on its outer surface finally will not can be done by NMR. For further information ESR studies were carried out.

The current in vitro ESR experiments on the nanoemulsion and on oil loaded GB-SLN demonstrate a preferable localization of the lipophilic model drug in the oil where it is better dissolved than in the solid lipid. Only decreasing MCT loads in the samples force TB molecules to concentrate on the lipid particle surface or to be dissolved in water. In pure SLN only a third of all TB molecules is located in a lipophilic compartment.

ESR reduction experiments show that all TB molecules in any compartment of SLN systems (including the more lipophilically localized molecules) are rapidly reduced from aqueous AA. NEmu-10% offered the best protection capacities for TB, a carrier which in general is known for immediate drug release! The inner volume of the droplets is better protected against water than the inner volume of SLN. NLC were found to lay in-between

SLN and NEmu-10%, according to their amount of oil content. The results of the ESR reduction experiments clearly show that the accommodation and protection of foreign lipophilic molecules is poor for SLN and NLC with low oil load.

By a further non-invasive technique, the fluorescence spectroscopy, the hydrophobic fluorescent marker NR indicates the polarity of its environment due to solvatochromism. SLN offered only one polar compartment for NR molecules, defined by water contact. Increasing MCT creates a hydrophobic compartment for NR. Spectrofluorometric studies show a poor incorporation capacity of the marker NR in SLN and NLC of low MCT load. Even the bulk weight of solid lipids can not accommodate reasonable amounts of the dye. Concerning incorporation capacity and protection from the outer water phase SLN and NLC are surpassed by a common nanoemulsion.

Measurements performed by X-ray and synchrotron radiation, densimetry, refractometry and Raman spectroscopy confirm the idea of intact GB lattices in spite of oil loading. The lipid crystals are not disturbed in their structure as it could be suggested in case of oil incorporation.

Beside incorporation capacity particle shape was investigated. Until now, solid lipid particles were described to be spherical [7,165,167,168] what should offer a maximal volume for drug and oil incorporation. Particle size analysis by PCS indicated differences between SLN and nanoemulsion. Assuming similar particle volumes after homogenization due to comparable homogenization efficiency and due to the same viscosity at the homogenization temperature for both lipid melts, the diffusion of anisometric shaped carriers in the PCS equipment is slower than for isometric particles. By inversion of an argument, the larger sizes obtained for SLN should reflect their anisometric shape.

In contrast to LD (and partly PCS) measurements, flow FFF discriminates between SLN, NLC and nanoemulsion. The droplets of the nanoemulsion are less retarded than NLC and SLN, above all. NEmu-10% eluted therefore earlier and showed smaller sizes. Together, it is a clear indication that the investigated solid lipid containing particles in general do not possess a spherical compact shape.

Finally, the ultra structure of the dispersions was revealed in TEM studies. The micrograph of the nanoemulsion shows only circular dark structures which are attributed to spherical nanodroplets. SLN present themselves as dark needle-shaped or weak ellipsoidal structures, i.e. platelets are viewed either in side or top view. For oil loaded solid particles

hybrid structures between nanoemulsion and SLN were found. Indeed, onto platelet-shaped particles oil spots or even little oil droplets (“nanospoons”) were found. In conclusion, the results on thin SLN platelets disprove the common assumption of incorporation of drug molecules or liquid oil compartments in voluminous SLN spheres. Liquid lipids adhere to the surface of thin crystalline lipid matrix particles forming clearly detectable droplets even at oil loads claimed to be completely incorporated [164,166].

The interesting thin platelet character of SLN combined with good drug access due to localization on the tremendous large particle surface area makes SLN attractive to be tested on ex vivo human skin by ESR. But SLN were not found to be superior to the established systems nanoemulsion and microemulsion. SLN platelets formed a wall made from solid lipid after water evaporation. This wall made further drug transport into the skin impossible. Although the drug is presented predominately on a large carrier surface, this did not correlate to a better bioavailability.

Summarizing, this thesis reveals the common theory of drug localization in the solid lipid particle core (SLN) as well as the incorporation of oily domains of high drug content in the particles (NLC) (figure 28 (a)). The results indicate that the studied colloidal lipid matrices show neither a protection from aqueous environment (what could be expected due to the solid matrix), nor retardation capacities, nor a sufficient incorporation rate. Instead of the postulated inner oil droplets (NLC) or incorporated drug molecules (SLN) in the solid matrix, the existence of drug or MCT molecules, respectively, presented on the solid particle surface is more probable in this complex system. Distribution of drug or oil (i.e. oil as molecules or as clusters) inside a crystallized matrix of a nanoparticle is not probable because crystals with their regular structures only tolerate rare defects to incorporate host molecules: Drug or oil, respectively, are ejected from the molten lipid mix during the lipid crystallization process at the cooling step. Even in case of 2 % oil loading (formulation NLC-0.2) oil expulsion happens, so the postulated oil incorporation rates up to 16 or 38 %, respectively [164,166], can not be confirmed. In case that it would have been successfully to incorporate at least this low amount of oil (what could not be found!) it would never be possible to reach a reasonable drug incorporation rate because of low drug solubility capacity in these few MCT molecules.

However, the liquid lipid in NLC remain adhered to the solid lipid particle surface. It forms spots on the particle surface (figure 28 (b)). Additionally, increasing oil rates (from

approximately 10 % up) lead to the formation of oily droplets sticking on comparatively small GB platelets (figure 28 (b)). Very short diffusion pathways in platelets, increased water-lipid interphases and low drug incorporation in crystalline lipids are the drawbacks of SLN and NLC compared to conventional nanoemulsions.

It should be remembered that all measurements were performed with a lipid consisting of glyceride mixtures with a less ordered matrix in  $\beta'$ -modification. X-ray diffraction patterns prove the  $\beta'$ -modification of SLN and NLC. By its numerous defects in crystal lattice GB should facilitate drug incorporation [35,182,226], i.e. show better accommodation than more regular structured triglycerides.

For all investigations lipophilic model drugs were used (TB, P3, NR). Even lipophilic substances did not show satisfactory incorporation in solid lipid carriers. It should be clearly pointed out that the concentrations of TB and NR amounted to 0.276 mg TB/g formulation or 0.25  $\mu$ g NR/g formulation, so the nanoparticles are only negligible loaded. It can be followed that attempts for higher loading rates or even the incorporation of hydrophilic molecules will be unsuccessful, although the latter is claimed in the literature [161].

Missing protection and failed incorporation of considerable drug amounts as well as solemn long-term stability problems (gelation, particle growth) will hinder the entrance of SLN and NLC into the industrial market in the future, too. Intravenous application is claimed but offers high potential risks due to particle size and platelet shape. Because of low incorporation rates in most cases SLN are not attractive to be given perorally, moreover, protection of drug molecules against acid or enzymes is not realizable.

The best opportunities for solid lipid nanoparticles are seen as compounds in cosmetic products. E.g. synergistic effects are known for sun blocker milks containing SLN where both sun rays are reflected at the particle surface and the sun blocking active substance absorbs ultraviolet radiation [227]. Disadvantageous is the use of lipids in sun screeners, modern formulations avoid the use of acne provoking ingredients. Skin caring creams with SLN promise an improved skin hydration due to occlusive effects of the SLN platelets [228].

In all key properties SLN are surpassed by a common nanoemulsion. The drawbacks of SLN are inherent due to the crystalline state of the nanocarrier. I.e., the crystalline state of SLN and NLC is the underlying idea of these nanocarriers, but in the same time the reason

for the above mentioned drawbacks. Modification changes or ad-mixtures of other lipophilic substances can not resolve the basic carrier conflict.

In general, lipid based drug carriers are very well tolerated in contact with human cells and there are worthy to be further investigated in the future - despite the disappointing results gained for SLN and NLC. Colloidal systems proposed as drug carriers do not at all present trivial systems. In the context of this thesis, their complexity is reflected in the choice of various, mostly non-invasive analyzing techniques. Drug delivery systems designed by nanotechnology are not a priori superior to conventional systems because of their colloidal size. Critical discussions on drug carriers which are basing on nanotechnology keep on being indispensable and highly fruitful.

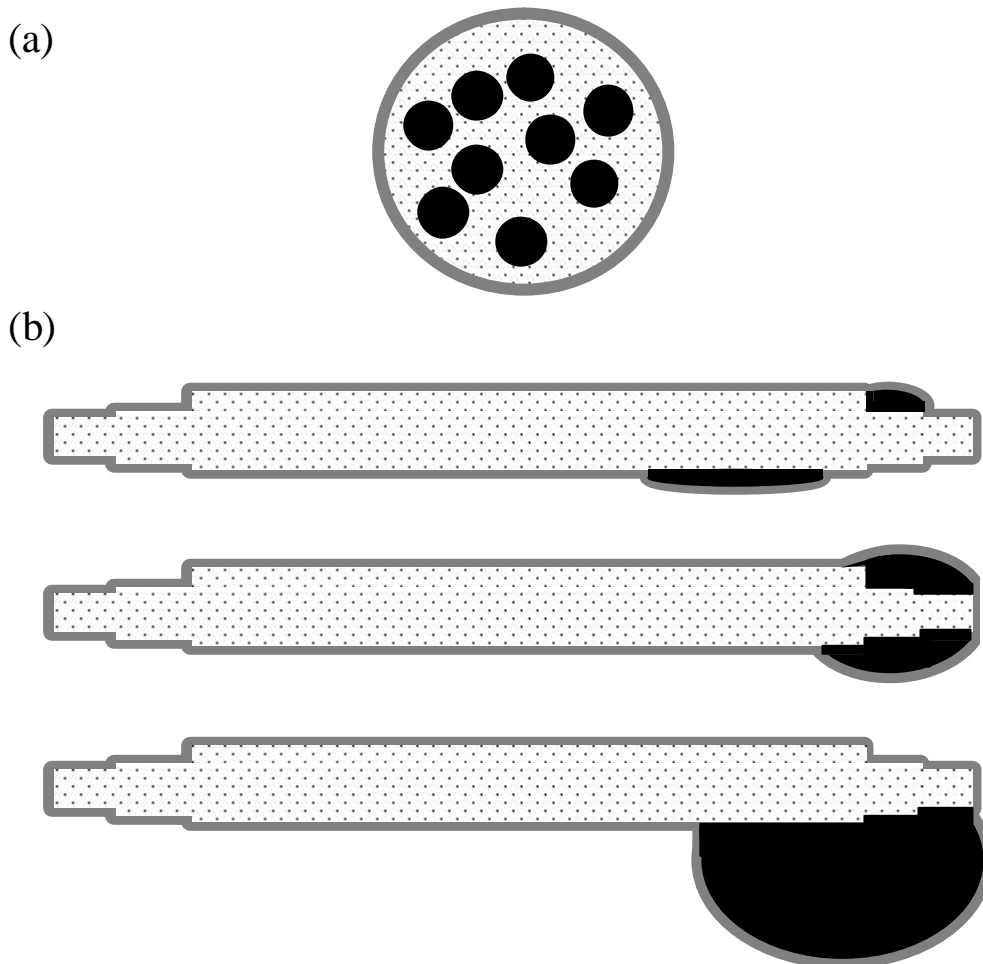


Fig. 28: Schematic structures of NLC, (a) model proposed in the literature, (b) models developed due to current experiments, varying with increasing amount of oil loading (■ oil (MCT), □ solid lipid (GB), ▒ stabilizer (poloxamer)).

### 5.2 German version

Zielsetzung der vorliegenden Arbeit war, Lipidnanodispersionen physikochemisch zu charakterisieren, wobei der Schwerpunkt der Untersuchungen auf kolloidalen festen Lipidpartikeln lag. Struktur und Dynamik dieser komplexen Arzneiträgersysteme sollten besser verstanden werden.

SLN und Nanoemulsionen lassen sich sowohl in kleinem Maßstab als auch großtechnisch herstellen. Alle im Rahmen dieser Arbeit hergestellten Proben erwiesen sich als sehr stabil innerhalb eines kurzen Zeitraumes von einem Monat, da sich Partikelgröße, DSC-Verhalten, Röntgendiffraktogramme, NMR- und ESR-Spektren nicht änderten. Ausgeprägte Alterungseffekte konnten für GB-Partikel nicht beobachtet werden, nur die Ramanspektroskopie wies leichte Spektrenveränderungen über den Lagerungszeitraum auf. Zudem trat über längere Lagerzeiträume gelegentlich und unvorhersehbar Gelierung der SLN auf - was jedoch im Gegensatz dazu für Nanoemulsionen nie feststellbar war.

NMR-Messungen zeigten eine Immobilisierung des Öls in den NLC-Formulierungen. Das Ausmaß der Immobilisierung von MCT in GB-Partikeln war jedoch unvergleichbar niedriger als die starke Immobilisierung von 2 % MCT-Zusatz in rekristallisiertem GB-Rohmaterial. Das ist ein deutlicher Hinweis darauf, daß die MCT-Moleküle nicht fest in der festen Matrix der Partikel verankert sind. Durch NMR-Messungen allein ist nicht eindeutig unterscheidbar, ob sich die Flüssiglipidmoleküle im Inneren oder an der Oberfläche der SLN aufhalten. ESR-Messungen sollten Klarheit schaffen.

Durch in vitro-ESR-Experimente an der Nanoemulsion und an ölbeladenen GB-SLN wurde der bevorzugte Aufenthalt des lipophilen Modellarzneistoffes im Öl nachgewiesen, wo er im Vergleich zum Festlipid besser gelöst wird. Lediglich abnehmende Ölbeladungen in den Proben zwingen die TB-Moleküle zu einer Aufkonzentrierung an der Lipidoberfläche oder zu einem Aufenthalt in Wasser. In konventionellen SLN ohne Ölbeladung fand sich nur ein Drittel aller TB-Moleküle in einem lipophilen Kompartiment lokalisiert.

ESR-Reduktionsexperimente zeigten, daß alle TB-Moleküle, unabhängig von ihrem Aufenthaltsort innerhalb der SLN-Dispersion, schnell von wäßriger Ascorbatlösung reduziert wurden. Das galt auch für TB-Moleküle in einem lipophilen SLN-Kompartiment. NEmu-10%, die Nanoemulsion, die im Allgemeinen für schnelle Arzneistofffreisetzung

bekannt ist, schützte TB am besten vor Reduktion! Das Innere der Emulsionstropfen hat weniger Kontakt zu der umgebenden Wasserphase als das Innere der SLN. NLC lagen bezüglich der Reduktionsgeschwindigkeit zwischen SLN und NEmu-10%, in der Reihenfolge ihres Ölgehaltes. Klar zeigten die ESR-Reduktionsexperimente, daß SLN und NLC mit geringer Ölbeladung nur wenige lipophile Fremdmoleküle aufzunehmen und kaum vor Reduktion/Wasserkontakt zu schützen vermögen.

Die Fluoreszenzspektroskopie als weitere Analysenmethode nutzt den Effekt der Solvatochromie. Das bedeutet, daß der hydrophobe Marker NR in Fluoreszenzspektren durch Wellenlängenverschiebung Auskunft über die Polarität seiner Umgebung gibt. SLN boten den NR-Molekülen nur eine polare Aufenthaltsmöglichkeit an, geprägt durch starken Wasserkontakt. Zunehmende Ölbeladung schuf ein stark hydrophobes Kompartiment für NR. Durch Spektrofluorometrie konnte zudem das geringe Inkorporierungsvermögen des Markers NR in SLN and NLC geringer Ölbeladung bestätigt werden. Sogar das Ausgangsmaterial der kristallinen Festfette duldet keine nennenswerte Einlagerung des Fluoreszenzfarbstoffes. Wiederum zeigte sich die Überlegenheit der Nanoemulsion gegenüber SLN und NLC in Bezug auf Inkorporierungsvermögen und Schutz vor umgebender Wasserphase.

Ergebnisse, die durch Röntgen- und Synchrotronmessungen, Densimetrie, Refraktometrie und Raman-Spektroskopie gewonnen wurden, bekräftigen die Idee intakter GB-Gitterstrukturen trotz vorhandener Ölbeladungen. Die Lipidkristalle sind in ihrem Aufbau nicht gestört, wie man es im Fall einer Ölinkorporierung erwarten könnte.

Neben der Inkorporierungskapazität wurde die Partikelform untersucht. Bis heute sind SLN in der Literatur als kugelförmig beschrieben [7,165,167,168], was maximalen Raum für Arzneistoff- und Öleinbettung bieten sollte. Partikelgrößenmessungen mittels PCS zeigten jedoch Unterschiede zwischen SLN und der Nanoemulsion. Unter der Voraussetzung, daß vergleichbare Homogenisierungskräfte auf beide Lipidschmelzen wirken und ihre Viskositäten bei der Homogenisationstemperatur übereinstimmen, sollten die Partikelvolumina annähernd vergleichbar sein. Die PCS-Methode detektierte für anisometrisch geformte Partikel eine langsamere Diffusion als für isometrische Teilchen. Im Umkehrschluß sollten die für SLN gemessenen höheren Partikelgrößen die anisometrische Form der Partikel widerspiegeln.

Im Gegensatz zu LD (und zum Teil PCS) vermag FFF zwischen SLN, NLC und

Nanoemulsion zu unterscheiden. Die Nanoemulsionströpfchen wurden weniger stark als NLC und SLN retardiert. Die Probe NEmu-10% wurde deswegen früher eluiert und zeigte kleinere Partikelgrößen. Zusammengefaßt wird deutlich, daß die untersuchten Partikel, sofern sie festes Lipid enthalten, keine kompakte Kugelform aufweisen.

Letzte Gewißheit über die Feinstruktur der Dispersionen wurde durch TEM-Studien erhalten. Die Aufnahmen der Nanoemulsion zeigten ausschließlich dunkle runde Strukturen, die kugelförmigen Nanotröpfchen zugeordnet werden konnten. SLN dagegen präsentierten sich als dunkle nadelförmige oder als leicht ellipsoide Gebilde, das heißt als Plättchen, die entweder von der Seite oder von oben betrachtet wurden. Für ölbeladene feste Teilchen wurden Mischformen zwischen Nanoemulsion und SLN gefunden. In der Tat saßen auf plättchenförmigen Partikeln punktförmig Ölsammlungen oder sogar kleine Öltröpfchen („Löffelstruktur“). In der Schlußfolgerung verwerfen die gewonnenen Ergebnisse (SLN als dünne Plättchen) die gängige Vorstellung voluminöser SLN-Kugeln, die Arzneistoff oder gar Ölkompimente einbetten sollen. Flüssiglipide haften an der Oberfläche der dünnen kristallinen Lipidmatrix, wo sie klar abgegrenzte Tröpfchen formen. Das war selbst bei Ölbeladungen zu beobachten, für die eine vollständige Inkorporierung postuliert wird [164,166].

Der dünne Plättchencharakter der SLN korreliert mit einer großen Oberfläche. Die große Oberfläche wiederum unterstützt eine Lokalisation von Arzneistoff auf der Oberfläche, was hervorragende Zutrittsmöglichkeit der umgebenden wäßrigen Phase bedeutet. Das interessante Aussehen der SLN macht sie attraktiv für ex vivo-ESR-Untersuchungen mit Humanhaut. Dort zeigten sie sich allerdings nicht überlegen im Vergleich zu bereits etablierten Systemen Nanoemulsion und Mikroemulsion. Die Plättchen formten nach Wasserverdunstung eine feste Lipidwand, die eine weitere Arzneistofffreisetzung verhinderte. Die starke Arzneistoffpräsentation an der Trägeroberfläche korrelierte nicht mit einer verbesserten Bioverfügbarkeit.

Zusammenfassend deckt die vorliegende Dissertation auf, daß die bis heute gängige Vorstellung einer Arzneistofflokalisierung im Festlipidkern (SLN) ebenso wie die Einbettung von Öldomänen mit erhöhtem Arzneistoffgehalt in den Partikeln (NLC) revidiert werden muß (Abbildung 1 (a)). Die Ergebnisse zeigen, daß die untersuchten kolloidalen Lipidmatrices weder einen Schutz vor umgebender Wasserphase bieten (was aufgrund der festen Matrix hätte erwartet werden können), noch retardierende

Eigenschaften oder ausreichende Inkorporierungskapazitäten aufweisen. Statt der postulierten inneren Öltröpfchen (NLC), beziehungsweise statt der inkorporierten Arzneistoffmoleküle (SLN) in der festen Lipidmatrix ist die Existenz von Arzneistoff- und/oder MCT-Molekülen auf der Partikeloberfläche dieser komplexen Systeme wahrscheinlicher. Die Arzneistoff- oder Ölverteilung (sei es als Ölmoleküle oder als Ölcluster) innerhalb des Kristallgitters eines Nanopartikels ist nicht wahrscheinlich, da Kristalle aufgrund ihrer regelmäßigen Strukturen nur wenige Fehlstellen zur potentiellen Einlagerung von Fremdmolekülen dulden: Arzneistoff beziehungsweise Öl werden während des Abkühlprozesses durch beginnende Kristallisation aus der (Misch-) Lipidschmelze herausgestoßen. Diese Ausstoßung findet sogar im Fall von nur 2 % Ölbeladung statt (Formulierung NLC-0.2), so daß die postulierten Ölinkorporierungsraten von 16 oder sogar 38 % [164,166] nicht bestätigt werden können. Selbst unter der Annahme, daß dieser geringe Anteil von 2 % Öl hätte eingebettet werden können (was nicht gefunden wurde!), so wäre es doch niemals möglich, in diesen wenigen Ölmolekülen eine ausreichend hohe Arzneistoffmenge zu lösen.

Festzuhalten bleibt, daß das flüssige Lipid in NLC an der Oberfläche der festen Lipidpartikel anhaftet, wobei es sich dort punktförmig ansammelt (Abbildung 1 (b)). Erst steigende Ölbeladungen (beginnend ab circa 10 %) führen zur Ausbildung von Öltröpfchen, die an vergleichsweise kleinen GB-Plättchen kleben (Abbildung 1 (b)). Die erforschten SLN und NLC zeigen Nachteile im Vergleich zu gewöhnlichen Nanoemulsionen, da der Plättchencharakter sehr kurze Diffusionswege bedingt, die Grenzfläche Wasser-Lipid erhöht wird und die Kristallinität der Lipide zu geringer Arzneistoffinkorporierung führt.

Zur Vollständigkeit sei daran erinnert, daß alle Untersuchungen an einem Lipid durchgeführt wurden, das ein Mischglycerid in relativ ungeordneter  $\beta'$ -Modifikation darstellt. Röntgendiffraktogramme bestätigen die  $\beta'$ -Modifikation von SLN und NLC. Durch die zahlreichen Kristallgitterdefekte sollte GB eine Arzneistoffeinlagerung erleichtern [35,182,226], in jedem Fall bessere Aufnahmekapazitäten als regelmäßiger strukturierte Triglyceride zeigen.

Für alle Untersuchungen wurden lipophile Modellarzneistoffe (TB, P3, NR) herangezogen. Sogar diese lipophilen Substanzen erreichten keine zufriedenstellende Inkorporierung in den festen Lipidpartikeln. Es muß klargestellt werden, daß die Konzentrationen 0,276 mg

TB/g Formulierung beziehungsweise 0,25 µg NR/g Formulierung betragen, so daß die Nanopartikel nur vernachlässigbar beladen waren. Daraus ist zu folgern, daß Bemühungen um eine höhere Arzneistoffbeladung oder gar die Inkorporierung hydrophiler Moleküle scheitern werden, obwohl letztere in der Literatur postuliert ist [161].

Fehlender Schutz, unzureichende Inkorporierung nennenswerter Arzneistoffkonzentrationen und bedenkliche Langzeitstabilitätsprobleme (Gelierung, Partikelwachstum) von SLN und NLC werden auch zukünftig eine erfolgreiche pharmazeutisch-industrielle Markteinführung verhindern. Die intravenöse Applikation der SLN wurde postuliert, birgt allerdings gefährliche Risiken aufgrund von Partikelgröße und -form. Perorale Gabe ist aufgrund der niedrigen Arzneistoffbeladungskapazität in den meisten Fällen nicht interessant, auch ist kein Schutz Arzneimoleküle vor Säure oder Enzymen realisierbar.

Als Zusatzstoffe in kosmetischen Produkten aber könnten SLN ihre besten Einsatzmöglichkeiten aufweisen. So sind synergistische Effekte bei Sonnenschutzmitteln beschrieben worden, bei denen die ultraviolette Strahlung sowohl an der Partikeloberfläche reflektiert als auch durch UV-Blocker absorbiert wird [227]. Nachteilig ist wiederum die Verwendung von Lipiden in den Sonnenschutzzubereitungen, moderne Mittel vermeiden den Zusatz dieser akneauslösenden Zusatzstoffe. Pflegende Hautcremes mit SLN versprechen eine verstärkte Hydratisierung der Haut, bedingt durch die okklusiven Effekte der SLN-Plättchen [228].

In allen Schlüsselparametern sind SLN einer gewöhnlichen Nanoemulsion unterlegen. Die Nachteile der SLN sind systembedingt aufgrund des kristallinen Zustands dieses Arzneistoffträgersystems. Der kristalline Zustand von SLN und NLC ist die zugrundeliegende Idee dieser Partikel, doch zugleich ist er der Hauptgrund für die oben angeführten Nachteile. Modifikationsänderungen oder Zumischung anderer lipophiler Substanzen können diesen Basiskonflikt nicht lösen.

Generell sind Arzneistoffträgersysteme auf Basis von Lipiden sehr gut humanverträglich, und sie lohnen zukünftige Forschungsaktivitäten – trotz der enttäuschenden Ergebnisse, die für SLN und NLC im Rahmen der vorliegenden Dissertation erhalten wurden. Kolloidale Arzneistoffträgersysteme stellen auf keinen Fall triviale Systeme dar. Ihrer Komplexität wurde im Rahmen der vorliegenden Arbeit durch Verwendung vielfältiger, meist nicht-invasiver Untersuchungsmethoden Rechnung getragen. Nanotechnologische Systeme sind konventionellen Systemen keinesfalls a priori überlegen, nur weil sie kolloidalen Charakter

aufweisen. Kritische Diskussionen über Arzneistoffträger, die auf Nanotechnologie basieren, bleiben unerlässlich und sind äußerst wertvoll.

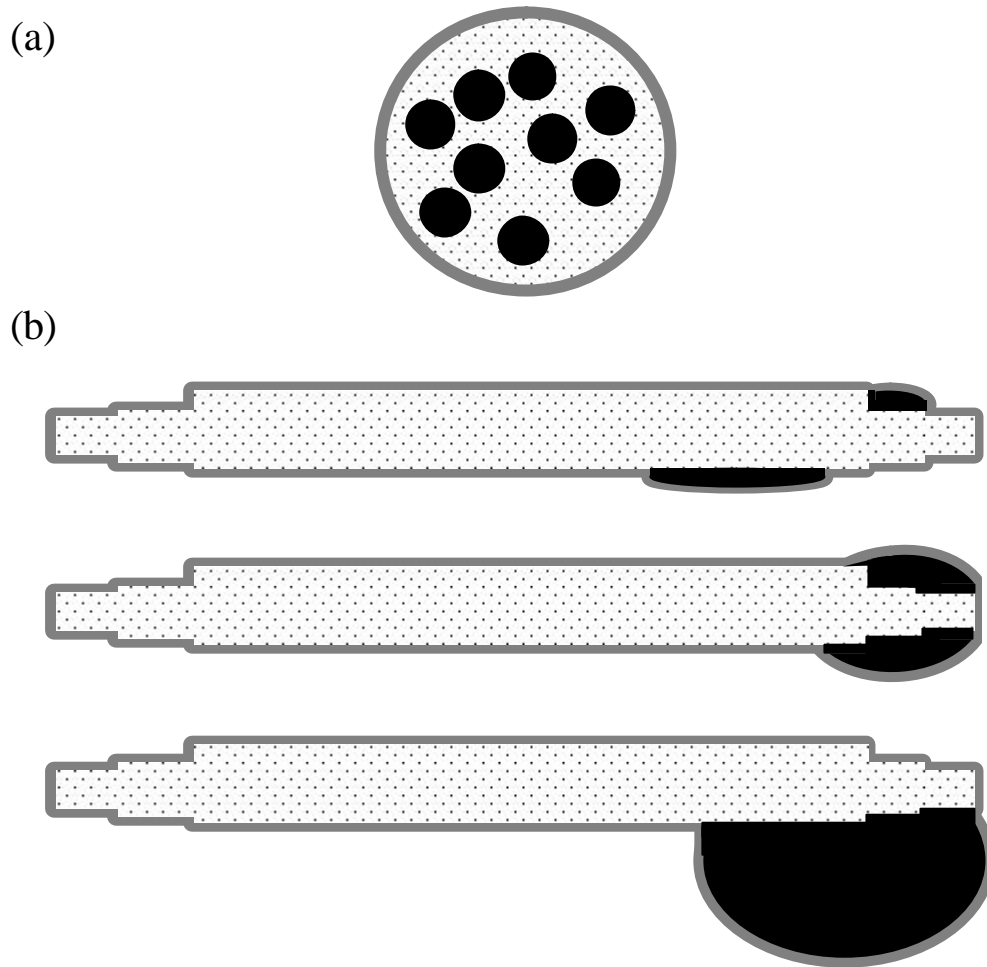


Abb. 1: Schematisch dargestellte Strukturen von NLC, (a) postuliertes Modell der Literatur, (b) aufgrund eigener Untersuchungen entwickelte Modelle, variierend durch zunehmende Ölbeladung (■ Öl (MCT), □ festes Lipid (GB), ■ Stabilisator (Poloxamer)).

## Bibliography

1. W. Mehnert and K. Mäder. Solid lipid nanoparticles: production, characterization and applications. *Adv. Drug Delivery Rev.* **47**:165-196 (2001).
2. G. M. Barratt. Therapeutic applications of colloidal drug carriers. *Pharm. Science and Technol. Today* **3**:163-169 (2000).
3. P. Couvreur, C. Dubernet, and F. Puisieux. Controlled drug delivery with nanoparticles: current possibilities and future trends. *Eur. J. Biopharm.* **41**:2-13 (1995).
4. G. L. Amidon, H. Lennernas, V. P. Shah, and J. R. Crison. A theoretical basis for a biopharmaceutic drug classification: the correlation of in vitro drug product dissolution and in vivo bioavailability. *Pharm. Res.* **12**:413-420 (1995).
5. R. Löbenberg and G. L. Amidon. Modern bioavailability, bioequivalence and biopharmaceutics classification system. New scientific approaches to international regulatory standards. *Eur. J. Biopharm.* **50**:3-12 (2000).
6. J. B. Dressman and C. Reppas. In vitro-in vivo correlations for lipophilic, poorly water-soluble drugs. *Eur. J. Pharm. Sci.* **11**:S73-S80 (2000).
7. R. H. Müller, M. Radtke, and S. A. Wissing. Solid lipid nanoparticles (SLN) and nanostructured lipid carriers (NLC) in cosmetic and dermatological preparations. *Adv. Drug Delivery Rev.* **54**:131-155 (2002).
8. Z. Cui and R. J. Mumper. Topical immunization using nanoengineered genetic vaccines. *J. Controlled Release* **81**:173-184 (2002).
9. R. Schubert. Liposomes in topical application and their mode of action in the skin. *Arch. Pharm.* **324**:627-633 (1991).
10. E. Allémann, J.-C. Leroux, and R. Gurny. Polymeric nano- and microparticles for the oral delivery of peptides and peptidomimetics. *Adv. Drug Delivery Rev.* **34**:171-189 (1998).
11. A. Meinzer, E. Müller, and J. Vonderscher. Perorale Mikroemulsionsformulierung - Sandimmun Optoral<sup>®</sup>/Neoral<sup>®</sup>. In: R. H. Müller and G. E. Hildebrand (eds), *Pharmazeutische Technologie: Moderne Arzneiformen*, Wissenschaftliche Verlagsgesellschaft mbH, Stuttgart, 1998, pp. 169-177.
12. A. K. Singla, A. Garg, and D. Aggarwal. Paclitaxel and its formulations. *Int. J. Pharm.* **235**:179-192 (2002).

13. M. Merodio, J. M. Irache, F. Valamanesh, and M. Mirshahi. Ocular disposition and tolerance of ganciclovir-loaded albumin nanoparticles after intravitreal injection in rats. *Biomaterials* **23**:1587-1594 (2002).
14. R. Abu-Dahab, U. F. Schäfer, and C.-M. Lehr. Lectin-functionalized liposomes for pulmonary drug delivery: effect of nebulization on stability and bioadhesion. *Eur. J. Pharm. Sci.* **14**:37-46 (2000).
15. J. B. Boyett and C. W. Davis. Injectable emulsions and suspensions. In: H. A. Lieberman, M. M. Rieger, and G. S. Banker (eds), *Pharmaceutical dosage forms - disperse systems*, Vol. 2, Marcel Dekker Inc., New York, 1989, pp. 379-416.
16. M. Nishikawa, Y. Takakura, and M. Hashida. Biofate of fat emulsions. In: S. Benita (ed), *Submicron emulsions in drug targeting and delivery*, Vol. 9, Drug targeting and delivery, Harwood academic publishers, Amsterdam, 1998, pp. 99-118.
17. A. N. Lukyanov, Z. G. Gao, L. Mazzola, and V. P. Torchilin. Polyethylene glycol-diacyllipid micelles demonstrate increased accumulation in subcutaneous tumors in mice. *Pharm. Res.* **19**:1424-1429 (2002).
18. K. K. Merdan, T. Hegener, O. Haberlein, and T. Kissel. Integrin targeting using RGD-PEI conjugates for in vitro gene transfer. *J. Gene Med.* **5**:588-599 (2003).
19. I. Brigger, J. Morizet, G. Aubert, H. Chacun, M.-J. Terrier-Lacombe, P. Couvreur, and G. Vassal. Poly(ethylene glycol)-coated hexadecylcyanoacrylate nanospheres display a combined effect for brain tumor targeting. *J. Pharmacol. Exp. Ther.* **303**:928-936 (2002).
20. A. N. Lukyanov, Z. Gao, and V. P. Torchilin. Micelles from polyethylene glycol/phosphatidylethanolamine conjugates for tumor drug delivery. *J. Controlled Release* **91**:97-102 (2003).
21. V. C. Mosqueira, P. Legrand, J. L. Morgat, M. Vert, E. Mysiakine, R. Gref, J. P. Devissaguet, and G. Barratt. Biodistribution of long-circulating PEG-grafted nanocapsules in mice: effects of PEG chain length and density. *Pharm. Res.* **18**:1411-1419 (2001).
22. G. Barratt. Colloidal drug carriers: achievements and perspectives. *Cell. Mol. Life Sc.* **60**:21-37 (2003).
23. C. Chauvierre, D. Labarre, P. Couvreur, and C. Vauthier. Novel polysaccheride-decorated poly(isobutyl cyanoacrylate) nanoparticles. *Pharm. Res.* **20**:1786-1793

- (2003).
24. C. Vauthier, C. Dubernet, C. Chauvierre, I. Brigger, and P. Couvreur. Drug delivery to resistant tumors: the potential of poly(alkyl cyanoacrylate) nanoparticles. *J. Controlled Release* **93**:151-160 (2003).
  25. B. P. C. Chow, E. A. Shaffer, and H. G. Parsons. Absorption of triglycerides in the absence of lipase. *Canadian J. Phys. Pharmacol.* **68**:519-523 (1990).
  26. J. Clement. Digestion and absorption of dietary triglycerides. *J. Physiologie* **72**:137-170 (1976).
  27. N. D. Gallagher and M. R. Playoust. Absorption of saturated and unsaturated fatty acids by rat jejunum and ileum. *Gastroenterology* **57**:9-18 (1969).
  28. G. Livesey. The absorption of stearic acid from triacylglycerols: an inquiry and analysis. *Nutrition Res. Rev.* **13**:185-214 (2000).
  29. U. Bracco. Effect of triglyceride structure on fat absorption. *Am. J. Clinical Nutrition* **66**:1002S-1009S (1994).
  30. L. P. Klemann, J. W. Finley, and G. A. Leveille. Estimation of the absorption coefficient of stearic acid in SALATRIM fats. *J. Agric. Food Chem.* **42**:484-488 (1994).
  31. J. W. Finley, L. P. Klemann, G. A. Leveille, M. S. Otterburn, and C. G. Walchak. Caloric availability of SALATRIM in rats and humans. *J. Agric. Food Chem.* **42**:495-499 (1994).
  32. H. Stricker. *Physikalische Pharmazie*, Wissenschaftliche Verlagsgesellschaft mbH, Stuttgart, 1987.
  33. B. Siekmann and K. Westesen. Thermoanalysis of the recrystallization process of melt-homogenized glyceride nanoparticles. *Coll. Surfaces B* **3**:159-175 (1994).
  34. L. H. Block. Emulsions and microemulsions. In: H. A. Lieberman, M. M. Rieger, and G. S. Banker (eds), *Pharmaceutical dosage forms - disperse systems*, Vol. 2, Marcel Dekker Inc., New York, 1989, pp. 335-378.
  35. V. Jennings and S. Gohla. Comparison of wax and glyceride solid lipid nanoparticles (SLN<sup>TM</sup>). *Int. J. Pharm.* **196**:219-222 (2000).
  36. A. Dingler, *Feste Lipid-Nanopartikel als kolloidale Wirkstoffträgersysteme zur dermalen Applikation*, PhD thesis, Berlin, 1998.
  37. J. Kreuter. Nanoparticles. In: J. Kreuter (ed), *Colloidal drug delivery systems*, Vol. 66, *Drugs and the pharmaceutical sciences*, Marcel Dekker Inc., New York, Basel

- and Hong Kong, 1994, pp. 219-342.
38. V. Jenning, M. Schäfer-Korting, and S. Gohla. Vitamin A-loaded solid lipid nanoparticles for topical use: drug release properties. *J. Controlled Release* **66**:115-126 (2000).
  39. J. Kristl, B. Volk, M. Gasperlin, M. Sentjurc, and P. Jurkovic. Effect of colloidal carriers on ascorbyl palmitate stability. *Eur. J. Pharm. Sci.* **19**:181-189 (2003).
  40. P. W. Atkins. *Physikalische Chemie*, VHC Verlagsgesellschaft mbH, Weinheim, 1990.
  41. T. Okubo and K. Kiriya. Structural and dynamic properties in the complex fluids of colloidal crystals, liquids and gases. *J. Mol. Liquids* **72**:347-364 (1997).
  42. A. z. Mühlen, C. Schwarz, and W. Mehnert. Solid lipid nanoparticles (SLN) for controlled drug delivery - drug release and release mechanism. *Eur. J. Biopharm.* **45**:149-155 (1998).
  43. A. Lamprecht, N. Ubrich, M. H. Pérez, C.-M. Lehr, M. Hoffmann, and P. Maincent. Biodegradable monodispersed nanoparticles prepared by pressure homogenization-emulsification. *Int. J. Pharm.* **184**:97-105 (1999).
  44. B. Magenheimer and S. Benita. Nanoparticle characterization: a comprehensive physicochemical approach. *S.T.P. Pharma Sciences* **1**:221-241 (1991).
  45. T. A. Barber. *Pharmaceutical particulate matter: analysis and control*, Interpharm Press Inc., Buffalo Grove, 1993.
  46. R. H. Müller. Nanosuspensionen - eine neue Formulierung für schwerlösliche Arzneistoffe. In: R. H. Müller and G. Hildebrand (eds), *Pharmazeutische Technologie: Moderne Arzneiformen*, Wissenschaftliche Verlagsgesellschaft mbH, Stuttgart, 1998, pp. 393-400.
  47. K. P. Krause and R. H. Müller. Production and characterisation of highly concentrated nanosuspensions by high pressure homogenisation. *Int. J. Pharm.* **214**:21-24 (2001).
  48. C. Jacobs, O. Kayser, and R. H. Müller. Production and characterisation of mucoadhesive nanosuspensions for the formulation of bupravaquone. *Int. J. Pharm.* **214**:3-7 (2001).
  49. E. Merisko-Liversidge, G. G. Liversidge, and E. R. Cooper. Nanosizing: a formulation approach for poorly-water-soluble compounds. *Eur. J. Pharm. Sci.* **18**:113-120 (2003).

50. A. T. Serajuddin. Solid dispersion of poorly water-soluble drugs: early promises, subsequent problems, and recent breakthroughs. *J. Pharm. Sciences* **88**:1058-1066 (1999).
51. R. H. Müller, C. Jakobs, and O. Kayser. Nanosuspensions for the formulation of poorly soluble drugs. In: F. Nielloud and G. Marti-Mestres (eds), *Pharmaceutical emulsions and suspensions*, Marcel Dekker Inc., New York and Basel, 2000.
52. A. E. Johnson. Analysis of the Young equation and use of the Kelvin equation in calculating the Gibbs excess. *Coll. Surfaces A* **202**:33-39 (2002).
53. K. H. Bauer, K.-H. Frömring, and C. Führer. *Lehrbuch der pharmazeutischen Technologie*, Wissenschaftliche Verlagsgesellschaft mbH, Stuttgart, 1999.
54. B. Siekmann and K. Westesen. Preparation and physicochemical characterization of aqueous dispersions of coenzyme Q10 nanoparticles. *Pharm. Res.* **12**:201-208 (1995).
55. Y. Barenholz and D. J. Crommelin. Liposomes as pharmaceutical dosage forms. In: J. Swarbrick and J. C. Boylan (eds), *Encyclopedia of pharmaceutical technology*, Vol. 9, Marcel Dekker Inc., New York, Basel and Hong Kong, 1994, pp. 1-39.
56. R. Schubert. Liposomen in Arzneimitteln. In: R. H. Müller and G. E. Hildebrand (eds), *Pharmazeutische Technologie: Moderne Arzneiformen*, Wissenschaftliche Verlagsgesellschaft mbH, Stuttgart, 1998, pp. 219-242.
57. M. Ghyczy. Arzneimittel mit Phosphatidylcholin und Liposomen: Entwicklung, Bewertung, Perspektiven. In: R. H. Müller and G. E. Hildebrand (eds), *Pharmazeutische Technologie: Moderne Arzneiformen*, Wissenschaftliche Verlagsgesellschaft mbH, Stuttgart, 1998, pp. 207-218.
58. D. D. Lasic. *Liposomes: from physics to applications*, Elsevier Science B.V., Amsterdam, 1993.
59. M. J. Otto. *Liposomes: from biophysics to therapeutics*, Marcel Dekker Inc., New York and Basel, 1987.
60. G. Gregoriadis, A. T. Florence, and H. M. Patel. Liposomes in drug delivery. A. T. Florence and G. Gregoriadis (eds), *Drug targeting and delivery*, Harwood Academic Publishers GmbH, Chur, 1993.
61. D. J. A. Crommelin and H. Schreier. Liposomes. In: J. Kreuter (ed), *Colloidal drug delivery systems*, Vol. 66, Drugs and the pharmaceutical sciences, Marcel Dekker Inc., New York, Basel and Hong Kong, 1994, pp. 73-190.

62. F. J. Martin. Pharmaceutical manufacturing of liposomes. In: P. Tyle (ed), *Specialized drug delivery systems*, Vol. 41, Drugs and the pharmaceutical sciences, Marcel Dekker Inc., New York and Basel, 1990, pp. 267-316.
63. A. T. Florence and C. Cable. Non-ionic surfactant vesicles (niosomes) as vehicles for doxorubicin delivery. In: G. Gregoriadis, A. T. Florence, and H. M. Patel (eds), *Liposomes in drug delivery*, Harwood Academic Publishers GmbH, Chur, 1993, pp. 239-253.
64. J. A. Bouwstra and H. E. J. Hofland. Niosomes. In: J. Kreuter (ed), *Colloidal drug delivery systems*, Vol. 66, Drugs and the pharmaceutical sciences, Marcel Dekker Inc., New York, Basel and Hong Kong, 1994, pp. 191-217.
65. H. Schreier and J. Bouwstra. Liposomes and niosomes as topical drug carriers: dermal and transdermal drug delivery. *J. Controlled Release* **30**:1-15 (1994).
66. H. Hauser. Short-chain phospholipids as detergents. *Biochim. Biophys. Acta* **1508**:164-181 (2000).
67. S. Segota, D. Tezak, and N. Ljubescic. Formation of vesicles in diluted aqueous solutions of surfactant investigated by direct analysis of light scattering. *Adv. Coll. Interface Sci.* **89-90**:283-291 (2001).
68. P. Alexandridis and T. A. Hatton. Poly(ethylene oxide)-poly(propylene oxide)-poly(ethylene oxide) block copolymer surfactants in aqueous solutions and at interfaces: thermodynamics, structure, dynamics, and modeling. *Coll. Surfaces B* **96**:1-46 (1995).
69. D. M. Small. *The physical chemistry of lipids: from alkanes to phospholipids*, Plenum Press, New York, 1986.
70. R. Voigt. *Pharmazeutische Technologie: für Studium und Beruf*, Deutscher Apotheker Verlag, Stuttgart, 2000.
71. I. Capek. Fate of excited probes in micellar systems. *Adv. Coll. Interface Sci.* **97**:89-147 (2002).
72. A. Meziani, A. Zradba, D. Touraud, M. Clause, and W. Kunz. Can aldehydes participate in the nanostructuring of liquids containing charged micelles? *J. Mol. Liquids* **73, 74**:107-118 (1997).
73. A. M. Wasserman, V. A. Kasaikin, Y. A. Zakharova, I. I. Aliev, V. Y. Baranovsky, V. Doseva, and L. L. Yasina. Molecular organization and dynamics of micellar phase of polyelectrolyte-surfactant complexes: ESR spin probe study.

- Spectrochimica Acta Part A* **58**:1241-1255 (2002).
74. K. Shinoda. Solvent properties of nonionic surfactants in aqueous solutions. In: K. Shinoda (ed), *Solvent properties of surfactant solutions*, Vol. 2, Surfactant science series, Marcel Dekker Inc., New York, 1967, pp. 27-63.
75. H. Wennerström and B. Lindman. Micelles. Physical chemistry of surfactant association. *Physics Reports* **52**:1-86 (1979).
76. R. Zana. Micellization of amphiphiles: selected aspects. *Coll. Surfaces A* **123-124**:27-35 (1997).
77. M. A. Hammad and B. W. Müller. Solubility and stability of tetrazepam in mixed micelles. *Eur. J. Biopharm.* **7**:49-55 (1998).
78. R. H. H. Neubert and M. Schwarz. Stable mixed micelles: a new efficient vehicle system for drugs. *Pharm. Res.* **14**:S707 (1997).
79. A. Supersaxo, W. R. Hein, and H. Steffen. Mixed micelles as a proliposomal, lymphotropic drug carrier. *Pharm. Res.* **8**:1286-1291 (1991).
80. G. A. Hussein, G. D. Myrup, W. G. Pitt, D. A. Christensen, and N. Y. Rapoport. Factors affecting acoustically triggered release of drugs from polymeric micelles. *J. Controlled Release* **69**:43-52 (2000).
81. A. Marin, M. Muniruzzaman, and N. Rapoport. Mechanism of the ultrasonic activation of micellar drug delivery. *J. Controlled Release* **75**:69-81 (2001).
82. V. P. Torchilin. Structure and design of polymeric surfactant-based drug delivery systems. *J. Controlled Release* **73**:137-172 (2001).
83. A. Krishnadas, I. Rubinstein, and H. Önyüksel. Sterically stabilized phospholipid mixed micelles: in vitro evaluation as a novel carrier for water-insoluble drugs. *Pharm. Res.* **20**:297-302 (2003).
84. N. Rapoport, W. G. Pitt, H. Sun, and J. L. Nelson. Drug delivery in polymeric micelles. *J. Controlled Release* **91**:85-95 (2003).
85. S. T. Hyde. Identification of lyotropic liquid crystalline mesophases. In: K. Holmberg (ed), *Handbook of applied surface and colloid chemistry*, John Wiley & Sons Ltd., Chichester, 2001.
86. S. Kutsumizu. The thermotropic mesophase: a curious mesophase. *Current opinion in solid state and materials science* **6**:537-543 (2002).
87. K. Larsson. Aqueous dispersions of cubic lipid-water phases. *Current opinion in colloid and interface science* **5**:64-69 (2000).

88. P. Garstecki and R. Holyst. Scattering patterns of self-assembled cubic phases. I. The model. *Langmuir* **18**:2519-2528 (2002).
89. P. Garstecki and R. Holyst. Scattering patterns of self-assembled cubic phases. II. Analysis of the experimental spectra. *Langmuir* **18**:2529-2537 (2002).
90. M. G. Carr, J. Corish, and O. I. Corrigan. Drug delivery from a liquid crystalline base across Visking and human stratum corneum. *Int. J. Pharm.* **157**:35-42 (1997).
91. B. Siekmann, H. Bunjes, M. H. J. Koch, and K. Westesen. Preparation and structural investigations of colloidal dispersions prepared from cubic monoglyceride-water phases. *Int. J. Pharm.* **244**:33-43 (2002).
92. M. L. Lynch, A. Ofori-Boateng, A. Hippe, K. Kochvar, and P. T. Spicer. Enhanced loading of water-soluble actives into bicontinuous cubic phase liquid crystals using cationic surfactants. *J. Coll. Interface Science* **260**:404-413 (2003).
93. B. J. Boyd. Characterisation of drug release from cubosomes using the pressure ultrafiltration method. *Int. J. Pharm.* **260**:239-247 (2003).
94. J. Patterson, A. Bary, and T. Rades. Physical stability and solubility of the thermotropic mesophase of fenoprofen calcium as pure drug and in a tablet formulation. *Int. J. Pharm.* **247**:147-157 (2002).
95. I. Danielsson and B. Lindman. The definition of microemulsion. *Coll. Surfaces B* **3**:391-392 (1981).
96. G. M. Eccleston. Microemulsions. In: J. Swarbrick and J. C. Boylan (eds), *Encyclopedia of pharmaceutical technology*, Vol. 9, Marcel Dekker Inc., New York, Basel and Hong Kong, 1994, pp. 375-421.
97. H. Wennerström, J. Daicic, U. Olsson, G. Jerke, and P. Schurtenberger. Sponge phases and balanced microemulsions: What determines their stability? *J. Mol. Liquids* **72**:15-30 (1997).
98. S. P. Moulik and B. K. Paul. Structure, dynamics and transport properties of microemulsions. *Adv. Coll. Interface Sci.* **78**:99-195 (1998).
99. R. Cortesi and C. Nastruzzi. Liposomes, micelles and microemulsions as new delivery systems for cytotoxic alkaloids. *Pharm. Science and Technol. Today* **2**:288-298 (1999).
100. L. M. Prince. *Microemulsions: theory and practice*, Academic Press Inc., New York, San Francisco and London, 1977.
101. D. Attwood. Microemulsions. In: J. Kreuter (ed), *Colloidal drug delivery systems*,

- Vol. 66, Drugs and the pharmaceutical sciences, Marcel Dekker, New York, Basel and Hong Kong, 1994, pp. 31-71.
102. M. Fanun, E. Wachtel, B. Antalek, A. Aserin, and N. Garti. A study of the microstructure of four-component sucrose ester microemulsions by SAXS and NMR. *Coll. Surfaces A* **180**:173-186 (2001).
103. M. Kreilgaard. Influence of microemulsions on cutaneous drug delivery. *Adv. Drug Delivery Rev.* **54**:S77-S98 (2002).
104. S. Klang and S. Benita. Design and evaluation of submicron emulsions as colloidal drug carriers for intravenous administration. In: S. Benita (ed), *Submicron emulsions in drug targeting and delivery*, Vol. 9, Drug targeting and delivery, Harwood academic publishers, Amsterdam, 1998, pp. 119-152.
105. P. Sherman. Emulsion science, Academic Press, London and New York, 1968.
106. E. Manegold. *Emulsionen*, Straßenbau, Chemie und Technik Verlagsgesellschaft mbH, Heidelberg, 1952.
107. P. Becher. *Emulsions: theory and practice*, New York, 1965.
108. K. Westesen and T. Wehler. Physicochemical characterization of a model intravenous oil-in-water emulsion. *J. Pharm. Sciences* **81**:777-786 (1992).
109. S. E. Tabibi. Production of disperse drug delivery systems. In: P. Tyle (ed), *Specialized drug delivery systems*, Marcel Dekker Inc., New York and Basel, 1990, pp. 317-331.
110. M. B. Schulz and R. Daniels. Hydroxypropylmethylcellulose (HPMC) as emulsifier for submicron emulsions: influence of molecular weight and substitution type on the droplet size after high-pressure homogenization. *Eur. J. Biopharm.* **49**:231-236 (2000).
111. M. Jumaa and B. W. Müller. The effect of oil components and homogenization conditions on the physicochemical properties and stability of parenteral fat emulsions. *Int. J. Pharm.* **163**:81-89 (1998).
112. I. B. Ivanov and P. A. Kralchevsky. Stability of emulsions under equilibrium and dynamic conditions. *Coll. Surfaces A* **128**:155-175 (1997).
113. H. Karbstein and H. Schubert. Simulation der Langzeitstabilität von O/W-Emulsionen. *Chem.-Ing.-Tech.* **66**:97-99 (1994).
114. D. Rousseau. Fat crystals and emulsion stability - a review. *Food Res. Internat.* **33**:3-14 (2000).

115. S. E. Friberg and K. Larsson. Food emulsions, *Food science and technology*, Marcel Dekker Inc., New York, Basel and Hong Kong, 1997.
116. J. Schmitt. Parenterale Fetteemulsionen als Arzneistoffträger. In: R. H. Müller and G. Hildebrand (eds), *Pharmazeutische Technologie: Moderne Arzneiformen*, Wissenschaftliche Verlagsgesellschaft mbH, Stuttgart, 1998, pp. 137-142.
117. L. C. Collins-Gold, R. T. Lyons, and L. C. Bartholow. Parenteral emulsions for drug delivery. *Adv. Drug Delivery Rev.* **5**:189-208 (1990).
118. S. Amselem and D. Friedman. Submicron emulsions as drug carriers for topical administration. In: S. Benita (ed), *Submicron emulsions in drug targeting and delivery*, Vol. 9, Drug targeting and delivery, Harwood academic publishers, Amsterdam, 1998, pp. 153-173.
119. S. Gohla. Multiple Emulsionen vom Typ Wasser-in-Öl-in-Wasser (W/O/W) in Kosmetika. In: R. H. Müller and G. Hildebrand (eds), *Pharmazeutische Technologie: Moderne Arzneiformen*, Wissenschaftliche Verlagsgesellschaft mbH, Stuttgart, 1998, pp. 195-206.
120. N. Garti, A. Aserin, I. Tiunova, and H. Binyamin. Double emulsions of water-in-oil-in-water stabilized by alpha-form fat microcrystals. Part 1: selection of emulsifiers and fat microcrystalline particles. *J. Am. Oil. Chem.* **76**:383-389 (1999).
121. N. Garti and A. Aserin. Double emulsions stabilized by macromolecular surfactants. *Adv. Coll. Interface Sci.* **65**:37-69 (1996).
122. P. Couvreur, P. Tulkens, M. Roland, A. Trouet, and P. Speiser. Nanocapsules: a new type of lysosomotropic carrier. *Fed. Eur. Biochem. Soc. Letters* **84**:323-326 (1977).
123. R. Alvarez-Román, G. Barré, R. H. Guy, and H. Fessi. Biodegradable polymer nanocapsules containing a sunscreen agent: preparation and photoprotection. *Eur. J. Biopharm.* **52**:191-195 (2001).
124. H. Fessi, F. Puisieux, N. Ammoury, and S. Benita. Nanocapsule formation by interfacial polymer deposition following solvent displacement. *Int. J. Pharm.* **55**:R1-R4 (1989).
125. M. Aboubakar, F. Puisieux, P. Couvreur, and C. Vauthier. Physico-chemical characterization of insulin-loaded poly(isobutylcyanoacrylate) nanocapsules obtained by interfacial polymerization. *Int. J. Pharm.* **183**:63-66 (1999).
126. T. Pitaksuteepong, N. M. Davies, I. G. Tucker, and T. Rades. Factors influencing

- the entrapment of hydrophilic compounds in nanocapsules prepared by interfacial polymerisation of water-in-oil microemulsions. *Eur. J. Biopharm.* **53**:335-342 (2002).
127. A. Lamprecht, Y. Bouligand, and J. P. Benoît. New lipid nanocapsules exhibit sustained release properties for amiodarone. *J. Controlled Release* **84**:59-68 (2002).
128. J. Kreuter. Nanoparticle-based drug delivery systems. *J. Controlled Release* **16**:169-176 (1991).
129. E. Allémann, R. Gurny, and E. Doelker. Drug-loaded nanoparticles - preparation methods and drug targeting issues. *Eur. J. Biopharm.* **39**:173-191 (1993).
130. L. Brannon-Peppas. Recent advances on the use of biodegradable microparticles and nanoparticles in controlled drug delivery. *Int. J. Pharm.* **116**:1-9 (1995).
131. P. Couvreur and C. Vauthier. Polyalkylcyanoacrylate nanoparticles as drug carrier: present state and perspectives. *J. Controlled Release* **17**:187-198 (1991).
132. J. Kreuter. Peroral administration of nanoparticles. *Adv. Drug Delivery Rev.* **7**:76-86 (1991).
133. M. C. Venier-Julienne and J. P. Benoît. Preparation, purification and morphology of polymeric nanoparticles as drug carriers. *Pharm. Acta Helveticae* **71**:121-128 (1996).
134. R. Gurny, N. A. Peppas, D. D. Harrington, and G. S. Banker. Development of biodegradable and injectable latices for controlled release of potent drugs. *Drug Dev. Ind. Pharm.* **7**:1-25 (1981).
135. R. Bodmeier and H. Chen. Indomethacin polymeric nanosuspensions prepared by microfluidization. *J. Controlled Release* **12**:223-233 (1990).
136. D. Lemoine, C. Francois, F. Kedzierewicz, V. Preat, M. Hoffman, and P. Maincent. Stability study of nanoparticles of poly(epsilon-caprolactone), poly(D,L-lactide) and poly(D,L-lactide-co-glycolide). *Biomaterials* **17**:2191-2197 (1996).
137. L. Illum, M. A. Khan, E. Mak, and S. S. Davis. Evaluation of carrier capacity and release characteristics for poly(butyl 2-cyanoacrylate) nanoparticles. *Int. J. Pharm.* **30**:17-28 (1986).
138. B. Siekmann and K. Westesen. Submicron-sized parenteral carrier systems based on solid lipids. *Pharm. Pharmacol. Lett.* **1**:123-126 (1992).
139. R. H. Müller, W. Mehnert, J.-S. Lucks, C. Schwarz, A. z. Mühlen, H. Weyhers, C. Freitas, and D. Rühl. Solid lipid nanoparticles (SLN) - an alternative colloidal

- carrier system for controlled drug delivery. *Eur. J. Biopharm.* **41**:62-69 (1995).
140. R. H. Müller and J. S. Lucks, Arzneistoffträger aus festen Lipidteilchen (Feste Lipidnanosphären (SLN)), European Patent EP 0 605 497 B1, 1996.
141. R. H. Müller, K. Mäder, and S. Gohla. Solid lipid nanoparticles (SLN) for controlled drug delivery - a review of the state of the art. *Eur. J. Biopharm.* **50**:161-177 (2000).
142. K. Westesen and B. Siekmann, Solid lipid particles, particles of bioactive agents and methods for the manufacture and use thereof, United States Patent 5,785,976, 1998.
143. R. H. Müller, S. Maaßen, H. Weyhers, F. Specht, and J. S. Lucks. Cytotoxicity of magnetite-loaded polylactide, polylactide/glycolide particles and solid lipid nanoparticles. *Int. J. Pharm.* **138**:85-94 (1996).
144. R. Lander, W. Manger, M. Scouloudis, A. Ku, C. Davis, and A. Lee. Gaulin homogenization: a mechanistic study. *Biotechnol. Prog.* **16**:80-85 (2000).
145. N. Rodriguez-Hornedo. Crystallization and the properties of crystals. In: J. Swarbrick and J. C. Boylan (eds), *Encyclopedia of pharmaceutical technology*, Vol. 3, Marcel Dekker Inc., New York and Basel, 1990, pp. 399-434.
146. S. Liedtke, S. Wissing, R. H. Müller, and K. Mäder. Influence of high pressure homogenisation equipment on nanodispersions characteristics. *Int. J. Pharm.* **196**:183-185 (2000).
147. M. R. Gasco, Method for producing solid lipid microspheres having a narrow size distribution, United States Patent 5,250,236, 1993.
148. B. Siekmann and K. Westesen. Investigations on solid lipid nanoparticles prepared by precipitation in o/w emulsions. *Eur. J. Biopharm.* **43**:104-109 (1996).
149. M. Trotta, F. Debernardi, and O. Caputo. Preparation of solid lipid nanoparticles by a solvent emulsification-diffusion technique. *Int. J. Pharm.* **257**:153-160 (2003).
150. F. Q. Hu, H. Yuan, H. H. Zhang, and M. Fang. Preparation of solid lipid nanoparticles with clobetasol propionate by a novel solvent diffusion method in aqueous system and physicochemical characterization. *Int. J. Pharm.* **239**:121-128 (2002).
151. P. Speiser, Lipidnanopellets als Trägersystem für Arzneimittel zur peroralen Anwendung, European Patent EP 0167825, 1990.
152. A. J. Domb, Lipospheres for controlled delivery of substances, United States Patent

- 5,188,837, 1993.
153. K. Sato. Solidification and phase transformation behaviour of food fats - a review. *Fett/Lipid* **101**:467-474 (1999).
154. F. D. Gunstone, J. L. Harwood, and F. B. Padley. The lipid handbook, Chapman and Hall, London and New York, 1986.
155. R. J. Hamilton and J. Cast. Spectral properties of lipids, Sheffield Academic Press Ltd, Sheffield, 1999.
156. S. Brösel and H. Schubert. Investigations on the role of surfactants in mechanical emulsification using a high-pressure homogenizer with an orifice valve. *Chem. Engin. Proc.* **38**:533-540 (1999).
157. K. Taiwo, H. Karbstein, and H. Schubert. Einfluß von Temperatur und Zusatzstoffen auf die Adsorptionskinetik von Lebensmittelemulgatoren. *Wiss. Abschlußberichte/Int. Sem. f. Forsch. u. Lehre in Chemieing.-Wiss., Techn. u. Phys. Chem. d. Univ. Karlsruhe* **28**:125-136 (1993).
158. H. Schubert and H. Armbruster. Principles of formation and stability of emulsions. *Int. Chem. Engin.* **32**:14-28 (1992).
159. E. Ugazio, R. Cavalli, and M. R. Gasco. Incorporation of cyclosporin A in solid lipid nanoparticles (SLN). *Int. J. Pharm.* **241**:341-344 (2002).
160. M. García-Fuentes, D. Torres, and M. J. Alonso. Design of lipid nanoparticles for the oral delivery of hydrophilic macromolecules. *Coll. Surfaces B* **27**:159-168 (2003).
161. W. Mehnert, A. z. Mühlen, A. Dingler, H. Weyhers, and R. H. Müller. Solid lipid nanoparticles - ein neuartiger Wirkstoff-Carrier für Kosmetika und Pharmazeutika. 2. Mitteilung: Wirkstoff-Inkorporation, Freisetzung und Sterilisierbarkeit. *Pharm. Ind.* **59**:511-514 (1997).
162. K. Westesen, H. Bunjes, and M. H. J. Koch. Physicochemical characterization of lipid nanoparticles and evaluation of their drug loading capacity and sustained release potential. *J. Controlled Release* **48**:223-236 (1997).
163. K. Westesen and B. Siekmann. Investigation of the gel formation of phospholipid-stabilized solid lipid nanoparticles. *Int. J. Pharm.* **151**:35-45 (1997).
164. V. Jennings, A. F. Thünemann, and S. H. Gohla. Characterisation of a novel solid lipid nanoparticle carrier system based on binary mixtures of liquid and solid lipids. *Int. J. Pharm.* **199**:167-177 (2000).

165. R. H. Müller, M. Radtke, and S. A. Wissing. Nanostructured lipid matrices for improved microencapsulation of drugs. *Int. J. Pharm.* **242**:121-128 (2002).
166. V. Jenning, K. Mäder, and S. H. Gohla. Solid lipid nanoparticles (SLN<sup>TM</sup>) based on binary mixtures of liquid and solid lipids: a <sup>1</sup>H-NMR study. *Int. J. Pharm.* **25**:15-21 (2000).
167. A. Dingler, R. P. Blum, H. Niehus, R. H. Müller, and S. Gohla. Solid lipid nanoparticles (SLN<sup>TM</sup>/Lipopearls<sup>TM</sup>) - a pharmaceutical and cosmetic carrier for the application of vitamin E in dermal products. *J. Microencapsulation* **16**:751-767 (1999).
168. A. z. Mühlen, Feste Lipidnanopartikel mit prolongierter Wirkstoffliberation - Herstellung, Langzeitstabilität, Charakterisierung, Freisetzungverhalten und -mechanismen, PhD thesis, Berlin, 1996.
169. H. P. Fiedler. *Lexikon der Hilfsstoffe für Pharmazie, Kosmetik und angrenzende Gebiete*, Editio Cantor Verlag, Aulendorf, 1996.
170. BASF. *Technical information for Lutrol F 68<sup>TM</sup>*, Ludwigshafen, Germany, 1997.
171. C. Kroll, Analytik, Stabilität und Biotransformation von Spinsonden sowie deren Einsatz im Rahmen pharmazeutisch-technologischer und biopharmazeutischer Untersuchungen, PhD thesis, Berlin, 1999.
172. M. Bockisch. *Nahrungsfette und -öle*, Ulmer, Stuttgart, 1993.
173. S. Jahnke. The theory of high-pressure homogenization. In: R. H. Müller and B. H. L. Böhm (eds), *Dispersion techniques for laboratory and industrial scale processing*, Vol. 42, paperback APV, Wissenschaftliche Verlagsgesellschaft mbH, Stuttgart, 2001, pp. 7-30.
174. U. Schäfer and H. Loth. An ex vivo model for the study of drug penetration into human skin. *Pharm. Res.* **13**:S399 (1996).
175. L. Wcislak, H. Klein, H. J. Bunge, U. Garbe, T. Tschentscher, and J. R. Schneider. Texture analysis with high-energy synchrotron radiation. *J. Applied Crystallography* **35**:82-95 (2002).
176. R. H. Müller and R. Schuhmann. *Teilchengrößemessung in der Laborpraxis*, Wissenschaftliche Verlagsgesellschaft mbH, Stuttgart, 1996.
177. R. J. Haskell, J. R. Shifflett, and P. A. Elzinga. Particle-sizing technologies for submicron emulsions. In: S. Benita (ed), *Submicron emulsions in drug targeting and delivery*, Vol. 9, Drug targeting and delivery, Harwood academic publishers,

- Amsterdam, 1998, pp. 21-98.
178. A. Fischer-Carius, Untersuchungen an extrudierten und sphäronisierten Matrixpellets mit retardierter Wirkstofffreigabe, PhD thesis, Berlin, 1998.
  179. C. R. Cantor and P. R. Schimmel. *Biophysical chemistry: techniques for the study of biological structure and function*, Freeman, San Francisco, 1980.
  180. B. Sjöström, A. Kaplun, Y. Talmon, and B. Cabane. Structures of nanoparticles prepared from oil-in-water emulsions. *Pharm. Res.* **12**:39-48 (1995).
  181. K. Westesen, M. Drechsler, and H. Bunjes. Colloidal dispersions based on solid lipids. In: E. Dickinson and R. Miller (eds), *Food colloids: fundamentals of formulation*, Royal society of chemistry, Cambridge, 2001, pp. 103-115.
  182. H. Bunjes, K. Westesen, and M. H. J. Koch. Crystallization tendency and polymorphic transitions in triglyceride nanoparticles. *Int. J. Pharm.* **129**:159-173 (1996).
  183. H. Bunjes, Einflußnahme unterschiedlicher Faktoren auf Struktur und Eigenschaften von Nanopartikeln aus festen Triglyceriden, PhD thesis, Jena, 1998.
  184. A. Lippacher, R. H. Müller, and K. Mäder. Semisolid SLN<sup>TM</sup> dispersions for topical application: influence of formulation and production parameters on viscoelastic properties. *Eur. J. Biopharm.* **53**:155-160 (2002).
  185. M. Schimpf, K. Caldwell, and J. C. Giddings. *Field-flow fractionation handbook*, Wiley-Interscience, New York, Chichester, Weinheim, Brisbane, Singapore, Toronto, 2000.
  186. L. Dulog and T. Schauer. Field-flow fractionation for particle size determination. *Prog. Org. Coatings* **28**:25-31 (1996).
  187. J. C. Giddings. Field-flow fractionation: analysis of makromolekular, colloidal, and particulate mater. *Science* **260**:1456-1465 (1993).
  188. B. Siekmann and K. Westesen. Submicron lipid suspensions (solid lipid nanoparticles) versus lipid nanoemulsions: similarities and differences. In: S. Benita (ed), *Submicron emulsions in drug targeting and delivery*, Vol. 9, Drug targeting and delivery, Harwood academic publishers, Amsterdam, 1998, pp. 205-218.
  189. M. Wohlgemuth, Diffusionsexperimente an Nanokapseldispersionen: Größenverteilung, Wirkstofffreisetzung und andere dynamische Phänomene, Ph. D. thesis, Duisburg, 2002.

190. A. A. Ribeiro and E. A. Dennis. Structure and dynamics by NMR and other methods. In: M. J. Schick (ed), *Nonionic Surfactants*, Physical Chemistry, Marcel Dekker Inc., New York, 1987, pp. 971-1009.
191. K. Jores, S. Liedtke, W. Mehnert, and K. Mäder. Characterization of solid lipid nanoparticles (SLN<sup>TM</sup>) - how to optimize the quantity of surfactants, *27th Intern. Symp. Control. Rel. Bioact. Mater.*, Vol. 27, Controlled release society, Paris, 2000, 1092-1093.
192. H. Bunjes, M. Drechsler, M. H. J. Koch, and K. Westesen. Incorporation of the model drug ubidecarenone into solid lipid nanoparticles. *Pharm. Res.* **18**:287-293 (2001).
193. H. Bunjes, B. Siekmann, and K. Westesen. Emulsions of supercooled melts - a novel drug delivery system. In: S. Benita (ed), *Submicron emulsions in drug targeting and delivery*, Vol. 9, Drug targeting and delivery, Harwood academic publishers, Amsterdam, 1998, pp. 175-204.
194. C. Mayer, D. Hoffmann, and M. Wohlgemuth. Structural analysis of nanocapsules by nuclear magnetic resonance. *Int. J. Pharm.* **242**:37-46 (2002).
195. K. Mäder, H. M. Swartz, R. Stösser, and H.-H. Borchert. The application of EPR spectroscopy in the field of pharmacy. *Pharm. Unserer Zeit* **49**:97-101 (1994).
196. A. Haberland, C. S. Maia, K. Jores, M. Dürrfeld, W. Mehnert, I. Schimke, B. Christ, and M. Schäfer-Korting. Albumin effects on drug absorption and metabolism in reconstructed epidermis and excised pig skin. *Altex* **20**:3-9 (2003).
197. V. Jennings, A. Gysler, M. Schäfer-Korting, and S. H. Gohla. Vitamin A loaded solid lipid nanoparticles for topical use: occlusive properties and drug targeting to the upper skin. *Eur. J. Biopharm.* **49**:211-218 (2000).
198. C. Santos-Maia, W. Mehnert, and M. Schäfer-Korting. Solid lipid nanoparticles as drug carriers for topical glucocorticoids. *Int. J. Pharm.* **196**:165-167 (2000).
199. R. Neubert and W. Wohlrab. In vitro methods for the biopharmaceutical evaluation of topical formulations. *Act. Pharm. Technol.* **36**:197-206 (1990).
200. B. W. Müller and P. Kleinebudde. Investigations of so-called microemulsions. Part 2. Investigations of drug-containing systems. *Pharmind* **50**:1301-1306 (1988).
201. J. Kemken, A. Ziegler, and B. W. Müller. Investigations into the pharmacodynamic effects of dermally administered microemulsions containing beta-blockers. *J. Pharm. Pharmacol.* **43**:679-684 (1991).

202. P. Greenspan and S. D. Fowler. Spectrofluorometric studies of the lipid probe nile red. *J. Lipid Res.* **26**:781-789 (1985).
203. C. Olbrich, O. Kayser, A. Lamprecht, C. Kneuer, C. M. Lehr, and R. H. Müller. Interactions of fluorescent solid lipid nanoparticles (SLN) with macrophage-like cells visualized by CLSM, *International Meeting on Pharmaceutics, Biopharmaceutics and Pharmaceutical Technology*, APV/APGI, Berlin, 2000, 331-332.
204. A. Hantzsch. Über die Halochromie und "Solvatochromie" des Dibenzalacetons und einfacherer Ketone, sowie ihrer Ketochloride. *Chem. Ber.* **55**:953-979 (1922).
205. M. M. Davis and H. B. Hetzer. Titrimetric and equilibrium studies using indicators related to nile blue A. *Anal. Chem.* **38**:451-461 (1966).
206. K. Westesen and H. Bunjes. Do nanoparticles prepared from lipids solid at room temperature always possess a solid lipid matrix? *Int. J. Pharm.* **115**:129-131 (1995).
207. S. Liedtke, K. Jores, W. Mehnert, and K. Mäder. Possibilities of non-invasive physicochemical characterisation of colloidal drug carriers, *27th Intern. Symp. Control. Rel. Bioact. Mater.*, Vol. 27, Controlled release society, Paris, 2000, 1088-1089.
208. S. Udenfriend. *Fluorescence assay in biology and medicine*, Academic press, New York, San Francisco, London, 1962.
209. S. Wartewig and R. Neubert. Nicht-invasive Analysenmethoden der Schwingungsspektroskopie in der pharmazeutischen Forschung. *Pharm. Ind.* **64**:863-869 (2002).
210. G. Rücker, M. Neugebauer, and G. G. Willems. *Instrumentelle pharmazeutische Analytik: Lehrbuch zu spektroskopischen, chromatographischen und elektrochemischen Analysenmethoden*, Wissenschaftliche Verlagsgesellschaft mbH, Stuttgart, 1992.
211. P. Tandon, R. Neubert, and S. Wartewig. Thermotropic phase behaviour of sodium oleate as studied by FT-Raman spectroscopy and X-ray diffraction. *J. Mol. Structure* **526**:49-57 (2000).
212. P. Pallas, S. Wartewig, I. Zimmermann, and H. Richter. Characterization of dimethyldiacetyloxysilanes by differential scanning calorimetry, Raman scattering and X-ray diffraction. *Pharmazie* **55**:503-507 (2000).

213. C. Beyer and J. Maasz. Röntgendiffraktometrie in der Pharmazie. *Pharm. Unserer Zeit* **1**:12-29 (1987).
214. K. Larsson. Classification of glyceride crystal forms. *Act. Chem. Scand.* **20**:2255-2260 (1966).
215. J. W. Hagemann. Thermal behavior and polymorphism of acylglycerides. In: K. Sato and N. Garti (eds), *Crystallization and polymorphism of fats and fatty acids*, Marcel Dekker Inc., New York and Basel, 1988, pp. 9-95.
216. L. Hernqvist. Crystal structures of fats and fatty acids. In: K. Sato and N. Garti (eds), *Crystallization and polymorphism of fats and fatty acids*, Marcel Dekker Inc., New York and Basel, 1988, pp. 97-137.
217. D. Thiele. Personal communication on the role of cocoa butter in chocolate, Laboratories of Nestlé, Berlin, 2001.
218. M. J. Ruocco and G. G. Shipley. Characterization of the sub-transition of hydrated dipalmitoylphosphatidylcholine bilayers. *Biochim. Biophys. Acta* **691**:302-320 (1982).
219. M. A. Kiselev, P. Lesieur, A. M. Kisselev, and M. Olivon. Ice formation in model biological membranes in the presence of cryoprotectors. *Nucl. Inst. Method. A* **448**:255-260 (2000).
220. M. A. Kiselev, P. Lesieur, A. M. Kisselev, D. Lombardo, M. Killany, S. Lesieur, and M. Ollivon. A sucrose solutions application to the study of model biological membranes. *Nucl. Inst. Method. A* **470**:409-416 (2001).
221. H. Bunjes, M. H. J. Koch, and K. Westesen. Effect of particle size on colloidal solid triglycerides. *Langmuir* **16**:5234-5241 (2000).
222. M. Y. Efremov, F. Schiettekatte, M. Zhang, E. A. Olson, A. T. Kwan, R. S. Berry, and L. H. Allen. Discrete periodic melting point observations for nanostructure ensembles. *Physical Review Letters* **85**:3560-3563 (2000).
223. V. Jenning, Feste Lipid-Nanopartikel (SLN<sup>TM</sup>) als Trägersystem für die dermale Applikation von Retinol: Wirkstoffinkorporation, -freisetzung und Struktur, PhD thesis, Berlin, 1999.
224. K. Jores, W. Mehnert, and K. Mäder. Physicochemical investigations on solid lipid nanoparticles (SLN) and on oil-loaded solid lipid nanoparticles: a nuclear magnetic resonance and electron spin resonance study. *Pharm. Res.* **20**:1274-1283 (2003).
225. T. Unruh, H. Bunjes, K. Westesen, and M. H. J. Koch. Observation of size-

- dependent melting in lipid nanoparticles. *J. Phys. Chem. B* **103**:10373-10377 (1999).
226. D. Precht. Fat crystal structure in cream and butter. In: N. Garti and K. Sato (eds), *Crystallization and polymorphisms of fats and fatty acids*, Marcel Dekker Inc., New York and Basel, 1988, pp. 305-361.
227. S. A. Wissing and R. H. Müller. Solid lipid nanoparticles as carrier for sunscreens: in vitro release and in vivo skin penetration. *J. Controlled Release* **81**:225-233 (2002).
228. S. A. Wissing and R. H. Müller. The influence of solid lipid nanoparticles on skin hydration and viscoelasticity - in vivo study. *Eur. J. Biopharm.* **56**:67-72 (2003).

## Publications

### Oral presentations

- K. Jores, S. Liedtke, K. Mäder, and W. Mehnert. Characterization of tensides in colloidal drug carrier systems. *Jahrestagung der Deutschen Pharmazeutischen Gesellschaft*, Münster, October 5th to 7th, 2000.
- K. Jores, W. Mehnert, and K. Mäder. A physicochemical characterization of drug containing lipid nanosuspensions. *Bayer AG*, Leverkusen, April 16th, 2003.
- K. Jores, W. Mehnert, and K. Mäder. Lipid nanodispersions as drug carrier systems – a physicochemical characterization. *Novartis Pharma AG*, Basel, June 20th, 2003.
- K. Jores, W. Mehnert, and K. Mäder. Visions and reality of solid lipid nanoparticles (SLN<sup>TM</sup>). *Novartis Pharma AG*, Basel, February 5th, 2004.
- K. Jores, W. Mehnert, and K. Mäder. From solid lipid nanoparticles (SLN) to nanospoons. Visions and reality of colloidal lipid dispersions. *International Meeting on Pharmaceutics, Biopharmaceutics and Pharmaceutical Technology*, APV/APGI, Nuremberg, March 15th to 18th, 2004.

### Poster presentations

- K. Jores, S. Liedtke, W. Mehnert, and K. Mäder. Characterization of solid lipid nanoparticles (SLN<sup>TM</sup>) - how to optimize the quantity of surfactants, *27th Intern. Symp. Control. Rel. Bioact. Mater.*, Controlled release society, Paris, July 7th to 13th, 2000.
- S. Liedtke, K. Jores, W. Mehnert, and K. Mäder. Possibilities of non-invasive physicochemical characterisation of colloidal drug carriers, *27th Intern. Symp. Control. Rel. Bioact. Mater.*, Controlled release society, Paris, July 7th to 13th, 2000.
- K. Jores, W. Mehnert, and K. Mäder. Incorporation of drug model substances in colloidal lipid carrier systems, *Jahrestagung der Deutschen Pharmazeutischen Gesellschaft*, Halle, October 10th to 13th, 2001.
- K. Jores, W. Mehnert, and K. Mäder. Non-invasive determination of the fate of colloidal lipid nanodispersions on human skin, *Jahrestagung der Deutschen Pharmazeutischen Gesellschaft*, Berlin, October 9th to 12th, 2002.

- K. Mäder, K. Jores, W. Mehnert, W. Herrmann, and T. Plauschin. Non-invasive characterization of drug release processes by low frequency ( 1GHz) EPR imaging, *Jahrestagung der Deutschen Pharmazeutischen Gesellschaft*, Berlin, October 9th to 12th, 2002.
- W. Mehnert, K. Jores, and K. Mäder. Lipid nanoparticles as possible drug carriers: a physicochemical characterization by spectrofluorometric studies, *Jahrestagung der Deutschen Pharmazeutischen Gesellschaft*, Berlin, October 9th to 12th, 2002.
- K. Jores, W. Mehnert, H. Bunjes, M. Drechsler, and K. Mäder. From solid lipid nanoparticles (SLN) to nanospoons. Visions and reality of colloidal lipid dispersions, *30th Intern. Symp. Control. Rel. Bioact. Mater.*, Controlled release society, Glasgow, July 19th to 23th, 2003.

#### **Conference proceedings**

- K. Jores, S. Liedtke, W. Mehnert, and K. Mäder. Characterization of solid lipid nanoparticles (SLN<sup>TM</sup>) - how to optimize the quantity of surfactants, *27th Intern. Symp. Control. Rel. Bioact. Mater.*, Vol. 27, Controlled release society, Paris, 2000, 1092-1093.
- S. Liedtke, K. Jores, W. Mehnert, and K. Mäder. Possibilities of non-invasive physicochemical characterisation of colloidal drug carriers, *27th Intern. Symp. Control. Rel. Bioact. Mater.*, Vol. 27, Controlled release society, Paris, 2000, 1088-1089.
- K. Jores, S. Liedtke, K. Mäder, and W. Mehnert. Characterization of tensides in colloidal drug carrier systems, *Arch. Pharm. Pharm. Chem.* **333**, Suppl. 2:21 (2000).
- K. Jores, W. Mehnert, and K. Mäder. Incorporation of drug model substances in colloidal lipid carrier systems, *Arch. Pharm. Pharm. Chem.* **334**, Suppl. 2:77 (2001).
- K. Jores, W. Mehnert, and K. Mäder. Non-invasive determination of the fate of colloidal lipid nanodispersions on human skin, *Arch. Pharm. Pharm. Chem.* **335**, Suppl. 1:113 (2002).
- K. Mäder, K. Jores, W. Mehnert, W. Herrmann, and T. Plauschin. Non-invasive characterization of drug release processes by low frequency ( 1GHz) EPR imaging, *Arch. Pharm. Pharm. Chem.* **335**, Suppl. 1:115 (2002).

- W. Mehnert, K. Jores, and K. Mäder. Lipid nanoparticles as possible drug carriers: a physicochemical characterization by spectrofluorometric studies, *Arch. Pharm. Pharm. Chem.* **335**, Suppl. 1:117 (2002).
- K. Jores, W. Mehnert, H. Bunjes, M. Drechsler, and K. Mäder. From solid lipid nanoparticles (SLN) to nanospoons. Visions and reality of colloidal lipid dispersions, *30th Intern. Symp. Control. Rel. Bioact. Mater.*, Vol. 29, Controlled release society, Glasgow, 2003, 181.
- K. Jores, W. Mehnert, and K. Mäder. From solid lipid nanoparticles (SLN) to nanospoons. Visions and reality of colloidal lipid dispersions. *Proc. International Meeting on Pharmaceutics, Biopharmaceutics and Pharmaceutical Technology*, APV/APGI, Nuremberg 2004.

### Research articles

- K. Jores, W. Mehnert, and K. Mäder. Physicochemical investigations on solid lipid nanoparticles (SLN) and on oil-loaded solid lipid nanoparticles: a nuclear magnetic resonance and electron spin resonance study. *Pharm. Res.* **20**:1274-1283 (2003).
- K. Jores, W. Mehnert, M. Drechsler, H. Bunjes, C. Johann, and K. Mäder. Investigations on the structure of solid lipid nanoparticles (SLN) and oil-loaded solid lipid nanoparticles by photon correlation spectroscopy, field-flow fractionation and transmission electron microscopy. *J. Controlled Release* **95**:217-227 (2004).
- K. Jores, W. Mehnert, and K. Mäder. Non-invasive determination of the fate of solid lipid nanoparticles (SLN) on human skin. (Submitted).
- K. Jores, A. Haberland, S. Wartewig, H. Rudolf, W. Mehnert, and K. Mäder. Non-invasive investigations on solid lipid nanoparticles (SLN) and on oil-loaded SLN by spectrofluorometric studies and by Raman spectroscopy. (Submitted).
- A. Haberland, C. S. Maia, K. Jores, M. Dürrfeld, W. Mehnert, I. Schimke, B. Christ, and M. Schäfer-Korting. Albumin effects on drug absorption and metabolism in reconstructed epidermis and excised pig skin. *Altex* **20**:3-9 (2003).

## Acknowledgements

I wish to express my gratitude to my supervisor, Prof Dr Karsten Mäder, for his valuable advice and continued kindness. His insightful suggestions and comments have provided the necessary progress of this thesis, even over the long distance between Freiburg/Breisgau and Berlin.

I thank my co-supervisor and leader of the DFG project, Dr Wolfgang Mehnert, for his support, kindness and patience I daily experienced in our small work group in Berlin.

My special thanks go to Deutsche Forschungsgemeinschaft (DFG) for the scholarship which has enabled these investigations.

Many different techniques for physicochemical characterization were used for this work. For support I would like to thank

- Mrs. S. Liedtke, Luisen Hospital, Aachen (introduction into the field of SLN)
- Dr H. Bunjes, Friedrich Schiller University, Jena, and Dr M. Drechsler, University of Bayreuth (TEM measurements)
- Mr. T. Plauschin, Magnettech GmbH, Berlin (technical ESR support)
- Mrs. H. Rudolf and Prof Dr S. Wartewig, Martin Luther University, Halle-Wittenberg (Raman spectroscopy)
- Mrs. T. Gartz, Free University, Berlin (NMR measurements)
- Dr C. Johann, Wyatt Technology Europe, Woldert (FFF measurements)
- Prof Dr H. Bunge, Technical University, Clausthal, and Dr M. A. Kiselev, Joint Institute for Nuclear Research, Dubna, Russia (synchrotron measurements)
- Dr A. Haberland, Free University, Berlin (advice in fluorescence measurements)
- Mr. S. Anger, Free University, Berlin (discussion on particle size measurements), and
- Dr U. Schäfer, University of Saarland, Saarbrücken (supply with human skin).

I thank all colleagues in the Institute of Pharmacy at Free University, Berlin for the friendly working atmosphere.

Most of all, I deeply thank my husband Thomas for his positive support, continued encouragement and appreciation of what I do.



# Curriculum vitae

## PERSONAL INFORMATION

Name	JORES, KATJA
Nationality	German
Marital status	married, no children
Date of birth	1972-06-10
Place of birth	Mainz, Germany

## WORK EXPERIENCE

Since 08/2003	position as Laboratory Head in Pharmaceutical Research and Development
Employer	Novartis Pharma AG, Basel, Switzerland
11/1999 to 07/2003	PhD study in Pharmaceutical Technology
Employer	Deutsche Forschungsgemeinschaft (DFG)
Place of work	Free University of Berlin, Institute of Pharmacy, Berlin, Germany
Supervisors	Prof Karsten Mäder (PhD) and Wolfgang Mehnert (PhD)
11/1999 to 07/2003	sidelines as pharmacist and as pharmaceutical consultant
Employers	Albrecht Apotheke and Schildhorn Apotheke, Berlin; Alpha Care, Celle, Germany

## EDUCATION AND TRAINING

03/2003	examination and certification for further education in Pharmaceutical Technology ("Fachapothekerin für Pharmazeutische Technologie")
From 11/1999 to 11/2002	further training measure in Pharmaceutical Technology ("Weiterbildung zur Fachapothekerin für Pharmazeutische Technologie")
07/1999	license to practice as pharmacist ("Approbatation als Apothekerin")
07/1999	third pharmaceutical state examination, Regensburg, Germany
From 11/98 to 04/99	second half of the practical year for pharmaceutical students
Employer	Universitäts Apotheke, Heidelberg; Germany
From 05/98 to 10/98	first half of the practical year for pharmaceutical students
Employer	Boehringer Ingelheim, Pharm. Development and Analytics, Buenos Aires, Argentina
From 04/94 to 04/98	pharmaceutical studies at Bayerische Julius Maximilian University, Würzburg, Germany
04/1998	second pharmaceutical state examination
04/1996	first pharmaceutical state examination
From 04/95 to 04/98	scholarship of Begabtenförderung Bischöfliche Studienstiftung Cusanuswerk
From 10/93 to 03/94	professional training
Technical college	Naturwissenschaftliches Technikum, Landau/Pfalz, Germany
Job title	technical assistant for environmental analytics ("Umwelt-technische Assistentin")
From 08/91 to 07/93	professional training
Technical college	Berufsbildende Schule Naturwissenschaften, Ludwigshafen, Germany
Job title	technical assistant for chemistry ("Chemisch-technische Assistentin")
From 08/78 to 05/91	elementary school and high school
Schools	Karmeliter Grundschule and Altsprachliches Rudi Stephan Gymnasium, Worms, Germany
Certificate (05/91)	Abitur



## **Erklärung**

Hiermit erkläre ich gemäß §5 (2) der Promotionsordnung der Mathematisch-Naturwissenschaftlich-Technischen Fakultät der Martin-Luther-Universität Halle-Wittenberg, daß ich die Ergebnisse der vorliegenden Dissertationsarbeit

Lipid nanodispersions as drug carrier systems –  
a physicochemical characterization

am Institut für Pharmazie der Freien Universität Berlin und an der Martin-Luther-Universität Halle-Wittenberg unter Anleitung von Herrn Prof. Dr. Karsten Mäder selbständig erarbeitet bzw. im Rahmen der angegebenen Kooperationen erhalten habe und nur die in der Dissertation angegebenen Literaturstellen und Hilfsmittel verwendet habe.

Weiterhin habe ich diese Arbeit bisher an keiner in- oder ausländischen Fakultät als Dissertationsschrift vorgelegt.

Halle (Saale), den 8. Juni 2004

Katja Jores